Towards Human-Centered Haptic Shared Autonomy for Assisted Driving Systems

by

Kenechukwu C. Mbanisi

PhD Dissertation

Submitted to the Faculty

of the

WORCESTER POLYTECHNIC INSTITUTE

In partial fulfillment of the requirements for the

Degree of Doctor of Philosophy

in

Robotics Engineering

by

April 2022

APPROVED:

_____

Prof. Michael A. Gennert, Advisor

_____

Prof. Karen L. Troy, Biomedical Engineering, WPI

_____

Prof. Candace Sidner, Computer Science, WPI

_____

Prof. Taskin Padir, Electrical and Computer Engineering, Northeastern University

_____

Prof. Soussan Djamasbi, School of Business, WPI

Abstract

Recent advances in sensor technology and declining computing costs have contributed to the rising adoption of intelligent assisted driving systems. These systems complement human efforts in vehicle navigation across various aspects of personal mobility including passenger vehicles, wheelchairs, and mobile telepresence robots. Shared autonomy (SA) formalizes this approach of synergistic collaboration of both the human and autonomous agent to achieve a common navigation task. Haptic shared autonomy (HSA) is a form of SA where both agents "blend" their control inputs by applying forces on a force-enabled control interface (such as a motorized steering wheel or haptic joystick). Existing research shows that HSA systems lead to improved driving task performance, increased situational awareness and reduced workload for the human. However, these systems still struggle with issues around control authority arbitration and intent misalignment which lead to undesirable conflict between the human and the autonomous agent, resulting in user dissatisfaction and, oftentimes, abandonment of the system altogether.

This dissertation presents a human-centered design approach with four proposed contributions to address these open challenges of haptic shared autonomy in assisted driving. The first contribution provides a better understanding of the implications of anticipation uncertainty on human motor control in force-based interactions. The second contribution is *SocNavAssist*, a multimodal (haptic + visual) shared autonomy framework that provides intuitive and intelligent navigation assistance for teleoperated mobile robots in human environments. The third is an extension to *SocNavAssist* to enable socially-aware assistance adaptation to different driving objectives/styles when navigating in dense, human-populated environments. Lastly,

a novel approach for modeling and simulating human driver control behavior for improved driving assistance system design is proposed.

Acknowledgements

First, I would like to acknowledge and thank my research advisor, Professor Michael Gennert, for his incredible support. I am so grateful for your willingness to serve as my advisor at a critical time, which gave me a lifeline to finish my PhD. Thank you for the constant guidance and encouragement you provided throughout my time at WPI, especially over the last year. I would like to thank my dissertation committee members, Professor Candace Sidner, Professor Soussan Djamasbi, Professor Karen Troy and Professor Taskin Padir for providing guidance and feedback in shaping my research.

I had the privilege of meeting and working with Dr. Hideyuki Kimpara on the Toyota-WPI research project during my doctoral work. The two years we worked together truly shaped me as a researcher. Thank you for your patience and humility in working with me. I am grateful to Professor Zhi (Jane) Li for her mentorship during the first four years of my PhD. Thank you for your caring, patient guidance, and support.

Over the years I have been blessed to know and work with many awesome colleagues in the Robotics Engineering department: Dr. Jayam Patel, Alexandra Valiton, Lening Li, Sihui Li, Abhishek Kulkarni, Heramb Nemlekar, Nathalie Majcherczyk, Dr. Adnan Munawar, Ahat Abudula, Tsung-Chi Lin and many others. Special thanks to Jayam for always being there to provide feedback and much-needed encouragement through the final months of my PhD.

I must acknowledge the many mentors who have had such a significant impact on my life and my time at WPI: Professor Nick Bertozzi, Professor Wole Soboyejo, and Professor Emmanuel Agu. I am also grateful to other faculty and staff who supported me throughout my time: Kristen Bronger, Katherine Crighton, Dr. Torbjorn Bergstrom, Professor Walter Towner, Professor Gbeton B. Somasse, Professor

Purvi Shah.

Many thanks to my wonderful local church family in Worcester (Grace Presbyterian Church) who brought so much life to my time in Worcester, such a long way from home. A big thank you to my dearest friends: Dr. Fyali Jibji-Bukar, Samuel and Oyin Iyiola, Joaquim Akinwunmi, Akachukwu Okafor, Babajide Owoyele, Adunola Fagbohungbe, Abisola Oni and many others, for their unending support and encouragement over the years.

I am grateful to my teachers and lecturers who helped me develop academically right from secondary school: Mr. Iyamu, Mr. Sebastian Eluehike, Mr. Ojukwu, Dr. A. Awelewa, Dr. Agboje and many others.

I would like to thank my wonderful family, Bishop Dr. Victor Mbanisi (Dad), Rev. Mrs Sophy Mbanisi (Mum), Victor, Juliet, Judith, Vivian, Chidi, Dinachi and all my brothers- and sisters-in-law. I am grateful for your love, support and belief in me. To my wonderful wife, Tumininu, I am so grateful for your unconditional love and support. I am very thankful for all the sacrifices you made so that I could get to where I am today.

I would like to thank the Toyota Motor Corporation, the Galkin Fund and the Glenn Yee Scholarship for providing financial support for my doctoral studies.

Lastly, but most importantly, I would like to give all the glory to God. Thank you God Almighty for giving me life, for sustaining me since my birth, and for guiding me through the challenging yet rewarding time at WPI. To God be the glory! Amen!

Contents

List of Figures

List of Tables

Chapter 1

Introduction

1.1 Motivation

The vehicles of today have more autonomous capabilities than ever before. Recent advances in sensor and computing technologies, coupled with the reduction in their costs, have contributed to this rise in vehicle autonomy. Increasingly, mobility systems (e.g. passenger vehicles, smart wheelchairs, mobile robots, drones, etc.) are being equipped with autonomous features that enable them to navigate in human environments either fully or semi-autonomously in a safe and reliable manner. The introduction of these autonomous features has the potential to alleviate some of the challenges of manual control in mobility systems, including minimizing accidents caused by human errors, eliminating the physical and cognitive strain of driving, and allowing individuals with physical or cognitive impairments greater autonomy.

However, these fully autonomous systems are yet to be fully reliable under all operational conditions. They remain prone to system malfunction caused by sensor failures and inaccuracies in traffic behavior prediction, etc., especially in safety-critical scenarios, requiring human intervention [4]. Moreover, researchers have

shown that factors such as a personal sense of control and limited trust in autonomy also contribute to humans' preference for staying in the control loop [5, 6].

A hybrid of full autonomy and manual control is *shared autonomy*, where humans and autonomous agents work collaboratively to accomplish navigation tasks, e.g., driving a passenger vehicle on a highway or operating a mobile telepresence robot across a hallway.

Shared autonomy enables the synergistic blending of the joint capabilities of the human and the autonomous agent leading to improved overall performance and reduced workload for the human [7]. However, open questions remain in shared autonomy around control authority arbitration i.e., *"Who has final control authority and how to blend control inputs?"* and shared intent misalignment, which leads to conflict and system abandonment by the human [8]. Oftentimes, these systems are designed with a focus on the technology (*machine-centered* approach) while limited attention is given to the crucial physical, cognitive, and social dimensions of the human operator which leads to poor overall performance as they interact with the system.

The alternative is to take a *human-centered* approach to the design of human-automation systems. The principles of *human-centered* design ensure that the considerations of human factors such as transparency, human supervision, and situation awareness are emphasized [8, 9]. Direct (or haptic) shared autonomy, where both agents "blend" their input commands by applying forces on a force-enabled control interface, is the framework favored in human-centered design because it provides a continuous feedback channel for the human and sustains situation awareness [8]. Existing research shows that *human-centered* shared autonomy systems lead to higher user acceptance, lower overreliance, reduced user workload, etc. [1, 10]. However, some challenges remain within the human-centered approach such as how to:

- improve robot-to-human intent transparency
- extend assistive driving applications from static environments to dynamic environments with social constraints,
- better model and understand human-vehicle interaction dynamics.

This dissertation is motivated by these challenges and contributes to the area of haptic shared autonomy by proposing solutions grounded in human-centered design principles.

1.2 Problem Statement and Research Objectives

This dissertation focuses on the following theme: "How to design shared autonomy frameworks for assistive driving systems considering human-centered factors?" Specifically, I examine the following research questions with the goal of understanding and improving the design of human-centered shared autonomy systems:

R1 *What are the implications of anticipation uncertainty on aligned intent and how can they be mitigated in force-based interactions?*

Mutual understanding is at the center of teamwork. This is not only true for human-human teams, but also human-robot teams as well. Transparency is crucial for maintaining mutual understanding between agents in a team [9]. In a human-centered shared autonomy system, the operator should be aware of and continuously updated on the system's actions; implying that the autonomous agent's actions should be understandable and predictable. This requirement is particularly relevant in haptic shared autonomy systems, where a haptic-enabled control device (e.g. motorized steering wheel) serves as the

shared control interface between the human and autonomous agent [1, 7]. Unanticipated haptic feedback forces on the control interface may adversely affect the human operator's response and thereby degrade task performance and driving safety [11]. Therefore, it is crucial to understand the effect of force anticipation uncertainty on human response and motor control in force-based interactions as it sheds light on the impact of system transparency on shared human-robot systems.

R2 *How to design human-centered socially-aware navigation assistance with improved system transparency?*

Given the insights on how force anticipation impacts human task performance, it is important to explore how to design human-centered shared autonomy systems that enhance mutual understanding and cooperation by improving system transparency. In this work, I consider the context of socially-aware navigation assistance, i.e., enabling non-intrusive, safe, and comfortable robot navigation around humans [12]. While research suggests that humans operating mobility systems (either proximally or remotely) would benefit from navigation assistance in dynamic, cluttered environments (e.g., at a busy conference hall, etc.), existing work on shared autonomy for navigation has focused on static environments or single moving pedestrian avoidance [6, 13]. An extension of existing approaches to the more realistic case of multi-pedestrian interaction is needed. In order to achieve effective navigation assistance in dynamic, multi-pedestrian scenarios, two questions arise: (i) How to plan and generate safe, socially-aware navigation paths within dynamic human environments? (ii) What interaction modalities (e.g. visual, haptic, auditory, etc.) work best to communicate the generated guidance cues to the human

operator in an intuitive and transparent manner? This dissertation proposes a multi-modal shared autonomy approach and evaluates its impact on improving system transparency, cooperation, and user preferences.

R3 *How to achieve assistance adaptation to distinct driving objectives/styles and how would this impact driving performance and human-automation cooperation?*

In real-world co-driving scenarios, the ability of autonomous agents to adapt to human characteristics, tasks, and/or environmental conditions is essential for enhancing alignment of control strategies and reducing conflict within shared tasks [14]. Additionally, adaptive support in assisted driving can lead to improved driving task performance over static, one-size-fits-all support [15]. Existing adaptation factors include risk, level of trust and confidence [16], task and skill level [17, 18], etc. Again, there has been limited work in the area of navigation assistance in dynamic human environments that takes user driving objectives and styles into account. It is important to explore approaches to adaptive navigation assistance in this context and how, if at all, they impact on driving performance and human-automation cooperation.

R4 *How to model and render complex human driver behavior in simulation to advance our understanding of human driver-vehicle interaction and improve the design of driver assistance systems?*

Increasing levels of autonomy in today's vehicles have impacted the way drivers interact, adapt, and respond to vehicle systems during shared driving. Having a thorough understanding of human driving behaviour is necessary for designing Assistive Driving Systems (ADS) that ensure safety and comfort when driving. ADS-driver interactions have traditionally been evaluated using sim-

ulated or real-world human driver experiments [19, 20], which have limited ability to provide objective evaluation of the dynamic interactions, and the control workload on the driver. An alternative approach is to use digital human driver models, since they enable accurate simulation of human behavior and dynamics, as well as providing access to hard-to-measure internal workload variables [21]. Yet, little work has been done on developing active digital human driver models and simulations to aid in the design of the next generation of commercial advanced driving assistance systems (ADAS). This dissertation examines how to model and simulate complex human driver behavior as well as how using digital driver models may open new horizons in model-based design and evaluation of human-centered ADAS.

1.3 Dissertation Structure and Research Contributions

The structure and contributions of this dissertation as well as the associated publications (published, under-review, or in preparation) are as follows:

- **Chapter 2** provides a brief review of the state of the art covering shared autonomy frameworks, haptics and human-centered design considerations for assistive autonomy in mobility applications.

- **Chapter 3** addresses Research Question **R1** by studying the impact of anticipation uncertainty and transparency on human motor control in force-based tasks. A simple pushing experiment was developed and conducted with ten participants to investigate this effect. Findings indicate that force anticipa-

tion, including the expected workload, affects human control strategy, such as whether feedforward- versus feedback-dominant control is used. The results also revealed that humans rely on internal predictive models for motor control, which is updated iteratively through interactions. The present findings shed light on the importance of transparency and anticipation in force-based interactions, such as haptic shared autonomy. The work in this chapter was first presented in:

  - [22] H. Kimpara, K. C. Mbanisi, Z. Li, K. L. Troy, D. Prokhorov, and M. A. Gennert, "Force Anticipation and its Potential Implications on Feedforward and Feedback Human Motor Control," *Human Factors*, Mar. 2020

- **Chapter 4** addresses Research Question **R2** by presenting SocNavAssist, a multimodal shared autonomy approach, leveraging visual and haptic guidance, to provide intuitive and transparent navigation assistance for mobile telepresence robots in dynamic human environments. The proposed framework uses a modified form of reciprocal velocity obstacles for generating safe control inputs while taking social proxemics constraints into account. Two different visual guidance designs, as well as haptic force rendering, were proposed to convey safe control input to the operator. I conducted a user study, with fifteen participants, to compare the merits and limitations of the multimodal approach to haptic or visual assistance alone in a shared navigation task. The key findings are that participants preferred multimodal assistance with visual guidance trajectory over haptic or visual modalities. Additionally, results also revealed that visual guidance trajectories conveyed a higher degree of understanding and cooperation than equivalent haptic cues in a navigation task. The work

in this chapter was first presented in:

  - [23] K.C. Mbanisi, M. A. Gennert, Z. Li, "SocNavAssist: A Haptic Shared Autonomy Framework for Social Navigation Assistance of Mobile Telepresence Robots", *IEEE International Conference on Human-Machine Systems (ICHMS)*, 2021
  - [24] K. C. Mbanisi, M. A. Gennert, "Multimodal Shared Autonomy for Social Navigation Assistance of Telepresence Robots", in submission to *IEEE Transactions on Human-Machine Systems (THMS)*

- **Chapter 5** addresses Research Question **R3** by presenting an extension to SocNavAssist that enables adaptive assistance to different driving objectives or styles while navigating in dense, human environments. This is accomplished by incorporating socially-relevant objective functions which reflect the distinct driving objectives. In particular, two assistance policies, safety-aligned and goal-aligned assistance, were designed and evaluated in autonomous mode using four typical navigation scenarios. An exploratory study, with five participants, was conducted to determine how adaptive assistance affects driving performance (efficiency and safety), human-automation cooperation and user preferences in shared navigation. The key findings are that, while assistance adaptation did not have a significant impact on driving performance, participants preferred safety-aligned assistance mode under both cautious and assertive driving objectives. This study provides a preliminary evaluation of how remote operators interact with different navigation assistance modes in response to typical driving behaviors in social navigation. The work in this chapter is under preparation for submission to:

– [25] K.C. Mbanisi, M. A. Gennert, "Adaptive SocNavAssist: Assistance Adaptation to Driving Objectives in Social Navigation", to be submitted to *IEEE/ACM International Conference on Human-Robot Interaction (HRI 2023)*

- **Chapter 6** addresses Research Question **R4** by presenting a novel approach for modeling and simulating human driver control behavior for improved driving assistance system design. Our simulation framework, Human Model-based Active Driving System (HuMADS), integrates a human driver model and a vehicle dynamics model to provide a high-fidelity simulation of driver-vehicle interaction. To generate human-like driver control motions on the digital human driver model, a learning-based approach is employed. Specifically, we recruited eight experienced drivers and recorded their vehicle control motions on a fixed-base driving simulation test bed. We further extracted a set of characteristic driver control styles (i.e. steering handling and pedal switching styles) from the demonstration data. Using a combination of imitation learning methods, we extracted the regularity and variability of driver control styles across participants, and modeled them as motion primitives that can be used for motion reproduction in simulation. The work in this chapter was first presented in:

  – [26] K. C. Mbanisi, H. Kimpara, Z. Li, and M. A. Gennert, "Learning Coordinated Vehicle Maneuver Motion Primitives from Human Demonstration," *2018 IEEE/RSJ International Conference on Intelligent Robots and Systems (IROS)*, Madrid, Italy, 2018, pp. 6560-6565.

  – [22] H. Kimpara, K. C. Mbanisi, J. Fu, Z. Li, D. Prokhorov, and M. A. Gennert, "Human model-based active driving system in vehicular dy-

namic simulation," *IEEE Transactions on Intelligent Transportation Systems*, vol. 21, no. 5, pp. 1903-1914, May 2020.

- [27] K. C. Mbanisi, H. Kimpara, Z. Li, and M. A. Gennert, "Analysis and Learning of Natural Driver Control Motion Primitives for Computational Human Driver Modeling", to be submitted to *IEEE Transactions on Intelligent Vehicles (TIV)*
- [28] K. C. Mbanisi, H. Kimpara, Z. Li, D. Prokhorov and M. A. Gennert, "Human Model-based Evaluation of Driver Control Workloads in Driver Assistance Systems", in submission to *IEEE Transactions on Human-Machine Systems (THMS)*

- **Chapter 7** concludes this thesis with a summary of contributions, insights into broader societal impacts, and a discussion of possible future directions from the work that I have presented.

Chapter 2

Background

2.1 Shared Autonomy Frameworks

Shared autonomy lies in the middle of the autonomy spectrum, with manual control and full autonomy at opposing ends [29] (Fig. 2.1). Abbink et al. [8] described shared autonomy (also known as shared control) as a scenario where "humans and robots are interacting congruently in a perception-action cycle to perform a dynamic task that either the human or the robot could execute individually under ideal circumstances". Petermeijer [30] considers shared control as "teamwork or joint action between human(s) and machines or robots in a shared task."

Therefore, as opposed to manual control (where the human is solely responsible for task execution) and full autonomy (where the autonomous agent is solely responsible), shared autonomy enables the cooperative sharing of responsibility for task execution between the human partner(s) and the robot (Fig. 2.1). Shared autonomy is a promising approach because it has to been shown to improve task performance and reduce the amount of operational workload for humans [7], while keeping humans in the loop for supervision and high-level decision making.

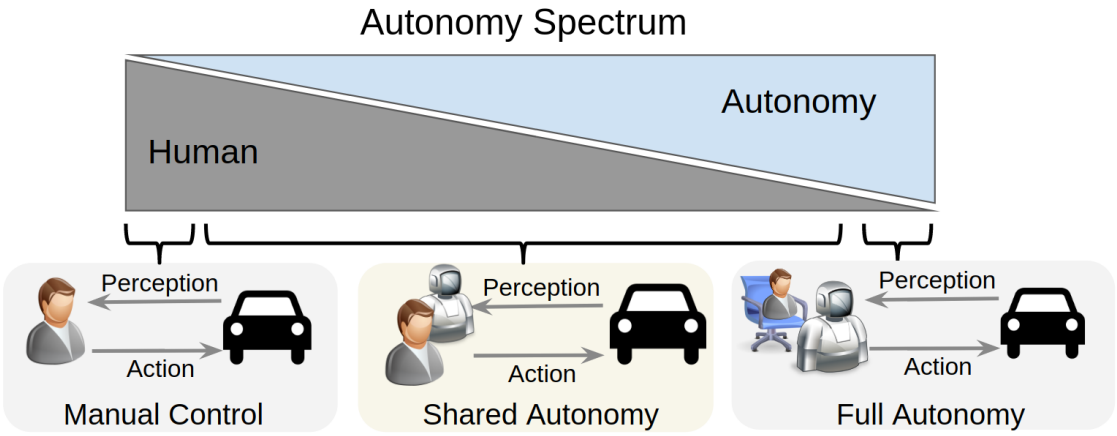

Figure 2.1: Spectrum of autonomy in human-machine systems

Existing approaches for shared autonomy (SA) can be defined into two categories based on how the task allocation and execution are performed: **task-level** SA and **servo-level** SA [31, 32] (Fig. 2.2). At the **task-level**, the human may assign a subtask completely to the machine/robot with precise task specifications, and then act in a solely supervisory role. As an example of task-level shared autonomy, consider the cruise control system in a passenger vehicle. The driver first assigns the longitudinal vehicle speed control (*subtask*) to the vehicle system by engaging the cruise control and setting the desired reference speed (*task specification*). Following that, the vehicle takes over longitudinal speed control entirely from the driver, who serves as a supervisor and decides when to disengage the cruise control and assume responsibility for the subtask. This level of shared autonomy is *discrete* in nature with only one agent handling low-level continuous control at any given time. When only the human is able to assign control authority, as described above, the system is considered to be human-initiated (HI) [33]. A mixed-initiative (MI) scenario occurs when both agents are able to assign control authority, i.e. both human and agent can request as well as relinquish control at different times [33].

Shared autonomy at the **servo-level**, on the other hand, refers to situations

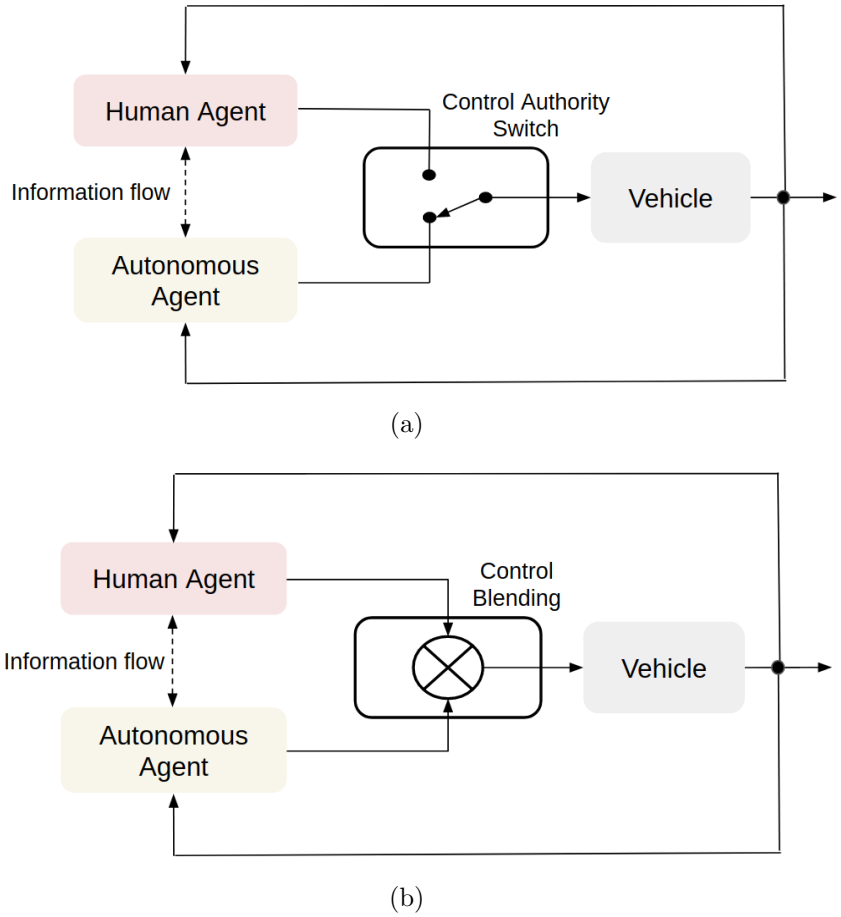

Figure 2.2: Taxonomy of shared autonomy based on task allocation and execution. a) Task-level SA; b) Servo-level SA.

in which both the human and the machine jointly control a given task and the final control commands combine the inputs of both agents. The weighted allocation function is a common blending approach in literature that adjusts the proportion of human and machine/robot input in the final command [32, 34]. A good example of servo-level SA is lane-keeping assistance in ADAS. Here, both the driver and the ADAS jointly contribute to the lateral steering control of the vehicle. Both agents must actively engage in the perception-action cycle and apply their control inputs on the steering wheel [7, 35]. This level of shared autonomy is *continuous* as both human and the autonomous agent must remain engaged in the control loop.

Two modalities of servo-level shared autonomy are prevalent in the literature based on how the control inputs of the agents are blended together: **direct** and **indirect** shared autonomy [7]. In **direct or haptic** shared autonomy, the autonomous agent and the human jointly apply their control inputs as forces on a force-based control interface (such as a motorized steering wheel or a haptic joystick) such that the human can directly negotiate the final control inputs to the vehicle by applying more or less force on the interface [7,35]. The advantage of haptic shared autonomy is that it enables the human to directly modulate their level of control authority based on the amount of force exerted on the shared control interface. However, one drawback is with control conflict and the resulting increased forces and physical workload on the human. We will discuss the subject of conflict in haptic shared autonomy further later in this chapter.

The second modality is **indirect** shared autonomy, also known as input-mixing. Here, no physical interaction or coupling exists between the human and the autonomous agent, but the human applies their input commands onto the control interface (such as a joystick or keyboard) and the autonomous agent is responsible for blending that command to reach a final command which is sent to the vehicle. This results in the autonomous agent retaining final control authority on the vehicle motion [35, 36]. Although entrusting the autonomous agent with final authority is useful in certain situations where human performance may be impaired (e.g., by drowsiness, low visibility, or presence of blind spots), it generally leads to lower situation awareness and sense of control for the human agent.

2.1.1 Haptics and Haptic Shared Autonomy

The haptic sensation is one of the five broad human senses; it refers to our sense of touch and plays a crucial role in how humans interact with and experience the

tangible world [37]. Haptic sensing can be divided into two general categories based on the physiological mechanisms used: *tactile (or cutaneous)* sensation and *kinesthetic* sensation. Tactile (or cutaneous) sensation refers to the deformations of the skin as a result of pressure, vibration or shear sensed by mechanoreceptor cells in the skin. Kinesthetic sensation is an internal perception of forces and torques, processed by sensory receptors in muscles, tendons, and joints [37, 38]. Researchers in the haptics field have explored how artificial haptic sensations can be applied when the traditional sense of touch is lost (e.g., due to remote or virtual interaction) or where it is needed as a communication medium (e.g., in human-robot interaction scenarios) [37, 39]. In robot-assisted surgery, the sense of touch can be restored using kinesthetic haptic feedback. This force feedback enables the surgeon to feel the interaction forces in real time while performing surgical tasks remotely with a leader-follower robot teleoperation system. [38]. Haptic feedback has also been applied, along with visual and auditory feedback, as a means to enable explicit communication and interaction between humans and machines (or robots). Vibrotactile cues on wearable or handheld tactile feedback devices can be used to provide guidance information between the human and a robot [39, 40].

In the context of shared autonomy, haptic feedback (primarily kinesthetic feedback) has been applied extensively in assistive navigation of unmanned aerial vehicles (UAVs), unmanned ground vehicles (UGVs), and passenger vehicles in order to provide navigation guidance cues to the human operator (e.g., for obstacle avoidance, path tracking, etc) as well as to augment perceptual awareness that may be lost in remote driving scenarios. Research has shown that haptic shared autonomy systems in assisted navigation: (i) improves driving task performance [10], (ii) enhances driver's situation awareness [8], (iii) enables the driver retain final control authority as a safety measure (as opposed to indirect shared autonomy described

above) [7, 35]. However, as highlighted earlier, these systems struggle with the issue of *conflict* between the human and the autonomous agent. Itoh et al. [11] defined conflict in haptic shared autonomy as "occurring as long as the human control input is inconsistent with the expected control input of the intelligent machine". This control mismatch results from a lack of intent alignment or control strategy among cooperating agents, which typically leads to increased control forces and torques as the human struggles to exert their control over the vehicle. The occurrence of mild conflicts—where the human can forcefully maintain control of the vehicle—can result in reduced user satisfaction and, sometimes, the abandonment of the shared autonomy system in favor of manual control [8,41]. A severe conflict, however, where the autonomous agent's control overwhelms the human operator, could significantly compromise vehicle safety, especially when the conflict is caused by a system failure. The tragic Boeing 737-MAX crashes in 2018 and 2019 [42] are one example of this. In this dissertation, we explore human-centered design approaches to conflict resolution.

Two broad approaches exist for haptic shared autonomy based on the type of haptic cue provided to the human: Trajectory-tracking and Guidance forces from forbidden regions [7].

Trajectory-Tracking: This is simply haptic guidance along a desired (or reference) trajectory and is well suited to scenarios where a reference trajectory is known (e.g. lane following on a road). The autonomous agent renders a restorative force to the interface to guide the human back if they veer off the reference trajectory. This approach has been extensively applied in advanced driver assistance systems (ADAS) for passenger vehicles for tasks including lane-keeping, curve negotiation and collision avoidance (for a review, see [10]). The guiding force or torque is gen-

erally estimated as proportional to the error between the current trajectory and the reference trajectory [7, 10, 43]. A major consideration in this approach is how to determine the reference trajectory for a given task [44]. In the automotive domain, a human-compatible reference trajectory is derived from a simplified driver model that characterizes driver steering behavior [45]. However, in other free-form navigation scenarios, reference trajectories would prove harder to retrieve [46].

Guidance forces from forbidden regions: This is a general case of haptic guidance that incorporates scenarios in which the driving task is not constrained to a reference trajectory. In this approach, haptic forces are applied to guide the human away from collision-bound motions or operational boundaries [7]. Virtual fixtures method was one of the earliest instances of this approach where repulsive forces are applied in different geometric directions to restrict motion in forbidden regions [47,48]. Force field-based approaches have also been proposed in the literature. Artificial potential fields (APF) have been used to estimate repulsive force feedback to guide the human away from obstacles in the environment [49]. Extending the APF approach, Lam et al [50] proposed parametric risk fields (PRF) which further generates repulsive forces based on the estimated risk of the maneuver. Predictive planning techniques such as model predictive control (MPC) have been used to plan collision-free maneuvers over a horizon, guiding the operator to the optimal maneuver [46, 51]. A recent study further explored control-theoretic maneuver selection by using control barrier functions (CBF) to bring maneuvers as close as possible to the operator's command (i.e., reducing conflict) and also ensuring safety [52]. The previous approaches have achieved improved navigation performance (e.g., reduced collision, faster completion times) but only in situations where the forbidden regions are static and unchanging in the environment. Limited work has explored haptic

guidance in the midst of dynamic obstacles. Battisti et al [53] proposed a velocity-obstacle-based approach to filter out collision-bound velocity commands and guide the operator towards collision-free maneuvers using haptic forces. This dissertation explores the use of haptic guidance in dynamic scenarios in the context of social navigation around pedestrians.

2.1.2 Human-centered Design Considerations for Shared Autonomy

Higher levels of autonomy and intelligence in mobility systems promises to enhance driving safety and efficiency and allow disabled and elderly people to travel independently. However, as long as these mobile systems do not possess robust failure detection and recovery capabilities and are not fully reliable across a wide range of drive conditions, humans will have to share the driving responsibilities while the system is in operation, whether that means operating at the task level, servo level or a combination of both [4]. So it is crucial to design these automated driving systems in a way that is human-compatible, ensuring cooperation between humans and machines. For highly automated systems to be reliable, safe, and trustworthy, Shneiderman [54] contends that both agents need to maintain a high level of control and involvement. To achieve this, a human-centered design approach must be considered in the design of human-automation systems.

Billings [9] formulated one of the earliest human-centered principles for the design of human-automation systems in the aviation industry. Recently, similar principles have been formulated to guide the design of human-automation collaboration strategies and interfaces for semi-autonomous vehicles [1, 7]. Human-centered principles converge on the following axioms (Fig. 2.3):

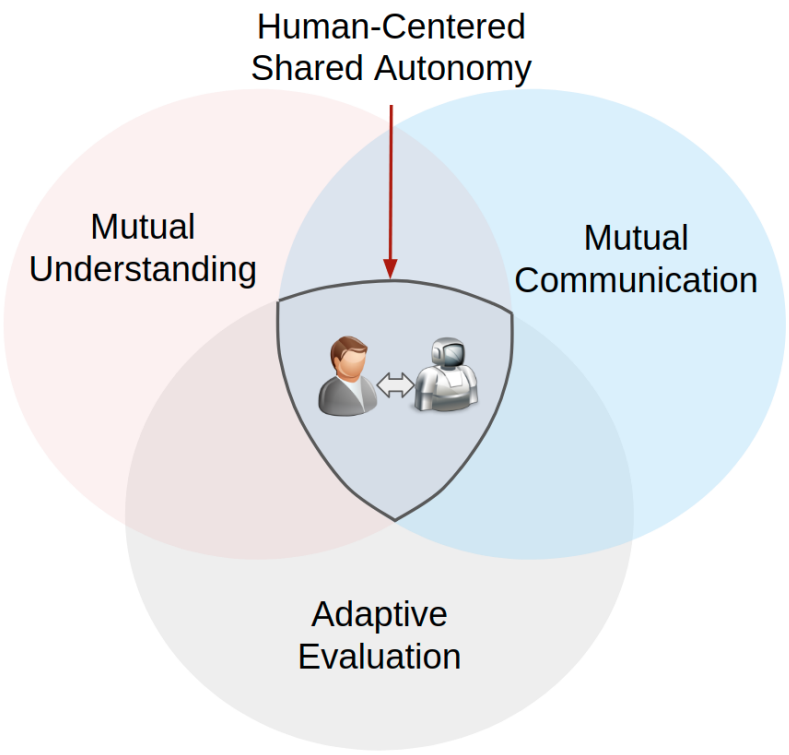

Figure 2.3: Human-centered design principles for shared autonomy systems [1]

1. **Mutual understanding:** *"Both agents should be able to understand each other's control actions."*

   Mutual understanding within a team is typically achieved via shared mental models of the collaborating agents [30]. A mental model is a description of the internal mental representation of how an agent (e.g. the autonomous agent) behaves in certain conditions. It is crucial for the human to have an accurate mental model of the autonomous agent, i.e. the capabilities, limitations and the intent of the autonomous agent [55]. With this knowledge, the human will be able to better understand the "*what*" and "*why*" of the autonomous agent's behavior and make predictions on what its future actions would be. We see evidence that humans use internal predictive models in their motor control, and that these models are constructed iteratively through interactions [56].

Inaccurate mental models lead to misjudgement of the autonomous agent's actions, over- or underreliance on the system, and unnecessary control conflicts [30]. In the context of shared autonomy, this question remains: how can the human be best informed of the autonomous agent's intent to maintain an accurate mental model?

On the other hand, a mental model of the human's behavior is also crucial if the autonomous agent is to accurately estimate the human's intent and provide synergistic assistance [1]. Various approaches to modeling driver behavior have been explored both at the operational level (such as steering, braking, or preference models) and the tactical level (including task intent inference, driver state, or skill models). See [1, 57] for a review on this topic.

2. **Mutual communication:** *"Both agents should be able to communicate the intent behind their respective actions."*

   To achieve effective communication between two entities, it is key to ensure that the right type of information is conveyed at the right time and in the right way. This will ensure that the human does not suffer from information overload, making it difficult for the human to interpret the task state and context [58]. Therefore, two crucial questions must be addressed in this context: (i) what information to communicate, (ii) how to communicate the information? Deciding what to communicate may be scenario- and task-dependent and would vary based on particular contexts and application. In their review paper, Petermeijer et al. [30] outlined the following information as candidates of what to communicate in a shared driving context: "(i) the current automation mode, (ii) time budgets to foreseen events, (iii) reasons for changes in automation models, (iv) reasons for planned maneuvers, etc."

Regarding how to communicate the information, it may be achieved via implicit (or indirect) communication or through explicit communication. Implicit communication is applied extensively in social human-robot interaction where robot posture, head or gaze movements are used to communicate the intent or the emotional state of the robot agent [59]. Explicit communication strategies are more prevalent in shared autonomy applications. Information can be communicated to the human agent through the different sensory modalities: visual channel (e.g. visual overlay display, virtual or augmented reality display, etc.) [60–62], the haptic channel (e.g. both kinesthetic and tactile feedback) [40, 52, 63] or the auditory channel (e.g. warning sounds, descriptive voice prompts, etc.) [64, 65]. Communication can occur through one or a combination of these channels. This dissertation investigates what interaction modalities are most effective for communicating the intent of autonomous agents to humans in a shared social navigation task.

3. **Adaptive evaluation:** *"Both agents should be able to monitor and adapt to the actions of the other agent in a cooperative fashion."*

   Adaptation is vital to maintaining robust team synergy in the face of changing environmental conditions, task specifications and agent states [14]. As an example, in shared driving, the autonomous agent would need to be able to adapt to and handle different driving objectives or styles, or changes in driver states (e.g., fatigue, distraction, etc.) that could impair drivers' performance and impact safety. The concept of adaptation is discussed in more detail later in this chapter.

Research has shown that haptic shared autonomy systems designed under human-centered principles are able to minimize human-automation conflict, and thus, im-

prove cooperation, user satisfaction and trust in the automation [1,15,41]. Following the axioms described above, two main factors are considered in the human-centered approach to conflict resolution are (i) system transparency, (ii) autonomy adaptation.

Transparency as Predictability

Transparency takes on different definitions in the literature when considering human-automation interaction [66], but here we explicitly consider the case of transparency as predictability, i.e., as the human and autonomy agent share a task, how predictable is the intent and action of the autonomous agent to the human operator. This is also called robot-to-human transparency [66]. The converse case, human-to-robot transparency, addresses how the agent understands the intent and actions of the human. Though it is also an important topic, in this dissertation we concentrate on the robot-to-human component. Transparency as predictability derives from the mutual understanding and communication axioms of human-centered design. In haptic shared autonomy, when the human cannot understand or anticipate what the autonomous agent is "doing" (action) or "trying to achieve" (intent), they may fight back over the force-based interface, hence generating resistive forces which increase workload and also lead to safety concerns in the navigation task.

Several methods have been proposed to improve the predictability of the autonomous agent's actions and intent. Balachandran et al [51] proposed an approach using haptic cues on the steering wheel to gradually communicate the autonomous agent's intent to steer away from a frontal collision. It is natural to consider using the shared haptic channel for intent communication as it elicits fast reflex responses to stimuli [67]. However, it is limited in the ability to convey contextual information such as the state of the task or future actions of the autonomous agent [68].

Because of this limitation in the haptic channel, researchers have favored visualization to augment haptic cues in intent communication. The human visual channel is significantly slower in processing stimuli than the haptic channel, but its trade-off is more bandwidth to convey richer information [69]. Hence, several works have been proposed to use visualization to communicate the intent of the autonomous agent in human-automation interaction. Augmented reality visualization has been applied for wheelchair navigation assistance [61], assisted telemanipulation to communicate the agent's estimate of the desired goal [70]. Visual feedback has been applied in advanced driver assistance systems (ADAS) for warning support (e.g., lane departure warning) as well as in action suggestion (e.g., recommended route display) [71]. Visualization of predicted trajectories was proposed to assist in a collision avoidance task in static environments [19, 68].

Research has also considered multimodal feedback combining visual and haptic modalities to improve system transparency and intent understanding. Vreugdenhil et al. [68] found that multimodal assistance improved user acceptance over haptic feedback alone. Berg [72] showed that compensating haptic forces with a visualization increased task performance in an industrial application. In a UAV collision avoidance task experiment, Ho et al. [73] evaluated two visualization designs combined with haptic feedback. They reported that participants preferred the visual design that showed a 1:1 representation of haptic forces. However, multimodal feedback may not always improve performance and may be dependent on the complexity of the task [74]. In Chapter 4, I investigate the effects of our multimodal approach in comparison with haptic or visual assistance alone on system transparency, cooperation and user preference in a shared social navigation task.

Autonomy Adaptation

The second human-centered design factor considered in this dissertation is adaptation. Adaptive automation systems do not remain "static" but can adjust to the task requirements, individual characteristics or preferences of the human operator. There are two modalities of robot adaptation explored in the literature: *adaptive* and *adaptable* systems. In *adaptive* systems, changes to the system's behavior are initiated by the system itself through monitoring of the task and the human behavior. Whereas in *adaptable* systems, the human is responsible for initiating changes to the system's behavior [7]. In this thesis, we consider *adaptive* automation because it designates the responsibility of adaptation to the autonomous agent. ~~thereby reducing the human's cognitive demand~~

Research has shown that adaptive assistance policies tend to outperform constant assistance policies in both overall task performance and human-automation cooperation [75]. Adaptation can be designed to occur along several dimensions, and we review a few of them below.

- *Risk-based adaptation* [43, 76]: This is analogous to an assist-as-needed approach where the level of haptic authority is low when the risk measure is low, but the level of haptic authority increases when the risk level is high. This approach ensures that conflict only occurs when they are desirable, i.e., when the risk is high and the vehicle is in a safety-critical situation.

- *Trust-based adaptation* [16]: Here, the intensity of the haptic feedback cues are regulated by the estimated level of trust the autonomous agent has in the human partner (robot-to-human trust). That is, when robot-to-human trust is high, the guidance forces on the control interface are reduced which leads to reduced physical workload. This approach differs from the risk-based

approach in that it formulates a computation model of mutual trust in the human-automation team.

- *Skill-based adaptation* [17]: In this approach, the adaptation occurs based on the operator's level of expertise in the task. This is often a latent variable that must be inferred by reasoning over the human's control inputs in task execution. The idea is that novice and expert human operators require various levels of support and a misalignment in the form of support may lead to conflict or task degradation.

- *Adaptation via personalization* [15, 41, 77]: In this approach, a model of the human operator is integrated into the control loop of the autonomous agent which allows for online adaptation of model parameters to individual users. This approach works well when human behavior and task specifications can be modeled quantitatively but may not scale to more general scenarios where human behaviors are very complex and hard to model.

- *Task-based adaptation* [18]: The approaches above assume a fixed task intent and adapt to it. The task-based adaptation relaxes this assumption by explicitly estimating the human partner's intent from control inputs and contextual information and provides the appropriate policy to maximize task performance and cooperation.

Chapter 5 explores the adaptation of navigation assistance to various operator driving objectives/styles and assesses the impact of the adaptation on human-automation cooperation and user preference.

2.2 Driving Assistance in Pedestrian-Rich Environments

Navigating a vehicle safely in a dynamic crowded environment can be challenging for humans, especially in remote teleoperation scenarios (e.g. driving a mobile telepresence robot) where situational awareness is limited and their field of view is narrow [78]. Therefore, shared autonomy with driving assistance is needed to support the operator in safe navigation around humans, not only in a physically safe way, but also in a comfortable, natural and socially consistent manner [12,79]. Real-world applications include smart wheelchair mobility, mobile telepresence robots and semi-autonomous parcel delivery robots. To achieve socially-aware navigation assistance, the autonomous agent must continuously execute the perception-planning-action control cycle while considering social constraints. However, there is limited work in this area as existing work has focused on navigation assistance in static environments alone [6,61,80]. The motion planning strategies employed in existing work [6,61,80] do not extend well beyond static environments. It is therefore necessary to develop driving assistance systems that are able to cope with dynamic obstacles and take social, cultural norms into consideration.

The topic of autonomous socially-aware robot navigation has drawn considerable attention in recent years (for reviews, see [81, 82]). Mavrogiannis et al [81] decomposes the problem of social navigation into two main components: prediction (i.e., estimating where the pedestrian(s) would be in the future) and planning (i.e., constructing a collision-free path to goal considering the predicted future states). These two components hinge on our understanding and modeling of human social and navigation behavior. Hall [83] pioneered the *proxemics theory* in the field of human psychology, which formalizes how humans manage their interpersonal spaces in

social contexts. Recent work in robotics has adapted this theory to reasoning about social constraints in motion planning around humans [12]. Several socially-aware planning approaches have been proposed in the literature and the prominent categories include sampling-based (e.g., RiskRRT [84]), model-based (e.g., social force model (SFM) [85], velocity-obstacles (VO) [86]) and learning-based methods (e.g., interacting Gaussian processes [87], SA-CADRL [88]).

However, there has been limited application of these methods to driving assistance, where the human is in the loop. In [13], Narayanan et al. formulated a semi-autonomous navigation framework for smart wheelchair assistance using RiskRRT. Kretzschmar et al. [89] took a different approach of learning the social constraints in navigation from human demonstration using inverse reinforcement learning and then deployed this trained policy as an assistive autonomy agent on a wheelchair. These works applied the indirect shared autonomy approach, and only considered either single pedestrian interactions or static group interactions. The work presented in this dissertation will consider a multimodal (haptic+visual) shared control framework for navigation assistance and extend the scenario from single pedestrian to multi-pedestrian interaction which is a more generalized and realistic problem.

2.3 Driving Assistance in Passenger Vehicles

Advances in sensor technology and the declining cost of computing hardware have accelerated the penetration of automated driving systems (ADS) in passenger vehicles. A taxonomy of driving automation levels (Levels 0-5) defined by the Society of Automotive Engineers International (SAE) [90], indicates that with higher autonomy levels, the human transfers increasing levels of driving responsibility and control authority to the automated driving system. However, as mentioned earlier,

systems with higher levels of autonomy (e.g. Levels 3-5) have yet to reach the level of robustness and reliability necessary for widespread deployment. Therefore, Level 2 systems which provide driver assistance while also keeping the driver in the loop, commonly known as advanced driver-assistance systems (ADAS), remain vital for driving safety [4]. ADAS can be classified in two broad categories: (i) based on the form of support and (ii) based on the driving task involved. For the former, driver-assistance systems can be *passive* in the form of a warning such as lane departure warning, or can be *active* such as automatic braking system [91]. For the latter, these systems can be classified into *lateral control* features such as lane-keeping assist or *longitudinal control* features such as adaptive cruise control [92]. It is hoped that these systems will reduce auto accidents and enhance driving experience by reducing human error [92].

Accurate computational driver models are crucial in the design of ADAS either in their operation, to define the appropriate complementary control actions to take in assisting the human [93], or to serve as surrogate models in place of human drivers in the testing and validation of the systems [94]. Cognitive driver models approximate driver behaviors in the context of driving task reasoning and decision-making which have been applied in developing and validating ADAS such as lane departure warning [95], collision avoidance [96], and steering assistance [93]. On the other hand, physical driver models are able to render human-like postures and movements in driving-related contexts and have been applied to analyzing in-vehicle tasks [97], ergonomics and vehicle occupant package design [98, 99], and driver assistance systems [100, 101].

However, limited work has been done on the development of an integrated physical driver model capable of rendering realistic driver control motions in normative driving scenarios. Such a surrogate driver model would provide new opportunities

for the evaluation of haptic-based ADAS, especially in the area of driver control workload. Conflict scenarios often arise between ADAS and the driver as a result of mismatches in situation awareness, intent, and task execution [11], as outlined in Section 2.1.1. This leads to higher interaction forces on the driver, which increases their physical workload and lowers their acceptance of the system. Existing studies assess the impact of haptic-based ADAS designs on driver control workload and physical stress by using one of two methods. Most studies rely on subjective evaluations of human subjects in simulated driving experiments to assess workload measures [102, 103]. Alternatively, some studies use suitably instrumented human subjects and/or vehicle control devices in driving studies to identify force interactions and the resulting internal dynamics of the human driver [20, 104, 105]. This dissertation presents the use of surrogate human driver models as a third approach since they enable the simulation of human behavior and dynamic characteristics as well as provide access to hard-to-measure internal workload variables.

Chapter 3

Role of Anticipation Uncertainty on Human Response in Force-based Tasks

3.1 Introduction & Background

In designing effective human-automation systems, mutual understanding through system transparency and predictability remains a crucial factor [1]. Predictability, in this context, suggests that the human has sufficient knowledge of the system capabilities and intentions to accurately anticipate its actions and react accordingly. Existing research on human motor control supports the fact that humans utilize both anticipatory (or feedforward) and compensatory (feedback) strategies to achieve fast and adaptive motions. [106]. These anticipatory behaviors in humans rely on internal predictive models learned over time [56]. It is important to better understand how human anticipatory behavior relates to human response in force-based tasks.

Several studies have examined the nature and effects of this anticipatory behavior

in a variety of scenarios. Serrien et al [107] recorded motion, grip, and load forces as subjects performed a task to pull open a drawer using precision grip on the handle. They observed a proactive increase in the grip force as the drawer approached the mechanical stop and concluded that this anticipatory behavior occurred to avoid slipping of the handle due to the emergent impact force. In manipulation tasks involving lifting objects of different weights, several experiments have demonstrated that humans predictively scale their lift-grip force according to their expectation of the object's weight [108]. The expected object weight may derive from internal models built for the object based on its mechanical properties or prior experience [109]. An extension of existing research is needed to consider the effect of correct and incorrect anticipation of force interaction during the execution of a force-based task. This finds relevance in the force-based interaction between a human and an autonomous agent over a shared haptic-enabled interface. Consider a scenario where a human driver and an advanced driving assistance system (ADAS) are jointly controlling a vehicle using haptic feedback on a steering wheel. A goal conflict between the driver and the ADAS can lead to sudden, unexpected haptic forces being applied by the ADAS on the steering wheel, which may affect the driver's response and compromise driving safety.

The goal of this chapter is to investigate the characteristics and effects of force anticipation uncertainty on human motor control in force-based interactions. To do so, a novel experimental study is designed and conducted to investigate human motion and force responses to a simple load pushing task in both expected and unexpected conditions. The hypotheses are that incorrect anticipation will lead to reduced task performance whereas when correct anticipation is sustained, task performance would be improved. Understanding how internal predictive models interact with anticipatory behavior and influence human motion are crucial to the

human-centered design of haptic shared autonomy systems.

This chapter is organized as follows: the experimentation and analysis methods are described in Section 3.2. The experiment results are presented and discussed in Sections 3.3 and 3.4, while concluding remarks are presented in Section 3.5. The work in this chapter was summarized in [22].

3.2 Experimental Design

3.2.1 Participants

Ten participants (9 males) participated in the study (age: 25.8 ± 2.5 years; height: 172.5 ± 5.3cm; mass: 70.6 ± 12.2kg). Data from one male participant who did not perform the tasks within the specified time period were excluded from the analysis. Participants with limited upper limb function due to injury, pre-existing condition, or disease were excluded from this study.

3.2.2 Experimental Setup and Task Description

With the participant seated in the experimental setup (as shown in Fig. 3.1), they performed a pushing task using their dominant arm. The handling plate contacted the loading plate through a uni-axial load cell (LCM300; FUTEK, CA) that was attached to the loading plate. The load cell measures the contact force as the handling plate pushes against the loading plate during the task. The participant pushed the handling plate directly, to move both plates forward along low-friction linear sliders (SRS15GMU; THK, Japan) until they come into contact with rubber stoppers. The initial positions of the loading and handling plates were established on the test bench using rubber stoppers. The loading plate was connected to different

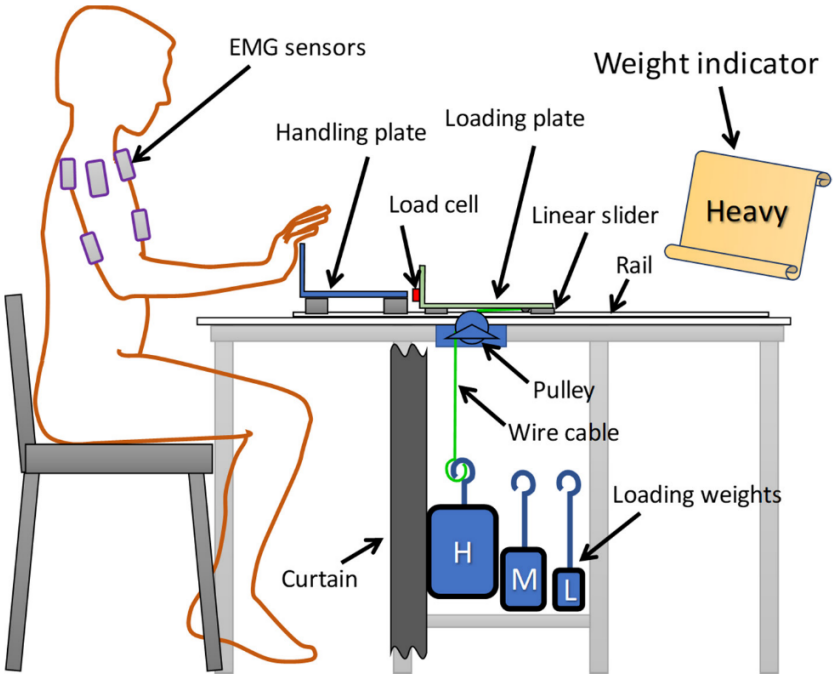

Figure 3.1: Experimental configurations of pushing task with a test-bench.

weights via a cable attached to a fixed pulley in order to establish the workload in a particular pushing trial. Loads were selected evenly along a log10 scale and included Heavy (5kg), Medium (1kg) and Light (0.2kg). A black curtain a set up to prevent participants from seeing the weights on the loading plate.

Linear sliders with low friction allowed the handling plate to slide easily. Because the handling plate was separated from the loading plate, if a participant pushed too hard anticipating a heavy workload, the displacement overshoot of the loading plate could not be corrected. Thus, undershooting was not included in the outcome of the loading plate displacement, and only pushing was possible.

3.2.3 Experimental Procedure

Upon arrival to the study, participants signed the IRB-approved informed consent form. The experiment comprised three sessions: *training* session (14 trials x 3

workload conditions = 42 trials), *checking* (2 trials x 3 workload conditions = 6 trials) and *testing* sessions (15 trials) in this order. The experimenter informed the participant of the type of workload prior to each trial, i.e. Heavy, Medium, or Light on the board display. A 3-s count-down was provided leading up to each pushing task. After the countdown reached "start", the participant was asked to immediately push the handle plate quickly and accurately with his/her hand. The instructions were to push the handling plate 10 cm in under one second while keeping the hand in contact with the plate. Breaks of 3–5 minutes were provided to the participant between each session.

The training and checking sessions were designed to calibrate the workload anticipation of the participants. In the *training* session, participants performed 14 pushing tasks with each workload setup and were informed of the correct workload before each trial. This was designed to familiarize participants with the workloads and to train their corresponding motion and force responses. Next, the participant performed six trials on the *checking* session with informed workloads matching the actual workloads. A participant was considered "trained" if they completed four out of six trials within 1 second with an error less than 2 cm for each workload condition in the checking trials. Additionally, the participant also verbally expressed that they were familiar with each workload. If a participant was unable to complete the checking session accurately, more training sessions were held until the participant met the requirement.

The *testing* session involved the participants performing 15 trials of the pushing task while the informed workload may or may not have reflected the actual workload. It was explained to participants that both the correct and incorrect information would be displayed during the test, but that they should rely on the displayed information. The sequencing of the actual workload and the matching of

Trial Case	Actual	Informed	Condition
LL	Light	Light	Correct
LM	Light	Medium	Over
LH	Light	Heavy	Over
ML	Medium	Light	Under
MM	Medium	Medium	Correct
MH	Medium	Heavy	Over
HL	Heavy	Light	Under
HM	Heavy	Medium	Under
HH	Heavy	Heavy	Correct

Table 3.1: Possible cases of the actual and informed workload in the experiment

the informed workload were both random. The 15 trials included 3 mismatching trials related to over-anticipation (i.e., the informed workload was greater than the actual workload) and 2 mismatching trials related to under-anticipation. Table 3.1 presents nine examples of the actual and informed workload setups experienced by participants during the testing session. The trials could be categorized into correct anticipation, under-anticipation, and over-anticipation. Our experiment required the handling plate displacement from the push to be 10 cm. With reference to this requirement, a trial may fall into the categories of "acceptable," "overshoot," and "undershoot." Specifically, the "maximum displacement" of each trial was normalized with respect to the average displacement in the "MM" trials for each participant. The performance of a trial was "acceptable" if the normalized displacement was within the range of 80%–120%. Displacement above 120% and under 80% was considered to be "overshoot" and "undershoot," respectively.

3.2.4 Data Collection

Wireless surface electromyography (sEMG) sensors were used to monitor the electrical activities of the relevant muscles on the participant's upper extremities. Our setup consisted of 14 channels of Delsys Trigno Avanti EMG sensors (Delsys, MA) attached to the anterior, middle, and posterior deltoid, biceps, triceps, brachioradialis, and trapezius muscles of both the left and right upper extremities. The signals were sampled at 1,111Hz using Delsys EMGWorks Acquisition Software (Delsys, MA). The sEMG recordings were normalized by the peak contraction value for each muscle from the maximal voluntary contraction (MVC) test [110]. A motion capture system (VICON Vero, 10 cameras) was used to track the arm and upper body motions of the participants at 100Hz. The pushing force was measured using a uni-axial load cell (LCM300, FUTEK, CA) at 1,111Hz. All data channels were synchronized together.

3.2.5 Data and Statistical Analysis

All recorded data were analyzed and processed using MATLAB (MathWorks, MA). The raw EMG signal was high-pass filtered at 35 Hz (second-order, zero-lag Butterworth filter), DC offset, rectified, and low-pass filtered at 40 Hz (second-order, zero-lag Butterworth filter), then resampled at 1,000 Hz [111]. Force and handling plate displacement data were resampled at 1,000 Hz and low-pass filtered at 40 Hz (second-order, zero-lag Butterworth filter). Figure 3.2 displays the synchronized displacement, force, and sEMG data for a single pushing trial from a representative participant. When the pushing task was performed, the anterior deltoid muscle, which is the dominant muscle involved in shoulder elevation, was the only muscle that demonstrated an initial spike in its EMG signal before the onset of force.

Therefore, the EMG signals from other muscles were excluded from our analysis. A composite plot of force, displacement, and EMG for a single trial of the pushing task is shown in Figure 3.3. Seven landmark points were identified for force anticipation analysis, which included EMG onset, force onset, displacement onset, the first force peak, the minimal point of the first force peak, maximum force, and maximum displacement. Since the EMG onset can be interpreted as the start of actuation, the lead time is expressed as the time interval between EMG onset and displacement onset. Also, the pushing task is completed when the loading plate reaches the maximum displacement. Accordingly, the task duration is defined as the interval from the onset of the EMG to the instant of maximum displacement. The force onset time was defined as the first instant the force exceeded 3 N and continuously increased.

The first and second peak forces were measured as local maxima occurring after onset. Displacement onset time was defined as the time after force onset, at which the loading plate displaced more than 5 mm from its initial position. To identify EMG onset time, a threshold was set equal to 1.2 times the maximum resting EMG value (from the beginning to 0.3 s prior to the instant of force onset). The EMG onset time was defined as the first instant the EMG signal exceeded this value. Initial velocity of the handling plate was calculated as the average velocity obtained from a displacement between the 5 and 10 mm marks. Our data preprocessing first normalized the EMG signals of a participant with respect to the MVC and the EMG magnitudes recorded in the "MM" trial of each participant (Table 3.1).

The time delays were calculated using the timings of the EMG onset, force onset, and displacement onset. Initial analyses compared force and displacement variables using ANOVA and Bonferroni-corrected post hoc t-tests in order to determine the main effects of actual versus informed workload. In the next step, the trials were

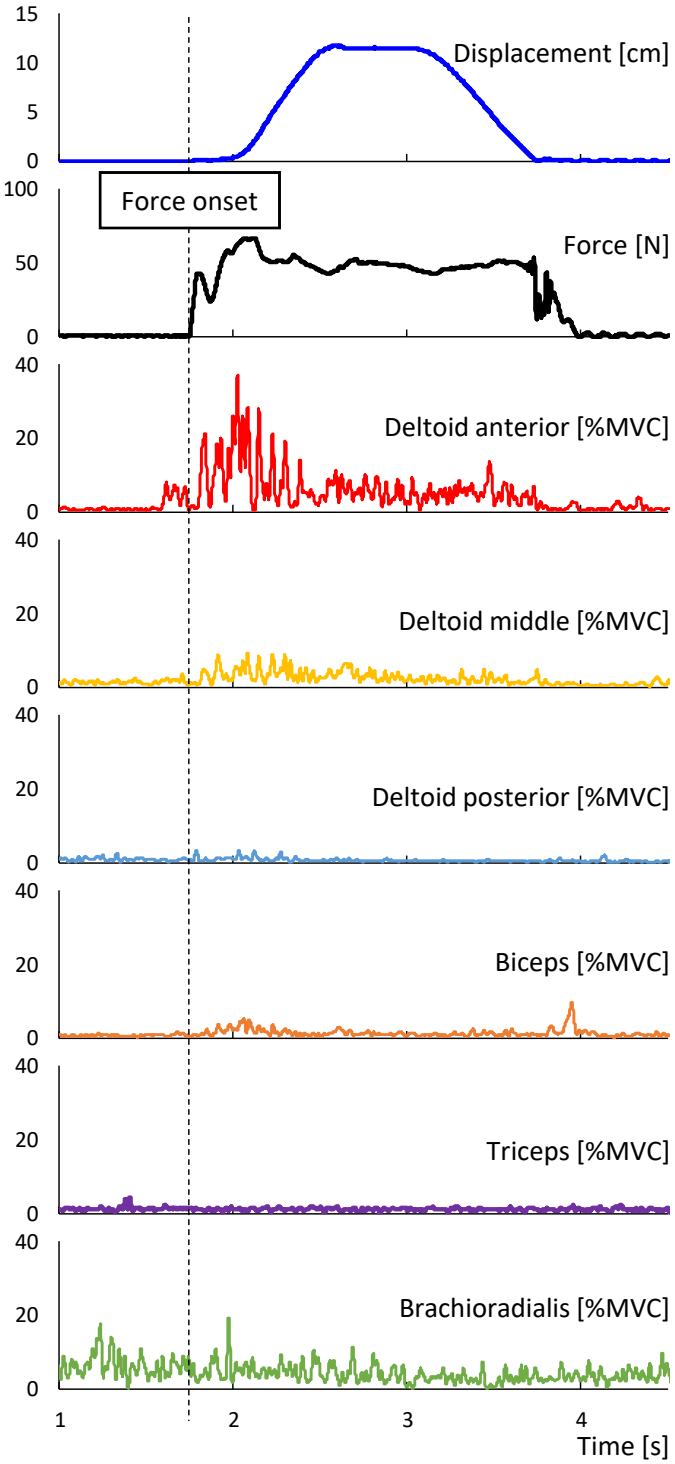

Figure 3.2: Recorded displacement and force data along with EMG signals from the deltoid (anterior, middle, and posterior), biceps, triceps, and brachioradialis muscles for a single pushing trial.

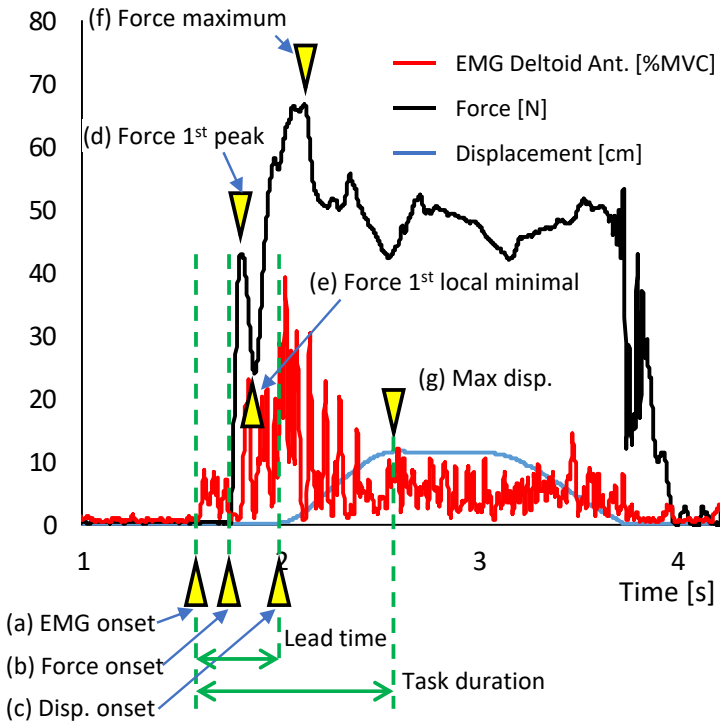

Figure 3.3: Force, displacement, and EMG data for a single trial, with the features for force anticipation analysis.

classified into feedforward-dominant and feedback-dominant cases based on the relative time delays between the force and displacement. To determine whether trials classified as feedforward-dominant were different from those classified as feedback-dominant, a Student's t-test was used to compare the first peak force, initial velocity, lead time, and task duration. In addition, to determine whether overshoot trials were different than acceptable trials, a Student's t-test was used to compare the normalized maximum first peak EMG, normalized integrated first peak EMG, first peak force, and initial velocity. Finally, to evaluate the effect of perceived weight from the preceding trial on performance of the current trial, one-way ANOVA was used to compare time delays and pushing performance for HH trials that followed various preceding conditions. Because of the limited sample size, the effect size (Cohen's d or η^2 , as appropriate) for the analyses were also calculated for differences.

3.3 Results

Accuracy of Motion Responses

When the correct information was provided to participants, nearly 80% of them were able to accurately hit the target distance of 10 cm, with the remaining 20% overshooting. The distribution was similar for cases of underanticipation (when incorrectly Light workloads were displayed). However, when incorrectly Heavy workloads were displayed (overanticipation trials), approximately 80% participants overshot the target. Due to the design of the task, undershooting was not possible. Figure 3.4 shows the distribution of participant responses with correct, under-, and overanticipation of task workload by their normalized displacement. Significant informed/actual workload interactions were observed in the displacement, with actual Light and Medium workloads being most affected by informed workload.

Figure 3.5 shows the mean and standard deviation of the normalized maximum displacement of the handling plate across all nine trial cases. When the actual workload was Light, the responses to the various informed workload cases mostly resulted in an overshoot. And, with Light workloads, the normalized maximum displacement increased with the workload anticipation ($p < .001$). When the actual workload was Medium, overshoot only occurred with a Heavy anticipated workload case, and displacements were different between ML and MM versus MH cases ($p < .037$). When the actual workload was Heavy, the normalized maximum displacement of all the trials remained within the acceptable error range, i.e. no overshoot was observed (see Figure 3.5). The task performance with heavier actual workloads was more consistent than with lighter workloads. Specifically, the standard deviations for HL, HM, HH were ± 9.97, ± 14.08, ± 17.64, respectively, while the standard deviations for LL, LM, LH is ± 31.15, ± 57.35, ± 79.49, respectively.

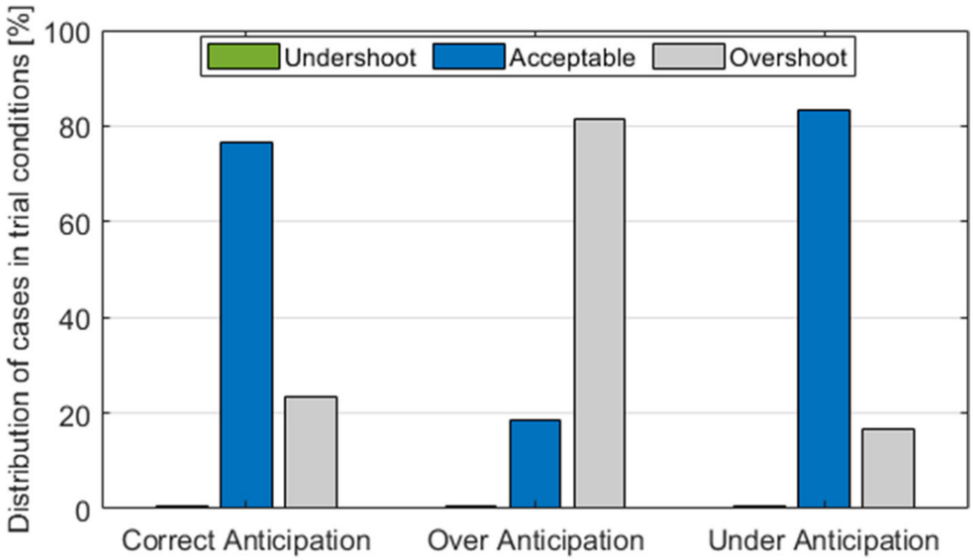

Figure 3.4: Distribution of displacement response across the three trial conditions: correct, over-, and underanticipation, in percentages.

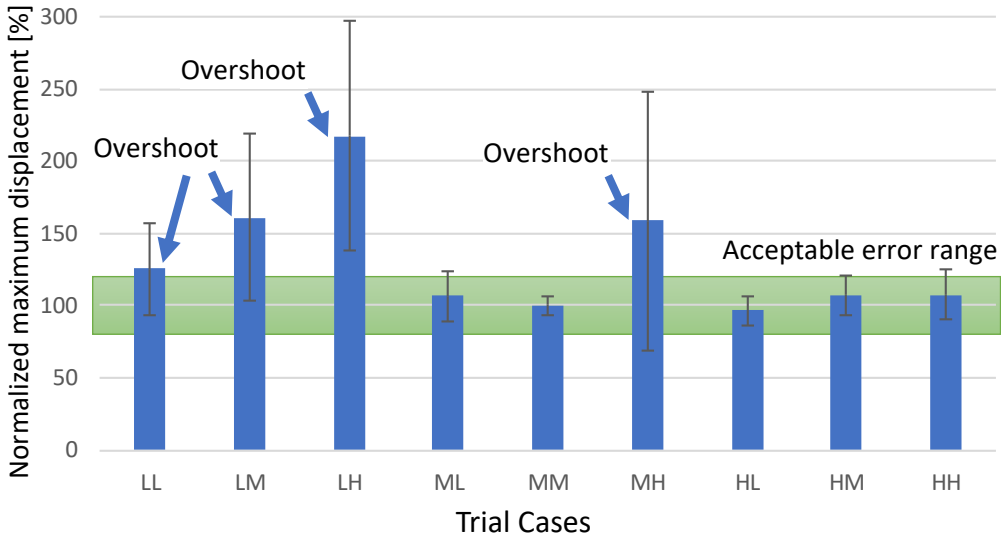

Figure 3.5: Mean and (error bars) standard deviation of the normalized maximum displacement of the handling plate with a description of the acceptable error range of $\pm 20\%$

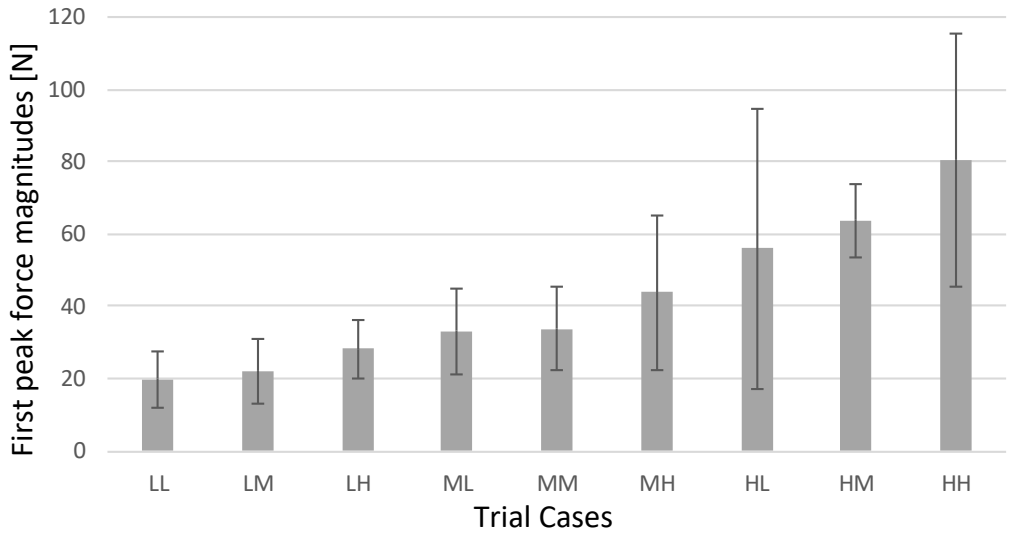

Figure 3.6: Mean and standard deviation of the first peak force magnitudes across all nine trial cases.

Effects of Informed Anticipation

By comparing the first force peak between two conditions, one can observe the effects of workload anticipation uncertainty. In general, the force profiles had a single pulse in the cases of overanticipation (LM, LH, and MH) and two pulses in the cases of underanticipation. Figure 3.6 shows the mean and standard deviation of the first force peak value of the force profiles across all the participants, for each trial case. Overall, the first force peak value increased as a function of both the actual and informed workload. However, the first force peak was only significantly different between informed conditions within the Light actual workload cases ($p = .028$, $\eta^2 = .13$). Light actual workloads had significantly lower first peak forces than Heavy workloads (33.9 (19.7) N vs. 50.0 (41.2) N, $p = .04$ from post hoc Bonferroni-corrected t-test). The effects of the informed workload were also reflected in the initial velocity of loading plate and task durations. Significant differences in initial velocity due to informed workload magnitudes were only observed in Light actual workload cases ($p = .046$, $\eta^2 = .12$). Task durations were significantly affected by

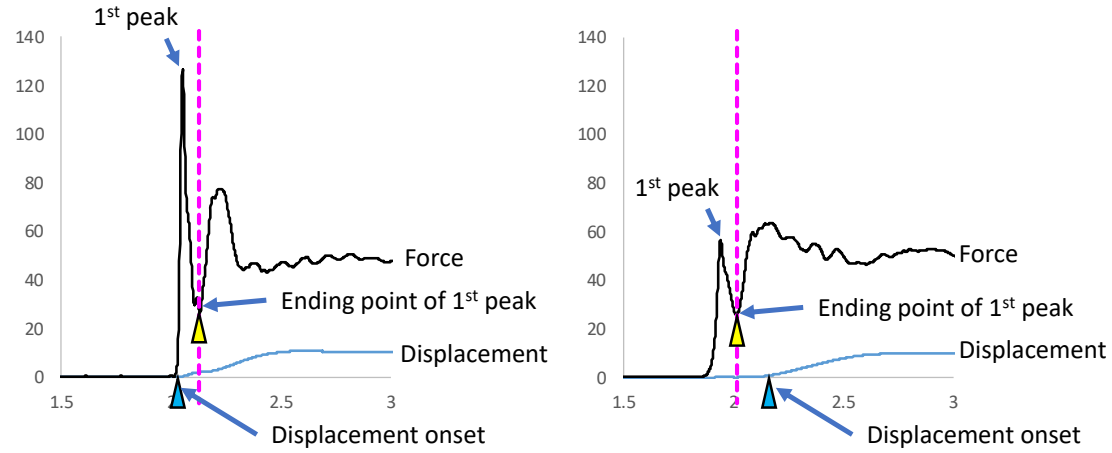

Figure 3.7: Force and displacement profiles in the first peak dominant (feedforward-dominant) cases (left) and the secondary force dominant (feedback-dominant) cases (right) for Heavy trials.

the actual, but not the informed workloads ($p < .001$, $\eta^2 = .14$). Specifically, Heavy actual workloads took longer to move than Light or Medium ones ($p < .001$).

Feedforward- and Feedback-Dominant Controls

By comparing the relative time delays between the first minimal point and the displacement onset, responses were classified as either feedforward or feedback-driven. Figure 3.7 presents the two types of force responses observed among participants when the actual workload was Heavy. The displacement onset (point c in Figure 3.3) may occur before or after the minimal point of the first force peak when comparing the displacement profile with the force profile. The end of the first peak force pulse may indicate that the participant has switched from feedforward to feedback force control, based on the perceived workload being heavier than anticipated. This is an important feature that may indicate whether a participant's force response is more or less dependent on the informed workload. Accordingly, it is proposed that feedforward dominant cases are those where the plate moves before the minimal point of the first peak force, whereas feedback dominant cases are those where the plate

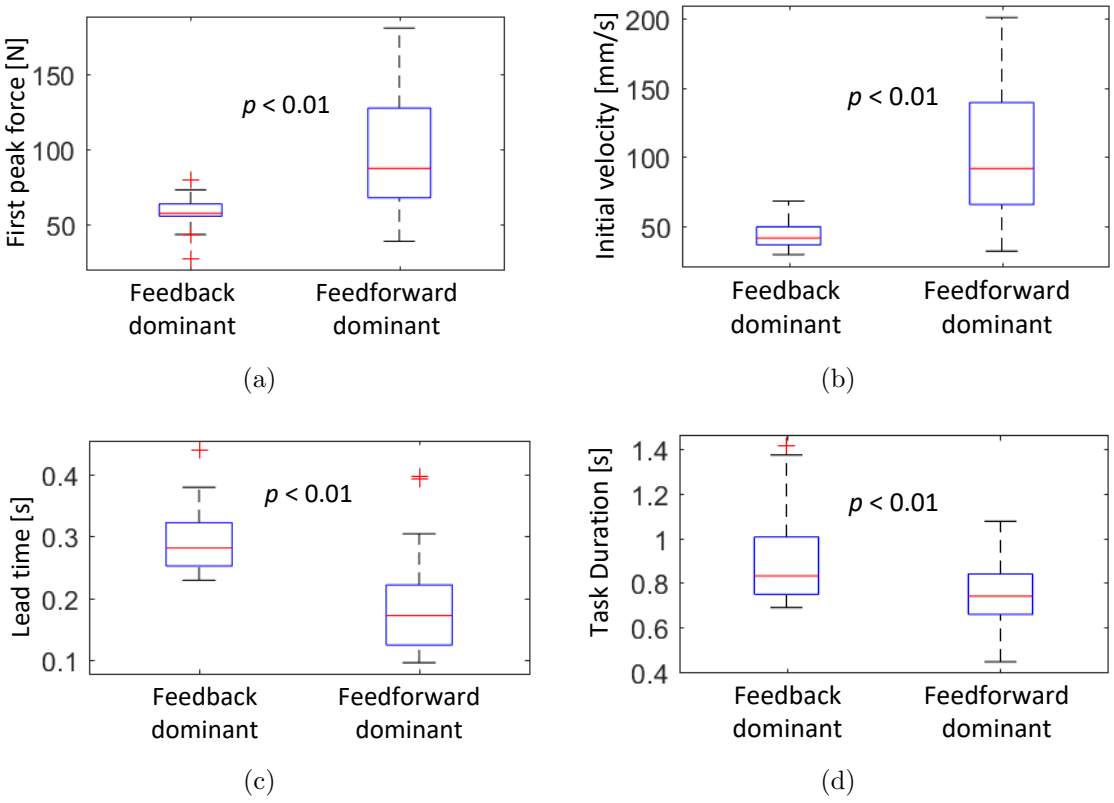

Figure 3.8: Comparison of the effect of feedforward/feedback controls on the first peak force, initial velocity, lead time, and task duration for Heavy load trial cases. a) First peak force; b) Initial velocity; c) Lead time; d) Task duration.

does not move until the first peak force has ended.

Based on this classification scheme, 44% of trials were classified as feedforward-dominant and 56% were classified as feedback-dominant with the Heavy actual workload cases. Feedback-dominant behaviors were not observed with the Light or Medium actual workload cases. Next, the force, motion, and EMG responses were compared between feedforward- and feedback-dominant responses. The results showed that, for the trials of Heavy actual workload, the feedforward-dominant responses had significantly higher first force pulse amplitude ($p < .001$, $d = 1.43$) and initial velocity ($p < .001$, $d = 1.64$) versus feedback-dominant responses (Figure 3.8). They also had significantly shorter lead time (the time from EMG onset

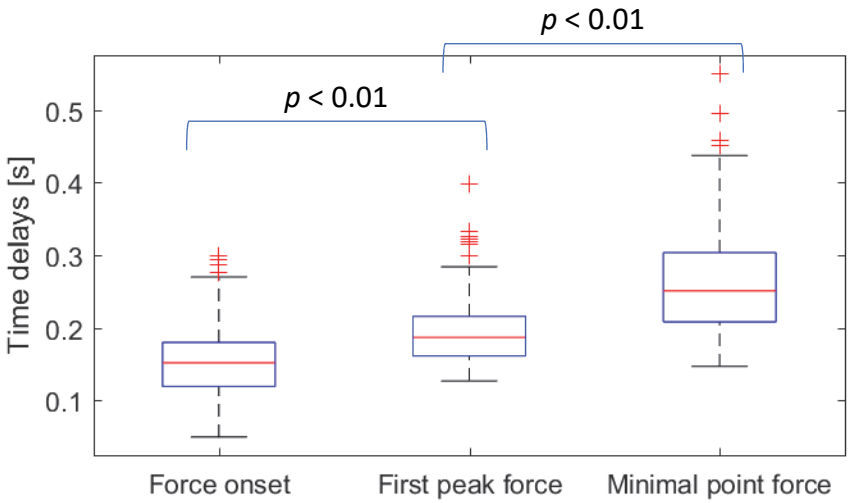

Figure 3.9: Time delays from EMG onset to the force onset, the first peak force, and the minimal point of force.

to displacement displacement onset) and task duration ($p < .001$, $d = 1.34$, and $p < .01$, $d = .86$, respectively). All responses, regardless of whether they were classified as feedforward or feedback, had similar time delays. These include time delays of (1) the force onset (156 ± 48 ms), (2) the first peak force (195 ± 48 ms), and (3) the first minimal point (265 ± 79 ms) from EMG onset. Each of these time delays were significantly different from each other (Figure 3.9) and occurred in a fixed sequence. The time duration of the first peak force (109 ± 63 ms) was an invariant parameter in the pushing task across all subjects and conditions, and was not different between trials classified as feedback or feedforward.

Effects on EMG Responses

EMG responses differed both between feed-forward- and feedback-dominant responses and as a function of overshoot. Shown in Figure 3.3, the EMG response of the anterior deltoid muscle typically had two bursts, with the first corresponding to the first peak of force response and feedforward control, based on the anticipated workload. With the normalized EMG data, it was observed that: compared to the

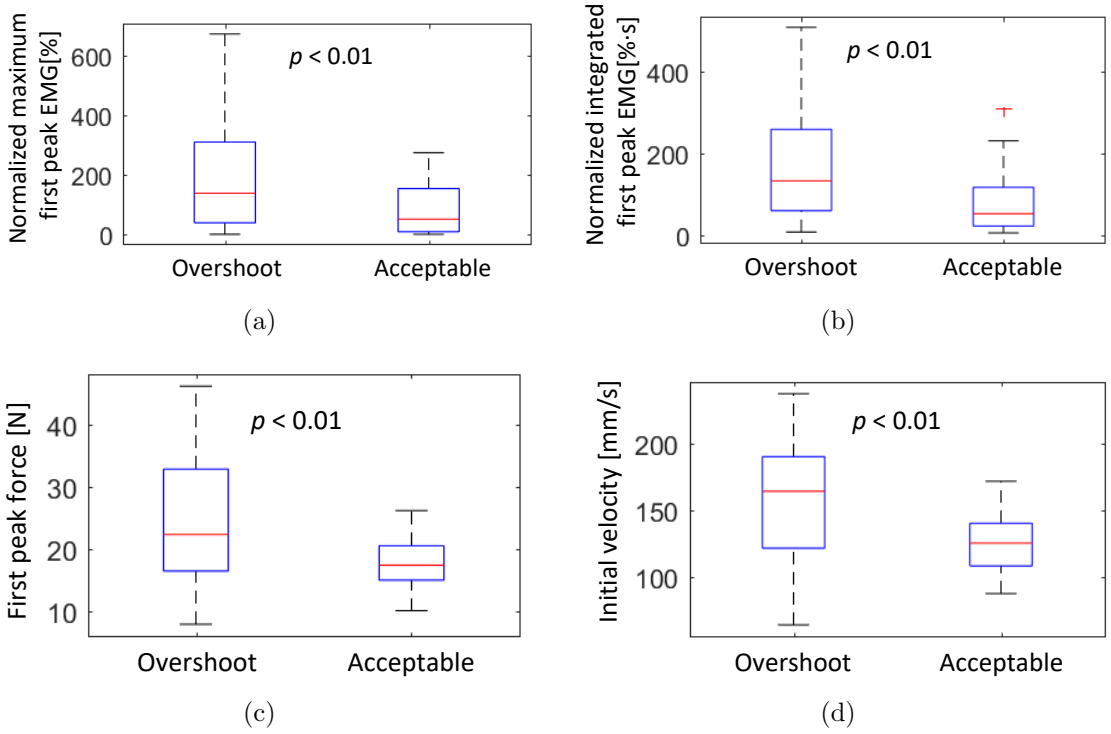

Figure 3.10: Comparison of maximum value and time integrated value of normalized initial burst EMG, first peak force, and initial velocity based on overshoot/acceptable task results in Light load trials. a) Maximum value of normalized initial burst of EMG signal; b) Time integrated value of normalized initial burst of EMG signal; c) First peak force; d) Initial velocity.

trials of acceptable motion accuracy, the trials of motion overshoot had significantly larger values for (1) the first peak value of the normalized EMG signal ($p = .005$, $d = .72$, Figure 3.10(a)) and (2) the time integrated value of the initial burst of normalized EMG signal ($p = .006$, $d = .72$, Figure 3.10(b)). These observations are consistent with the significant differences found by comparing the first peak force ($p = .001$, $d = .83$) and initial velocity ($p = .002$, $d = .83$) between overshoot and acceptable motion accuracy (Figure 3.10(c–d)).

Effect of Preceding Trial

HH performance was moderately affected by the condition of the trial immediately preceding the HH task. Actual workload in preceding trials affected first peak force ($p = .077$, $\eta^2 = .18$), initial velocity ($p = .057$, $\eta^2 = .20$), lead time ($p = .005$, $\eta^2 = .33$), and task duration ($p = .029$, $\eta^2 = .24$; Figure 3.11). Post hoc t-tests showed that Light actual workloads significantly increased the lead time of the current HH trial ($p < .01$). Furthermore, a preceding trial of Light workload increased the task duration compared to a preceding Heavy workload ($p < .05$). We found no significant effect of preceding trials of Light versus Medium workload.

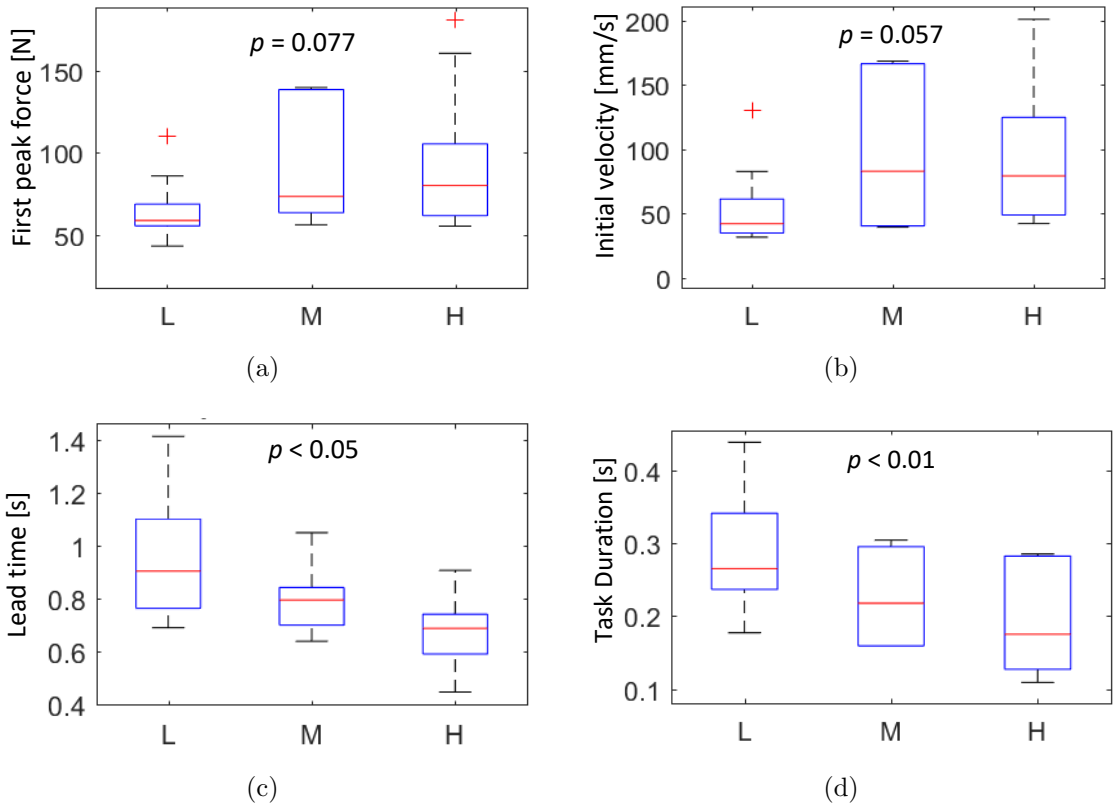

Figure 3.11: Comparing the effect of preceding trial workload on the first peak force, initial velocity, lead time, and task duration of current trials of Heavy workload. a) First peak force; b) Initial velocity; c) Lead time; d) Task duration.

3.4 Discussion

This study compared human motion and force responses in a simple load pushing task under workload anticipation uncertainty. Because pushing-only tasks do not necessarily require hand deceleration to manage position control, they could produce unique behaviors, such as displacement overshoot. The results show that when participants had the correct anticipation of the workload, they completed the task more accurately compared to when they had an incorrect anticipation (especially in over-anticipation cases) of the workload. This trend is consistent in the force and EMG response as well. Both the first peak values of the force and normalized EMG magnitude were significantly higher in these overshoot cases compared to the acceptable cases. This suggests that participants trusted the informed workload and responded based on their pre-calibrated internal models of the task and workload [56].

To investigate further, the extracted response features were used to classify the responses into feedforward-dominant and feedback-dominant control based on the phases of the responses. This classification is consistent with existing studies in human motor control [56,112]. The results show that feedback-dominant control was used more frequently when the actual workload was Heavy, while only feedforward-dominant control was used (and usually sufficient) when the actual workload was Light or Medium. It appeared that despite being properly informed of the actual workload to expect, participants tended to underestimate the workload for Heavy cases. The first peak force in the heavy trials were less than 50N (approximately the actual load being moved). Because of this, a second force pulse was often required in a feedback manner to overcome the perceived resistance and initiate movement of the handling and loading plates.

In evaluating response timings, it was found that the time delays for force response is consistent with the time delays of feedback control (about 100ms) in the task of balancing in the presence of floor perturbations [111]. The fast response of force and tactile feedback is especially advantageous in continuous coupled co-driving between a human and an autonomous system. The fast feedback loop allows for tight coupling and information exchange [67, 113]. This is in contrast to other feedback modalities such as visual and auditory feedback which are reported to be much slower (0.18s and 0.3-0.4s respectively) in ideal conditions [114]. However, one challenge with the haptic feedback channel is the limited bandwidth in communicating sufficient information to elicit the right response [69]. As previously highlighted in Section 3.1, unexpected forces may occur due to conflicts in intent between driver and assisted driving system [76]. Our results in this chapter suggest that these unexpected forces may result in high feedback forces from the human driver to resist the unanticipated maneuver, leading to increased physical workload, degraded driving performance and vehicle safety. A possible solution is to improve the transparency (or predictability) of the system so that drivers have a better understanding of the system's intent, allowing them to anticipate and interpret interaction haptic forces.

The limitations of the study must also be acknowledged. The sample was small and skewed heavily toward men. It is possible that the results are not generalizable to other populations, especially those with neuromotor impairments. A small sample size made it difficult to detect all of the effects of trial order and anticipation. However, performing additional conditions would have resulted in an excessively long experimental protocol. Despite the small number of participants, the repeated-measures design resulted in a study that was adequately powered to detect differences in our dependent variables. Additionally, the measured effect sizes were generally large (Cohen's $d > .5$, $\eta^2 > .15$), supporting the significance of the

findings [115–117].

3.5 Chapter Summary

This study investigated the effects of correct and incorrect force anticipation on the human performance of a simple pushing task. The main finding of the study is that task anticipation, including expected workload, influences human control strategy, particularly during force-based interactions. Specifically, the results show that the first peak of the pushing force increases consistently with anticipated workload. This suggests that with proper calibration of their internal model, humans can accurately anticipate and predict force interactions. Also, overshooting was observed in the case of over-anticipation (i.e., when the anticipated workload was greater than the actual workload). Participants used feedforward-dominant control to achieve the rapid task with Heavy workloads. In addition, when Heavy trials were preceded by Light trials, participants tended to perform slower and with initially lower force.

These findings reveal how force anticipation affects task performance in motion and force control, and how the workload of preceding tasks may influence the performance of the current task. These considerations are crucial in understanding the important role of transparency and anticipation in force-based interaction, such as in haptic shared autonomy. The following chapters incorporate the findings from this user study as design considerations for haptic shared autonomy. Specifically, Chapter 4 discusses how to develop a more transparent and intuitive shared autonomy system for assisted driving by using a multimodal interface approach.

Chapter 4

SocNavAssist: Multimodal Shared Autonomy for Social Navigation Assistance of Mobile Telepresence Robots

4.1 Introduction

We established in the previous chapter that the level of system transparency, i.e. the ability to understand and anticipate the force cues in shared interaction, is crucial to maintaining appropriate human responses and overall performance. This chapter, therefore, examines how to design a human-centered haptic shared autonomy system that enhances system transparency and cooperation between the human and the assistive agent.

We consider the problem of navigation assistance in this chapter within the context of remote driving of mobile telepresence robots (MTR). Mobile telepresence

robots enable people to extend their presence to remote locations and provide new opportunities for remote participation. Recent years have seen an increase in adoption of these robots throughout various spheres of life. Today, MTRs make it possible for people to remotely participate in corporate meetings, academic conferences, college classes, elder care visits, and even medical appointments [5, 78]. Advances in immersive technologies (e.g. Virtual Reality (VR), Head-mounted displays), as well as sensing and computing capabilities applied to telepresence robots continue to improve their ease of use in navigation and overall user experience [118].

However, one of the challenges with MTRs is navigating around humans in cluttered environments without having a clear picture of the surroundings, due to their limited situational awareness and narrow field of view [78]. As a result, it reduces their ability to engage in non-navigational activities, such as interacting with others or exploring the remote area. One way to address this challenge is to provide fully autonomous features to handle the low-level navigation task. Considerable work has been done on autonomous socially-aware navigation algorithms, such as robust pedestrian motion prediction and tracking and dynamic collision avoidance [79,119]. However, these fully autonomous systems are yet to be fully reliable, especially in safety or time-critical scenarios and may require human intervention in edge cases. Moreover, research suggests that MTR operators may prefer to remain in the control loop for reasons such as a sense of agency, control, and a limited level of trust in autonomy [5,6]. Shared autonomy, which is a middle ground between full autonomy and manual control, could, therefore, prove to be a promising approach for providing navigation assistance to human operators of MTRs [6].

Studies have shown that haptic shared autonomy in assisted navigation improves driving performance [10], as well as situation awareness [8]. Yet, these systems struggle with the issue of conflict between the human and the autonomous agent often

resulting from a lack of alignment of shared intent or control strategy among cooperating agents [11]. One way to mitigate this intent misalignment is by improving system transparency, i.e. how well the human operator can understand the intent and anticipate the actions of the autonomous agent [66]. The shared haptic channel is a natural option for communicating intent as it leads to fast, reflexive responses. However, due to limited bandwidth, it may only be applicable in situations where the task is clear and unambiguous, requiring less descriptive information [67, 120]. As a result, researchers have favored visualization to augment haptic cues in intent communication. While the visual channel is slower in processing stimuli than the haptic channel, its trade-off is more bandwidth to convey richer, contextual information [69]. Thus, several works have proposed using visualization to communicate the intent of the autonomous agent in human-automation interaction. Augmented reality visualization has been applied for wheelchair navigation assistance [61], assisted telemanipulation to communicate the agent's estimate of the desired goal [70]. Recent studies have explored the benefits of combining both haptic and visual information in a multi-modal fashion [68, 72].

In this chapter, we present a multimodal shared autonomy approach for social navigation assistance. Firstly, we present a method for socially-aware navigation assistance using a modified reciprocal velocity obstacle (RVO) approach that generates safe control signals for the operator when navigating a telepresence robot in dynamic environments. Consequently, we implement different modes of communicating the generated control signals as guidance cues including haptic forces, visual feedback, and a combination of both in a multimodal manner. We further conduct a user study experiment to investigate the effects of our multimodal approach in comparison with haptic or visual assistance alone on navigation safety, system transparency and cooperation as well as user preference.

This chapter is organized as follows: the socially-aware navigation assistance system design is described in Section 4.2 and the user study design is presented in Section 4.3. Results from the user study experiment are presented and discussed in Sections 4.4 and 4.5, while concluding remarks are presented in Section 4.6. The work in this chapter was summarized in [23, 24].

4.2 System Design

Our socially-aware navigation assistance approach incorporates three key elements: (1) socially-aware collision avoidance via reciprocal velocity obstacles (SA-RVO), (2) guidance using haptic forces, and (3) guidance using visual cues.

4.2.1 SA-RVO: Socially-aware collision avoidance via reciprocal velocity obstacles

To enable effective navigation assistance in dynamic environments, it is crucial to generate safe control signals that can guide human operators towards socially acceptable and collision-free movements. We base our approach on the reciprocal velocity obstacle (RVO) method [86]. RVO and its variants have been successfully implemented in multi-robot systems and autonomous socially-aware navigation [121]. RVO is an extension of the classic velocity obstacle method of dynamic collision avoidance, which guarantees collision- and oscillation-free motions in the presence of moving obstacles (such as other robot agents). This is accomplished by planning motions in the 2D velocity space of the robot and surrounding static or dynamic obstacles. Specifically, the robot A measures the relative velocities of other agents (i.e. pedestrian B) within its vicinity and constructs a collision cone ($RVO_{A|B}$) which is a region in the velocity space that would lead to a collision with the other

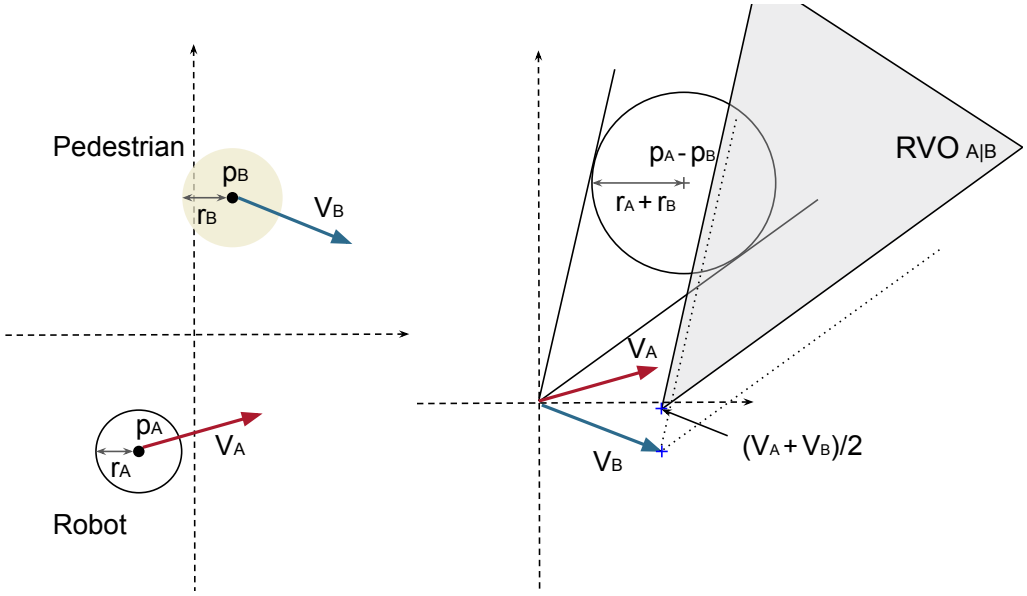

Figure 4.1: Schematic describing the reciprocal velocity obstacles (RVO) formulation

agent [86] (Fig. 4.1).

In the original RVO formulation, the optimal velocity is calculated as the candidate velocity within the space of collision-free velocities (i.e. $v \notin RVO_{A|B}$) that minimizes the distance to the maximum allowable velocity to the goal as follows:

$$v_A^{optimal}(t) = \underset{v \notin RVO_{A|B}}{\arg\min} \|v(t) - v^{goal}(t)\|^2 \tag{4.1}$$

where $v^{goal}(t)$ is the maximum velocity to the goal location [86].

We modify the search for optimum velocity by taking into account additional factors for navigation assistance, resulting in a weighted sum of objective functions:

$$v_A^{optimal}(t) = \underset{v \notin RVO_{A|B}}{\arg\min} \sum_{i=1}^{n} w_i G_i(t) \tag{4.2}$$

where w_i and G_i are the ith weight and objective function respectively. In this work, we consider three objective functions ($n = 3$), with $G_1 = \|v(t) - v_A^{pref}(t)\|^2$ where v_A^{pref} represents the current input velocity command from the human operator.

This objective looks for a velocity that is as close as possible to the operator's commanded velocity, preserving the original control intent of the operator. The second objective, $G_2 = \|v(t) - v_A^{optimal}(t-1)\|^2$, controls for change in consecutive optimal velocities to enable smooth guidance cues to the operator. Finally, the third objective compensates for goal-directed motion as in equation 4.1, $G_3 = \|v(t) - v^{goal}(t)\|^2$. This requires that the autonomous system is aware of the operator's goal either explicitly or by inference [122]. For this study, we assume that the operator's goal location is known.

The RVO formulation only accounts for disc-shaped objects, therefore, we perform a static obstacle avoidance step as a preprocessing step to the RVO, in order to account for static obstacles in the environment such as walls and tables. Specifically, using velocity sampling, we filter out velocities that would lead to collision over a time horizon based on a pre-defined map of the environment. The resulting samples of 'statically' safe velocities is then fed into the SA-RVO to account for dynamic obstacles.

In addition, our proposed approach follows Truong et al. [121] by explicitly accounting for social proxemics constraints. Based on the proxemics theory proposed by Hall [83], an individual's interpersonal space can be divided into concentric circles, with the radius of the circles representing different levels of intimacy and comfort: intimate space (<0.45m), personal space (0.45-1.2m) and then social space (>1.2m). Hence, SA-RVO defines the collision cone for each pedestrian based on the radius of their personal space, thus taking into account their social constraints.

Furthermore, in addition to the proxemics constraints imposed on single pedestrians, we look at human group interactions and their corresponding social constraints. Human groups are detected and tracked based on the multi-model multiple hypothesis tracker (MHT) approach proposed by Linder and Arras [123]. The open-source

ROS implementation [1] was used in this study.

4.2.2 Guidance using Haptic forces

The haptic guidance mode generates appropriate haptic feedback cues on the haptic interface so that the operator's control input can be guided towards alignment with the optimal velocity command, $v_A^{optimal}(t)$, computed by SA-RVO. The haptic forces are computed as proportional to the error between $v_A^{optimal}(t)$ and v_A^{pref}, which is the current velocity command from the human operator:

$$F(t) = K_p(v_A^{optimal}(t) - v_A^{pref}(t)) \tag{4.3}$$

where K_p is the fixed haptic gain. This value regulates the level of haptic authority assigned to the autonomous agent. With a low haptic gain, the operator is able to override low haptic guidance forces easily, thereby retaining control. A high haptic gain, however, may make it difficult for the operator to counteract the haptic forces being generated, leaving final control to the autonomous agent [7].

4.2.3 Guidance using Visual cues

Visual feedback in mobile telepresence robots typically serves two purposes. It provides the operator with information about the remote environment in which the robot operates, and it also enables audio-visual social interaction with the remote individuals. However, existing studies have shown that augmented visualizations on the visual feedback display can be used to provide guidance cues [61, 69] and communicate the intent of the autonomous system to the human operator [60, 124].

In this study, we examine two visual cue designs. First, a visual trajectory trace is

[1] `https://github.com/spencer-project/spencer_people_tracking`

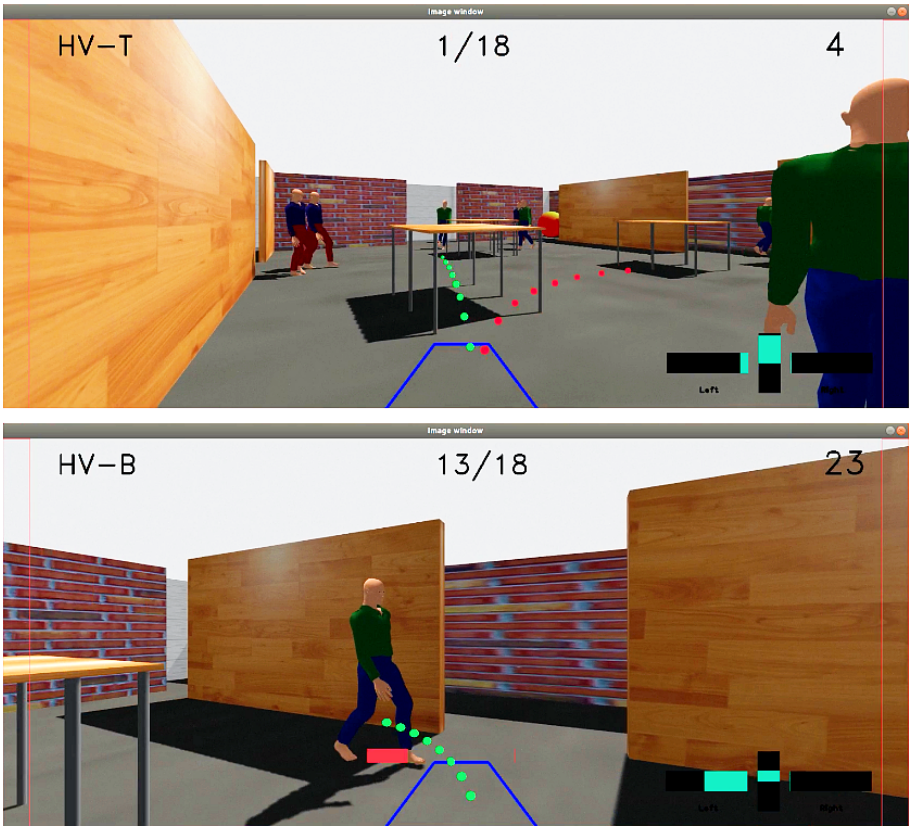

Figure 4.2: Illustration of the visual guidance cues. **Top**: visual guidance trajectory. **Bottom**: visual steering bars. In both designs, the green trajectory trace presents a feedback on the dynamics of the robot, while the guidance cues are in red. A projection of the robot's occupied space is in blue, and a speed indicator display is in aqua on the bottom right.

presented as an overlay to communicate the predicted future states of robot based on the instantaneous control input from the shared haptic interface as in [68]. Predicted trajectories are computed using a simple kinematics model of the differential drive robot, which propagates the current state by the control input. This helps the operator form an improved mental model of the robot dynamics.

Secondly, we seek to provide visual cues on the visual display to guide the operator towards the optimal control input computed by SA-RVO and consistent with the haptic guidance mode. To achieve this, we consider two visualization designs:

1. *Visual guidance trajectory*: Inspired by [68], we also present the visual guid-

ance cue as a visual trajectory trace as above. In contrast to [68] however, the predicted robot future states are computed based on the optimal control command computed by SA-RVO rather than the operator's control input. The result is a suggested path visualization that shows contextual information about the direction the autonomous agent suggests the operator to go. Note that we display the trajectory only when the difference between the operator's control input and the optimal control input exceeds a threshold, in order to avoid display clutter.

2. *Visual steering bars*: Instead of showing a suggested path, this approach presents steering magnitude bars on the left and right of the visual display (Fig. 4.2). They indicate how much the robot needs to be steered in order to align with SA-RVO's optimal control inputs. In this design, instantaneous steering corrections consistent with the haptic cues are communicated to the operator over the visual display. This provides the operator with limited information about the suggested future states and may be viewed as a visual representation of the haptic cues.

4.3 User Study Design

We conducted a user study with a within-subject repeated-measures design to compare the effects of multimodal navigation assistance with single-modality (haptic and visual) and no assistance cases, as a baseline, in terms of navigation safety, interface transparency and user preference in a social navigation task. The study design and procedure was duly approved by Worcester Polytechnic Institute's Institutional Review Board (IRB).

Our study hypotheses are as follows: First, we hypothesize that multimodal

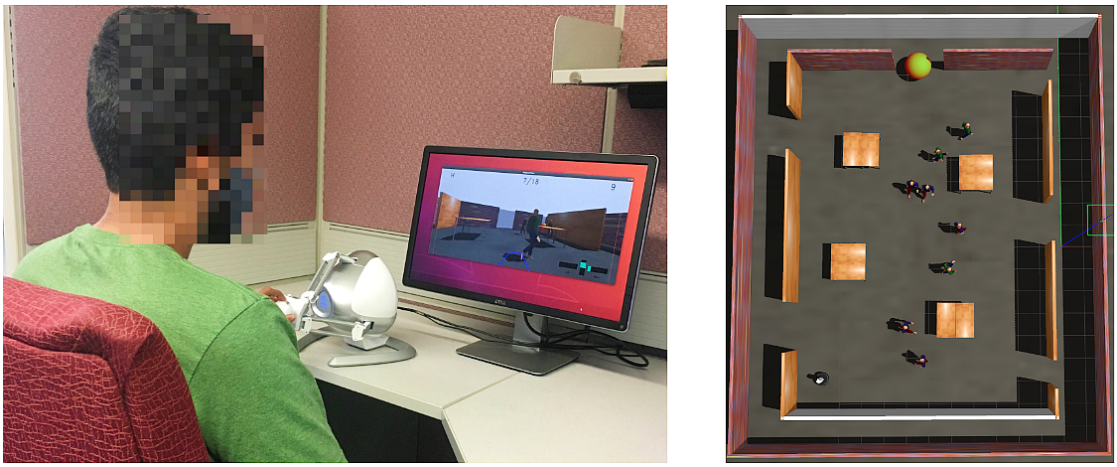

Figure 4.3: Simulated experiment setup. *Left:* Each participant controls a virtual wheeled robot using a haptic joystick with visual feedback from the forward-facing camera on the robot *Right:* Snapshot of the simulated social navigation task.

assistance will outperform both haptic and visual modalities alone in regards to navigation safety, system transparency and cooperation, and user preference (**H1**). Additionally, we anticipate that all guidance modes will outperform manual control in navigation safety and user preference when considered as a baseline condition (**H2**). Furthermore, we hypothesize that visual modality will lead to greater system transparency and cooperation than haptic modality (**H3**).

4.3.1 Participants

Fifteen (15) participants (7 males and 8 females; age: 25.3 ± 4.1) were recruited for the user study from the university student community. Twelve participants (80%) reported to have no prior experience with a haptic device. Seven stated that they had only 1-2 years of driving experience (47%), whereas 8 had more than three years of driving experience (53%). Based on self-reported gaming experience (gaming frequency, skill level and average gaming duration), we classified participants into two categories: non-gamer (6, 40%), gamer (9, 60%).

4.3.2 Experimental Setup

The user study was designed as a virtual social navigation task. Participants were asked to control a simulated differential drive mobile telepresence robot in a dynamic, human-populated virtual environment to navigate from start position in a hall to specified goal location in a safe and socially acceptable manner. The virtual mobile robot and the populated environment were simulated using Gazebo Simulator. Participants received visual feedback from a forward-facing camera mounted on the virtual mobile robot through a 24-inch computer monitor (see Fig. 4.3). The visual guidance methods were presented as a visual overlay on the camera display using OpenCV.

The virtual environment was modeled after a conference hall with tables and space for walking (see Fig. 4.3). Two different hall layouts were adopted and randomly applied based on table positions to prevent participants from memorizing the hall layout across trials. We modeled the virtual pedestrian motion using a Gazebo actor plugin[2][3] based on the social force model [85] to enable reactive navigation behavior to obstacles and the robot. Three pedestrian motion configurations were implemented in the study: (a) approach, (b) crossing, (c) random, to encompass a wide variety of real-life crowd navigation scenarios.

Human control inputs and haptic guidance forces were applied through a commercially available haptic-enabled device (Novint Falcon, Novint Technologies). To provide 2D control inputs (linear and angular velocity) for robot control, only two of the 3-DOFs on the haptic interface were mapped to the differential-drive robot controller using a position-velocity mapping.

[2] `https://github.com/robotics-upo/gazebo_sfm_plugin`
[3] `https://github.com/robotics-upo/lightsfm`

4.3.3 Evaluated Conditions

In the study, participants drove the virtual mobile robot in six control conditions based on the presence and form of navigation assistance provided. They are as followed:

1. **Manual control (MC)**: No navigation assistance is provided to the participant in the task. This is our baseline condition in the study.

2. Single modal assistance:

   (a) **Haptic guidance (H)**: Navigation assistance is provided in the form of haptic guidance forces on the haptic interface based on Section 4.2.

   (b) **Visual guidance trajectory (V-T)**: A suggested path visualization is presented along with the predicted robot path based on the instantaneous control input as described in Section 4.3.

   (c) **Visual steering bars (V-B)**: Steering correction cues are presented along with the predicted robot path based on the instantaneous control input as described in Section 4.3.

3. Multimodal assistance:

   (a) **Haptic + Visual trajectory (HV-T)**: Combines the haptic guidance cues with the visual guidance trajectory cues.

   (b) **Haptic + Visual bars (HV-B)**: Combines the haptic guidance cues with the visual steering bars.

4.3.4 Experimental Procedure

Upon arrival to the study, participants signed the IRB-approved informed consent form. Thereafter, the study commenced with an introduction to the study procedure

and how to control the virtual mobile robot. The study comprised three phases: familiarization, learning, and testing phases.

Familiarization Phase: Here, participants were allowed to drive the virtual mobile robot in an open space (with no obstacles or people) for up to 5-7 minutes to get familiar with the robot controls. Participants held the haptic interface using their preferred hand. This phase was completed in manual control (MC) condition, without any navigation assistance. After participants report confidence in their control of the robot, they are moved to the next phase.

Learning Phase: In this phase, the participants completed 12 trials of the navigation task. In each trial, they were told to control the robot from its start location in the virtual environment to a specified goal location within the hall while driving in a socially-acceptable manner without colliding with moving pedestrians and obstacles. A trial starts when the participant started the timer by pressing a button on the haptic interface and ended once the robot reaches within a threshold distance of the goal location. Each trial was randomly assigned an evaluated condition, resulting in participants experiencing all six conditions at least twice. This allowed participants to build familiarity with the assisted control conditions before the main testing phase. A break time option was provided to avoid fatigue during the study.

Testing Phase: In this phase, the participants completed a block of three trials for each control condition, resulting in six blocks and 18 trials in total. Each trial block comprised the three pedestrian configurations described above. The order of the conditions were randomized and counterbalanced to reduce learning effect, recency bias and fatigue. After each block, participants completed a post-block questionnaire to provide subjective responses to their experience. At the completion of all six trial blocks, participants completed a post-study questionnaire where they provides subjective ranking of the six control conditions according to several

criteria. Section 5.4.4 provided more details on the two questionnaires administered. The entire user study took approximately 1.5 hours to complete, depending on the participants.

4.3.5 Measures

Objective Measures

Three objective measures were computed to evaluate (i) the safety of the navigation, and (ii) the level of agreement or cooperation between the human operator and the navigation assistance.

1. *Number of intimate and personal intrusions*: We counted the number of instances of both intimate and personal space intrusions per trial. An intrusion occurs when the clearance between the robot and a pedestrian is below 0.45m for the intimate space and below 1.2m for the personal space [125].

2. *Mean disagreement*: Following [52], this is measured as the mean of the norm of the difference between the human operator's velocity input and the optimal velocity input from the navigation assistant.

Subjective Measures

Post-block Questionnaire: At the end of each trial block with each control condition, participants completed the following questionnaire using a 7-point likert scale to evaluate the condition:

1. *System helpfuless and ease of use*: (1 - Strongly disagree, 7 - Strongly agree)

    - *Helpfulness*: "This interface condition was very helpful for completing the navigation task."

- *Ease of use*: "I found this interface condition to be easy to use for navigating the robot."

2. *System transparency*: (1 - Understood nothing at all, 7 - Understood extremely well)

   - *Intent understanding*: "To what extent did you understand the intentions of the navigation assistance?"
   - *Force anticipation*: "To what extent could you anticipate the haptic forces provided by the navigation assistance?"

3. *Level of cooperation*: "To what extent did you cooperate or agree with the navigation assistance in the task?" (1 - Never agreed, 7 - Always agreed)

4. *Sense of control*: "To what extent did you feel you had control over the robot?" (1 - No control, 7 - Complete control)

Post-study Questionnaire and Interview: After all six trial blocks were completed, participants completed the following questionnaire to reflect on their experience and rank each of the control conditions.

1. *Skill confidence level*: "How confident are you that you can complete the task successfully without navigation assistance?" (1 - Not confident at all, 7 - Extremely confident)

2. Rank the six conditions in terms of the *most helpful* in completing the tasks successfully.

3. Rank the five assisted conditions in terms of the *most intent understanding* of the navigation assistance.

4. Rank the five assisted conditions in terms of the *most cooperation (or agreement)* with the navigation assistance in the task.

5. Rank the six conditions in terms of the *most preferred* (considering all factors) for completing the task.

At the end of the user study, we conducted a short, semi-structured interview for each participant to understand the reasons for how they ranked the conditions and other follow-up questions.

4.4 Results

All statistical analyses were performed in R [126]. Main effects across evaluated conditions was analyzed using the Friedman test and significance levels were estimated at $p < 0.05$ for statistical significance and $p < 0.1$ for marginal statistical significance. Pair-wise comparisons were performed as post-hoc tests using the Wilcoxon sign-test with Bonferroni correction for multiple comparisons. A summary of statistical results is shown in Table 4.1. We scored the subjective rankings using the Borda count. The order of ranking across various criteria is presented in Table 4.2.

1. *Navigation safety*: In evaluating the impact of navigation assistance on navigation safety, we found that control condition had no significant effect on the number of intimate intrusions, $\chi^2(5) = 6.741, p = 0.357$, but had a marginally significant effect on the number of personal intrusions, $\chi^2(5) = 10.279, p = 0.067$. Furthermore, no significant effects were found in pairwise comparison between control conditions. It is noteworthy to mention that both safety measures had very high variability across conditions, further reflecting a lack of substantial effect on safety.

Measures		Conditions						Friedman Test
		MC	H	V-T	V-B	HV-T	HV-B	
Intimate intrusions$^-$	M	0.40	0.51	0.80	0.49	0.60	0.53	*p = 0.240*
	SD	0.315	0.280	0.450	0.354	0.422	0.451	$\chi^2(5) = 6.741$
Personal intrusions$^-$	M	2.38	3.134	3.089	2.711	**2.245**	3.267	***p = 0.067****
	SD	1.033	1.464	1.890	1.320	1.642	1.733	$\chi^2(5) = 10.279$
Mean disagreement$^-$	M	-	0.37	0.28	0.30	0.30	0.28	*p = 0.735*
	SD	-	0.186	0.121	0.152	0.183	0.112	$\chi^2(4) = 2.000$
Interface helpfulness	M	5.33	4.27	**5.73**	5.20	5.40	5.40	***p = 0.026***
	SD	1.633	1.831	0.961	1.207	1.595	1.352	$\chi^2(5) = 12.68$
Interface ease of use	M	5.80	4.27	**6.07**	5.67	5.40	5.40	***p = 0.012***
	SD	1.639	1.831	1.100	0.976	1.765	1.639	$\chi^2(5) = 14.51$
Intent understanding (Transparency)	M	-	3.73	**5.80**	5.40	5.33	5.47	***p = 0.008***
	SD	-	2.120	1.146	1.404	1.799	1.506	$\chi^2(4) = 13.72$
Force Anticipation (Transparency)	M	-	3.20	-	-	3.93	**4.47**	***p = 0.049***
	SD	-	1.935	-	-	1.710	1.922	$\chi^2(2) = 6.00$
Cooperation	M	-	3.67	**5.267**	4.93	4.93	4.67	***p = 0.019***
	SD	-	1.345	0.961	1.280	1.580	1.345	$\chi^2(4) = 11.76$
Sense of control	M	**6.47**	4.80	6.33	6.27	5.47	5.40	***p = 0.000***
	SD	0.915	1.474	0.724	0.704	1.125	1.29	$\chi^2(5) = 27.89$

Table 4.1: Means (M), standard deviations (SD) and statistical analysis results for the objective and subjective measures across control conditions. The symbol $^-$ denotes the measure is of negative scale.

2. *System helpfulness and ease of use*: The subjective ratings of helpfulness and ease of use were compared across all six control conditions. We found statistical significance for both helpfulness, $\chi^2(5) = 12.68, p = 0.026$, and ease of use, $\chi^2(5) = 14.51, p = 0.012$ (Table 4.1, Fig. 4.4(a)). However, a post-hoc pairwise comparison found no statistical significance between the conditions. V-T has the highest mean rating for both helpfulness ($M = 5.73$) and ease of use ($M = 6.07$) among all the conditions. In the subjective ranking, HV-T was ranked most helpful 8 times (53%), more than every other condition, leading to the highest score on the borda ranked-order count (see Table 4.2). Additionally, visual trajectory-based conditions (HV-T and V-T) were ranked most helpful a combined 11 times (73%).

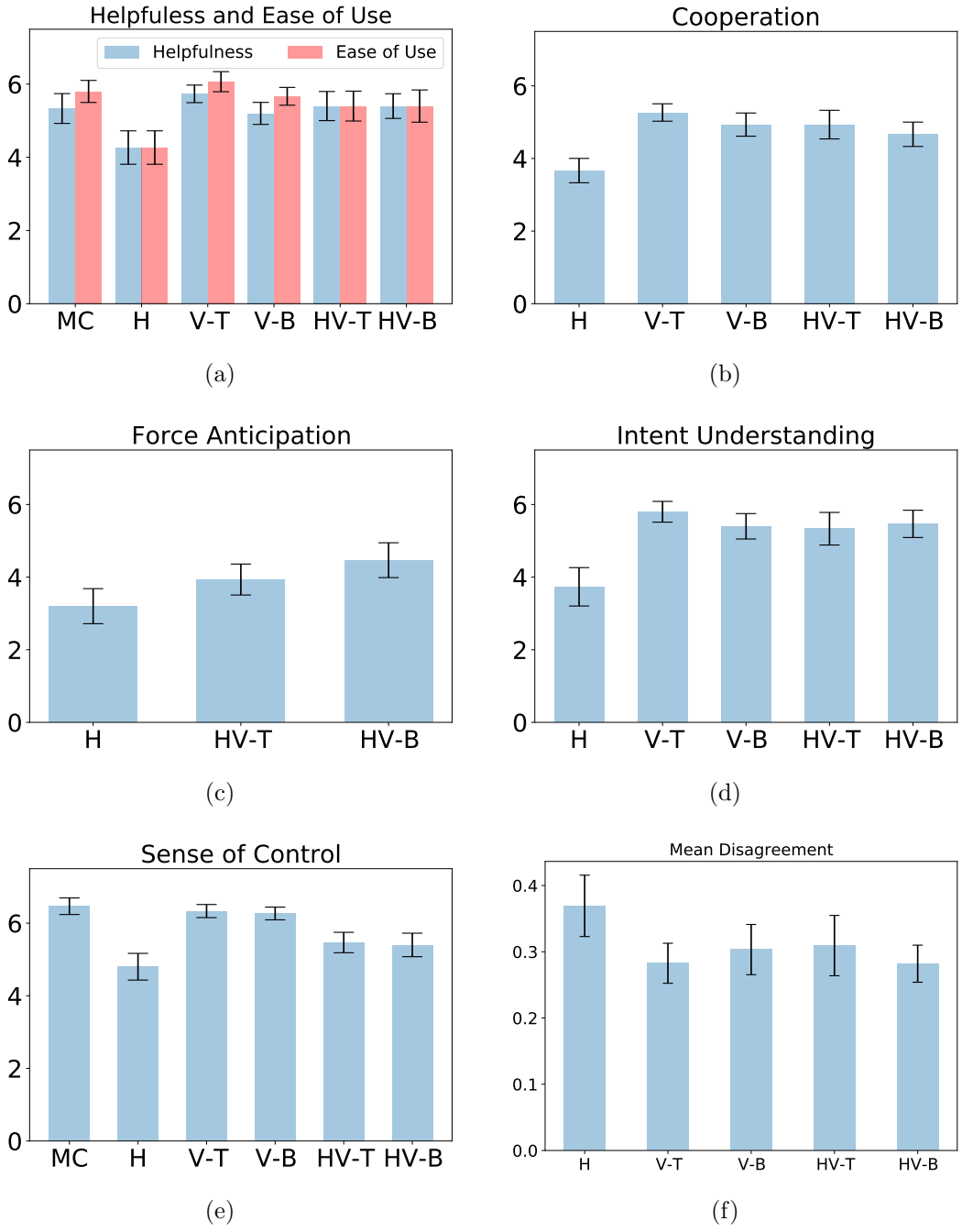

Figure 4.4: Bar plots showing comparison of the different control conditions

3. *System transparency*: Our analysis on the transparency measures revealed statistical significance in intent understanding, $\chi^2(4) = 13.72, p = 0.008$, across the five assisted control conditions (H, V-T, V-B, HV-T, HV-B) and force anticipation, $\chi^2(2) = 6.0, p = 0.049$, across the haptic-based control conditions (H, HV-T, HV-B) (see Fig. 4.4(c–d)). Further post-hoc analysis found marginal difference between V-T and H ($p = 0.072$) for intent understanding and between HV-B and H ($p = 0.051$) for force anticipation. Other pairwise comparisons were not statistically significant. In the subjective ranking, the haptic (H) condition was ranked as hardest to understand 13 times (87%) whereas HV-T (7 times) and V-T (5 times) were ranked easiest to understand a combined 12 times (80%).

4. *Cooperation and agreement*: We measured the user's subjective rating of the level of cooperation with the navigation assistance. Our results show that the assisted control condition type (H, V-T, V-B, HV-T, HV-B) had a significant effect on the level of cooperation, $\chi^2(4) = 11.76, p = 0.019$ (see Fig. 4.4(b)). A post-hoc test revealed that only V-T led to marginally significant effects over H ($p = 0.058$). We assessed the mean disagreement metric and found that the navigation assistance condition had no such effects across control conditions ($p = 0.738$). In the subjective ranking, visual trajectory-based conditions (HV-T and V-T) were ranked with most cooperation a combined 11 times (73%), with HV-T topping the rank with 7 first place rankings (47%). Again, the haptic (H) condition was ranked as least in cooperation 13 times (87%).

5. *Sense of control*: When evaluating the participant's sense of control across control conditions, we found a significant effect of control condition on reported sense of control, $\chi^2(5) = 27.89, p = 0.000$ (Fig. 4.4(e)). A post-hoc test

Borda Count Ranking	1st	2nd	3rd	4th	5th	6th
Helpfulness	HV-T (73)	V-T (63)	HV-B (58)	V-B (51)	MC (49)	H (21)
Intent Understanding	HV-T (63)	V-T (58)	HV-B (45)	V-B (40)	H (19)	-
Cooperation	HV-T (57)	V-T (55)	V-B (48)	HV-B (42)	H (23)	-
Overall Preference	HV-T (68)	V-T (66)	V-B (55)	HV-B (54)	MC (50)	H (22)

Table 4.2: Subjective ranking and calculated scores (in parentheses) of control conditions based on Borda count method

demonstrated that MC ($p = 0.054$), V-T ($p = 0.067$) and V-B ($p = 0.081$) conditions led to marginally significant increase in perception of control compared to the H condition.

6. *Overall preference*: When asked to rank the control conditions in terms of overall preference, six participants (40%) ranked HV-T condition in first place, whereas three participants each ranked V-T, HV-B and MC conditions instead (see Fig. 4.5). Haptic (H) condition was ranked least preferred 11 times (73%). Table 4.2 shows the rank order and calculated scores for overall preference as well as other subjective measures.

4.5 Discussion

In this study, our proposed multi-modal shared autonomy system for assisting in social navigation was evaluated and compared with single-modality designs (haptic or visual) and manual control (no assistance) as the baseline based on metrics such as navigation safety, interface transparency, cooperation and user preference.

Effect on Navigation Safety

We hypothesized that multimodal assistance will lead to higher navigation safety compared to single modal assistance (haptic and visual) and our baseline condi-

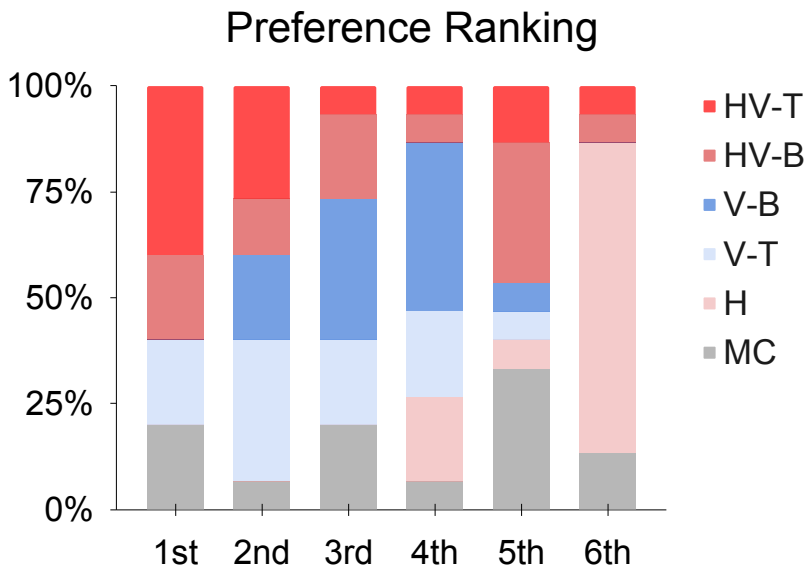

Figure 4.5: Distribution of overall preference ranking across control conditions.

tion. However, we observed that neither the presence nor the type of assistance modality had a significant effect on the navigation safety of the telepresence robot. Furthermore, we observed large variance in the results across control conditions (see Table 4.1). Previous studies on assisted navigation show evidence that visual and/or haptic navigation assistance improves performance and reduces collisions [52, 127]. However, we note that these studies consider navigation in static and structured environments. A recent study on telepresence navigation showed that navigation assistance methods may not always improve navigation safety especially in dynamic environments in interaction with people [128]. In our study, one possible explanation for this may be with task difficulty. Kuiper et al. [69] found that navigation assistance systems are more effective when the task is more difficult. However, in our final questionnaire, participants reported high confidence in their skill to complete the task without navigation assistance ($M = 5.07, SD = 1.39$). Also, a study on automation usage by Lee et al. [129] noted that people use autonomous systems

based on the difference between their trust in the system and their self-confidence in performing the task. This may imply that, on average, participants did not rely on the navigation assistance in the task. This warrants further investigations in two directions. First, further experimental manipulations on the task difficulty may be needed to provide more insight into its effects on shared navigation tasks. The second direction is to investigate the effect of training and learning on operator trust and reliance on the navigation assistance by manipulating practice duration.

Effect on System Transparency and Cooperation

Regarding system transparency and cooperation, we hypothesized that (i) multi-modal assistance will result in higher rating than both single modal cases, and (ii) visual modality will result in higher rating than the haptic modality. Our results only partially support these hypotheses. In the case of intent understanding, our results revealed that the control condition type significantly impacted the level of intent understanding. Specifically, we found that visual cues delineate the intent of the autonomous agent significantly more than the haptic cues alone. This is consistent with existing work on the visual channel for intent communication [60, 124]. However, we do not see a significant difference between visual-based single modal conditions (V-T, V-B) and multi-modal conditions (HV-T, HV-B), i.e. the combination of haptic and visual cues didn't lead to higher intent understanding over visual only conditions. A possible explanation for this is that due to the dynamic nature of our task, the haptic guidance forces tended to be fast changing and sometimes caused a distraction. Some participants commented that they were unable to understand why or what the haptic condition was trying to do.

Considering force anticipation, our results show that including visual information significantly improved the force anticipation over haptic cues alone, especially when

the visual cue is presented as steering magnitude bars (V-B). This is consistent with the findings by Ho et al. [73]. V-B provided a more consistent interpretation of the haptic forces than the suggested path visuals (V-T).

An interesting finding was the result showing the influence of video gaming experience on system transparency. Fig. 4.6 presents the participants' rating of intent understanding and force anticipation based on their gaming experience. Our results showed that participants classified as gamers (i.e. based on self-reported gaming frequency and skill level) reported higher ratings for intent understanding and force anticipation across all control conditions. This suggests that prior video gaming experience may have impacted the participant's ability to understand, interpret and anticipate the guidance cues. Takayama et al. [6] observed a similar influence in a remote telepresence navigation study where gaming experience decreased the perceived level of physical effort in the task and increased enjoyability.

Additionally, in considering human-automation cooperation and agreement, our subjective results revealed that level of cooperation was significantly impacted by assistance condition. Participants reported least cooperation for haptic only and highest with V-T. This pattern is consistent with the intent understanding rating and in line with existing studies on mutual understanding on human-machine cooperation [ref]. We must reflect on these results with caution as we found no significant difference when objectively estimating the degree of agreement (via the mean disagreement measure) between haptic only and visual conditions (see Table 4.2). However, in the subjective ranking, we see that Borda score placed HV-T over others consistently across all factors. Nine participants commented that visual information helped them better understand the haptic forces. This is supported by existing studies on multimodal feedback [68, 72].

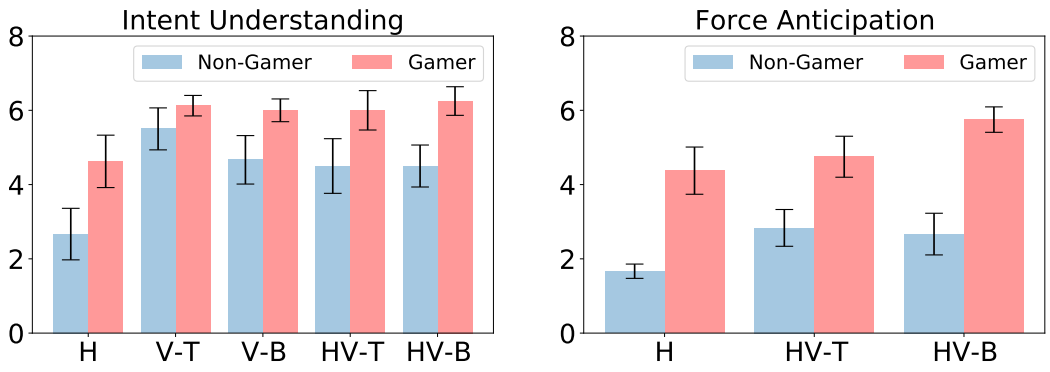

(a) (b)

Figure 4.6: Comparing the effect of gaming experience on the system transparency across different control conditions

Effect on User Preferences

We hypothesized that multi-modal assistance will be preferred over single modality assistance for both visual and haptic only cases. The results of our subjective ranking only partially support this hypothesis. Participants ranked both multi-modal assistance conditions, HV-T and HV-B, higher than H, with high Borda score margins in both cases, 46 and 32 points respectively (see Table 4.2). In fact, haptic only (H) condition was ranked last by 73% of participants in the study (11 times). This probably occurred because of the dynamic nature of the navigation task. Though the haptic channel enables faster response through reflexes [67], it suffers from low bandwidth limiting the amount of intent information that can be communicated to the operator [69]. In our results, we found that providing guidance information in visual form led to higher preferences. This is supported by existing multimodal studies [68, 72]. In the post-study interviews, nine participants reported that visual information enabled them to better understand the haptic forces.

We additionally hypothesized that multi-modal assistance will be preferred over visual only cases. Our results show only partial support for this. For visual trajec-

tory case, although HV-T is ranked higher, it is with a weak margin (only 2 points) (see Table 4.2). As for visual magnitude bars case, we see the reverse case with V-B ranked higher in the overall preference by only 1 point. When asked why they prefer multi-modal assistance over visual only assistance, participants reported that though visual information helped with understanding, the haptic cues "served as a reminder", "pushed you a little when a person is behind you", "moves you especially in moments of confusion on where to go".

Effect of Visual Guidance Design

In our study, we considered two designs for visual guidance: visual guidance trajectory and visual steering bars, as described in Section 4.2.3. According to our results, objective and subjective ratings did not differ significantly between both designs. However, in analyzing the subjective rankings, we found that trajectory conditions (V-T & HV-T) consistently had higher rank-score over steering bar conditions (V-B & HV-B) (see Table 4.2). Specifically, visual trajectory conditions were ranked most preferred 9 times (60%) compared to 3 times (20%) for visual steering bar conditions. Five participants reported that the suggested path in V-T was easier to match in terms of where to go. Also, one participant remarked that the suggested path conveyed more information than the steering bars. This is consistent with the operator display design paradigms in literature [60]. In [68], the authors suggest that a predicted trajectory expressing an autonomous agent's intent provides more information about the driving context than just an instantaneous maneuver suggestion (which reflects the haptic forces). Nevertheless, some participants reported they preferred steering bars for two main reasons. First, some participants found the steering bars easier to follow than the suggested path, possibly because it provided specific correction on what control input to apply. The other reason involved visual

attention and distraction. Three participants said that visual steering bars were less invasive on the screen, leading to less visual distraction. These findings provide insights for further research into human-centered visual design options in assistive systems.

4.6 Chapter Summary

In this chapter, we presented a multi-modal shared autonomy approach for navigation assistance in dynamic, human-populated environments. This approach included both active haptic guidance and passive visual feedback by using two distinct visualizations of the safe control input. We conducted a user study ($n = 15$) to evaluate how our proposed multimodal approach affects navigation safety, interface transparency, and user preference compared to single modality (haptic or visual alone) and no assistance cases. Our results revealed that more operators preferred multi-modal assistance (especially when visualization is in trajectory form) over both visual or haptic only in the shared navigation task. While we did not find any significant differences in navigation safety, we did find that visual cues significantly increased participants' understanding of intent and level of cooperation over haptic guidance. In this chapter, we have made important advances towards our understanding of how to design navigation assistance systems within the complex context of socially-aware navigation in cluttered environments. We conclude that further research is needed to validate these findings in a real-world context.

Chapter 5

Adaptive SocNavAssist: Assistance Adaptation to Driving Objectives in Social Navigation

5.1 Introduction

Assisted driving systems are increasingly relevant for supporting people in personal mobility (such as passenger drivers, wheelchair users, mobile telepresence robots, etc.) in order to relieve some of the physical and cognitive workload required for safe navigation. However, due to mismatches in intent across various levels of information processing [11], conflict occurs, which degrades trust and cooperation in the human-automation system. Chapter 4 presented increasing system transparency as one of the human-centered approaches to improve intent understanding and force anticipation in a haptic shared autonomy framework. However, while improving system transparency alone may positively impact shared driving in some scenarios, it may not be adequate in resolving conflicts in different scenarios, environments and

human states and factors. This is true of all "static" assistance systems that are tailored to a specific operating condition. As described in Chapter 2, another crucial factor for human-centered design is autonomy adaptation. Adaptive SA systems are able to adjust their control level or strategy to better align with the human state or behaviors, task and environment conditions. There's growing body of work on automation adaptation in the context of intelligent driving systems and and robot teleoperation [16, 17, 76]. In recent work, Zwaan et al. [43] proposed a risk-adaptive driving assistance system that reduces the level of haptic authority on the steering wheel when the risk of collision is low, but increases it when the risk is high by monitoring the environmental conditions. Luo et al. [130] monitored the level of driver fatigue or workload and modulated the level of assistance to assist the driver as needed.

While the above studies have modulated the level of assistance on a specific task objective based on several factors, Gao [131] took a different approach to consider task adaptation. In a navigation scenario, they showed that inferring and adapting to the current navigation task objective executed by the operator such as doorway crossing, object inspection or wall following led to improved task performance and reduced overall workload. Our work in this chapter extends this task objective adaptive approach to the context of social navigation assistance by enabling adaptation to specific context-dependent preference or objectives drivers may have in a navigation task. For instance, a telepresence robot operator or a wheelchair user may have different objectives in mind while controlling the vehicle. If they are at a conference hall, they may wish to get across a hall as quickly as possible to meet a deadline or they may wish to drive as cautiously as possible so as not to distract other people. Hence, we focus on the spectrum of driving behavior from cautious to assertive. Numerous studies have identified these as distinct behaviors in how humans inter-

act while walking through a crowd or driving a vehicle on a highway either tied to personality traits or conditioned based on the task requirement [132–134].

In this chapter, two questions arise in exploring adaptive navigation assistance in social navigation: (i) How to design socially-aware navigation assistance that is adaptive to user driving objectives/styles?, (ii) Will such an adaptive system impact task performance and human-robot cooperation, and if so, by how much? We build on SA-RVO presented in the previous chapter by extending it to incorporate further socially-relevant objective functions that characterize these distinct driving objectives/styles. We further conduct a pilot user study experiment to evaluate the impact of objective-aligned navigation assistance on driving performance, human-robot cooperation and user preference in a social navigation task.

This chapter is organized as follows: the adaptive socially-aware navigation assistance system design is described in Section 5.2. The two proposed assistance policies are evaluated in Section 5.3. The pilot user study design is presented in Section 5.4. We present and discuss the user study results in Section 5.5 and Section 5.6 respectively. Finally, concluding remarks are presented in Section 5.7.

5.2 System Design

The adaptive socially-aware navigation assistance system comprises two main components: (i) a modification of collision avoidance via socially-aware reciprocal velocity obstacles (SA-RVO), (ii) a multimodal (haptic + visual) interface to provide guidance cues to the operator.

5.2.1 Adaptive SA-RVO: Socially-aware collision avoidance via reciprocal velocity obstacles

The navigation assistance system proposed in this work builds on the SA-RVO presented in Chapter 4. To recap, the SA-RVO approach is based on the reciprocal velocity obstacle (RVO) method [86] which is a well studied approach for dynamic collision avoidance in the presence of both static and dynamic obstacles by planning for collision-free motions in the 2D velocity space of the robot. SA-RVO extends the original RVO formulation by explicitly accounting for social proxemics constraints by expanding the region of the pedestrian to cover their personal space [23]. In the original RVO formulation, the optimal velocity is calculated as the candidate velocity within the space of collision-free velocities (i.e. $v \notin RVO_{A|B}$) that minimizes the distance to the maximum allowable velocity to the goal. SA-RVO modifies this process by taking into account additional factors for navigation assistance while evaluating candidate velocities, resulting in a weighted sum of objective functions:

$$v_A^{optimal}(t) = \underset{v \notin RVO_{A|B}}{\arg\min} \sum_{i=1}^{n} w_i G_i(t) \tag{5.1}$$

where w_i and G_i are the ith weight and objective function respectively. Three objective functions were considered in Chapter 4:

1. *Operator alignment cost*: This objective function seeks to find a velocity that is as close as possible to the operator's commanded velocity v_A^{pref} thereby preserving the operator's original intent.

$$G_1(t) = \|v(t) - v_A^{pref}(t)\|^2$$

2. *Motion smoothness cost*: This objective ensures smooth guidance cues to the

operator by penalizing rapid changes in consecutive optimal velocities $v_A^{optimal}$.

$$G_2(t) = \|v(t) - v_A^{optimal}(t-1)\|^2$$

3. *Goal-directed cost*: This objective penalizes velocities that deviate from the direction to goal ensuring the operator is guided towards the goal. To achieve this, the autonomous system needs to know the goal of the operator either explicitly or by inference [122]. In this study, we assume the location of the operator's goal is known.

$$G_3(t) = \|v(t) - v^{goal}(t)\|^2$$

Three additional objective functions are included to the adaptive SA-RVO to explicitly model different social navigation behaviors (Fig.5.1) including clearance from static obstacles, clearance from pedestrians to maintain personal space, and consideration for passing in in front of a moving pedestrian. To account for discrete future poses of the robot over a finite time horizon t_p, candidate trajectories are computed using a constant velocity projection of the candidate velocities with time delta, Δt. The following objective/cost functions then evaluate each candidate trajectory based on the criteria.

1. *Static obstacle cost*: This objective corresponds to the cumulative cost of the candidate trajectory resulting from static obstacles in the environment. This cost is computed using the static costmap generated from the environment occupancy grid map which captures the static structures in the environment. For this, we used the 2D costmap package [1] in the ROS (Robotics Operating

[1] `http://wiki.ros.org/costmap_2d`

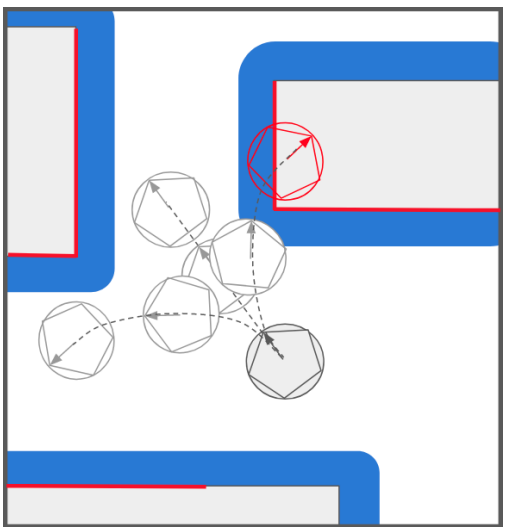

(a) Static obstacle cost

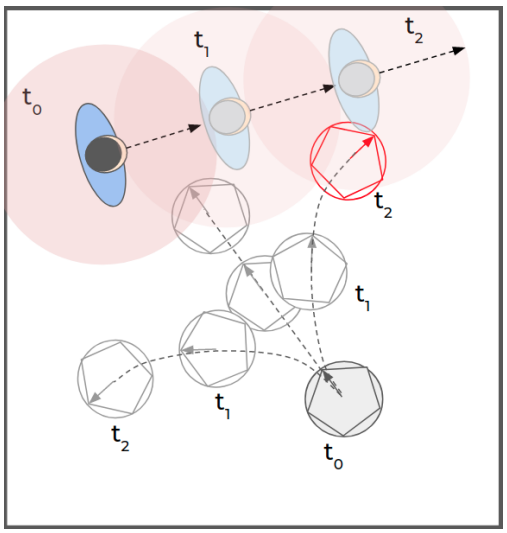

(b) Social intrusion cost

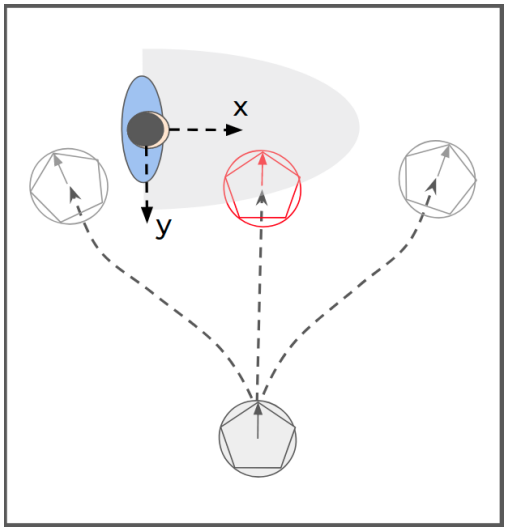

(c) Frontal intrusion cost

Figure 5.1: Three additional objective/cost functions to model different social navigation behaviors are included in SA-RVO. Using projections of candidate velocities, candidate robot trajectories are generated and evaluated over a finite finite horizon. The **red** future robot projection in (a-c) would be penalized since it would lead to collision-bound or unsafe behavior.

System) [2]. The range of static cost C_{static} for the robot's pose $X_r^{t'}$, at time t' in the candidate trajectory is 0–255, where zero means the pose is in free-space and hence, collision-free, while 255 means the robot will be in collision at that pose. Fig. 5.1(a) shows an illustration of static obstacle costmap with inflation region around obstacles (blue areas) for a robot showing $N_p = 2$ trajectory projection steps.

$$G_4(t) = \sum_{t'=t+\Delta t}^{t+N_p\Delta t} C_{static}(X_r^{t'})$$

where t is the current time, $t' \in [t, t + N_p\Delta t]$ is the projected time in the prediction horizon, Δt is the prediction time step.

2. *Social intrusion cost*: This corresponds to the cumulative cost of the candidate trajectory resulting from static and moving pedestrians in the environment. A disc-shaped social costmap C_{social} with radius corresponding to the proxemics space, is defined around each pedestrian pose representing the cost of the robot being at that position relative to the pedestrian (Fig. 5.1(b)). The cost value is computed proportional to the distance to the pedestrian. To account for dynamic pedestrians, the future poses of each pedestrian is predicted using a simple constant velocity model based on their current pose and velocity. This way, we can account for the dynamic costmaps of each of the pedestrians at different times over the prediction time horizon, t_p (see Fig. 5.1). As a result, this objective prioritizes candidate trajectories with fewer intersections with the costmaps of predicted pedestrian paths [135]. This is consistent with how humans plan their motions around other moving entities in their proximity by

[2] `http://wiki.ros.org`

anticipating their motions.

$$C_{social}(X_r, X_{ped}) = \begin{cases} \xi - \|X_r - X_{ped}\|^2, & \text{if } \|X_r - X_{ped}\|^2 < \xi \\ 0, & \text{otherwise.} \end{cases}$$

$$G_5(t) = \sum_{t'=t+\Delta t}^{t+N_p\Delta t} max\{C_{social}(X_r^{t'}, X^{t'}_{ped,j}), \forall j \in [1, N_{ped}]\}$$

where $X_r^{t'}$ and $X^{t'}_{ped,j}$ are the predicted poses of the robot and j-th pedestrian at time $t^{'}$ respectively, ξ is the distance threshold value and represents the radius of the costmap, N_{ped} is the total number of pedestrians and pedestrian groups under consideration, N_p is the number of trajectory projection steps.

3. *Frontal intrusion cost*: This objective corresponds to the cumulative cost of the candidate trajectory resulting from frontal intrusion of pedestrians in the environment. Inspired by [136], the frontal intrusion costmap $C_{frontal}$ is modeled as a truncated 2D Gaussian function placed in front of each pedestrian representing the cost of the robot being at that pose relative to the pedestrian (Fig. 5.1(c)). The shape of the truncated Gaussian function is asymmetric and is defined by the two standard deviations, $\sigma_{frontal} = 1.2m$ and $\sigma_{side} = \sigma_{frontal}/1.5$ relating to the x and y axes respectively (in Fig. 5.1(c)). The truncation occurs along the y-axis of the pedestrian ensuring only robot poses in front of the robot are considered. As above, the future poses of each pedestrian are predicted using a simple constant velocity model to enable dynamic costmaps at different times over the prediction time horizon.

$$G_6(t) = \sum_{t'=t+\Delta t}^{t+N_p\Delta t} max\{C_{frontal}(X_r^{t'}, X^{t'}_{ped,j}), \forall j \in [1, N_{ped}]\}$$

Consistent with SA-RVO in Chapter 4, we perform a static obstacle avoidance step as a preprocessing step in order to account for static obstacles in the environment such as walls and tables. In particular, we filter out any velocities that generate candidate trajectories that lead to collisions using the static costmap(see Fig. 5.1(a)). The resulting samples of 'statically' safe velocities is then fed into the SA-RVO in order to account for dynamic obstacles.

5.2.2 Multimodal Assistance Interface

Following the findings from Chapter 4, the multimodal (combining haptic and visual channels) approach is adopted to provide guidance feedback cues to the operator. The haptic channel generates appropriate force feedback cues on the control interface (3 DOF haptic-enabled joystick) so that the operator's control input can be guided towards alignment with the optimal velocity command, $v_A^{optimal}(t)$, computed by adaptive SA-RVO. As described in Section 4.2.2, the haptic forces are computed as proportional to the error between $v_A^{optimal}(t)$ and v_A^{pref}, which is the current velocity command from the human operator:

$$F(t) = K_p(v_A^{optimal}(t) - v_A^{pref}(t)) \tag{5.2}$$

where K_p is the fixed haptic gain. This value regulates the level of haptic authority assigned to the autonomous agent. Low haptic gain allows the operator to override low guidance forces easily, thereby maintaining control. However, high haptic gain may hinder the operator from counteracting the haptic forces being generated, leaving final control to the autonomous agent [7].

For visual feedback, two visual trajectory traces are displayed as overlays on the display window as described in Section 4.2.3. The first trajectory trace (green

dotted trace in Fig. 4.2(top)) communicates the predicted future states of the robot based on the instantaneous velocity control input from the shared haptic interface as in [68]. The second trajectory trace (red dotted trace in Fig. 4.2(top)) represent the predicted future state of the robot based on the optimal velocity control command computed by adaptive SA-RVO rather than the operator's control input. This results in a suggested path visualization that shows contextual information about the direction the autonomous agent suggests the operator to go.

5.3 Evaluation of Driving Objective-dependent Assistance Policies

Two navigation assistance policies—Safety-Aligned and Goal-Aligned—are considered in this study as they correspond to the two ends of the spectrum of driving behaviors/styles found in literature, namely, cautious and assertive driving [134]. Both assistance policies were realized based on setting the weights of the objective function described in Section 5.2.

The **Safety-Aligned (SA)** assistance policy corresponds to the cautious driving behavior. Here, the static obstacle and social intrusion costs weights (w_4 and w_5) are increased to penalize driving too close to pedestrians and obstacles. Additionally, a high objective weight, w_6, was set to the frontal intrusion cost function to penalize robot trajectories that cross right in front of the pedestrian.

The **Goal-Aligned (GA)** assistance policy was designed to correspond to the assertive driving behavior. Here, the social-related costs, w_{4-6}, are reduced to make cautious behavior to be less prominent while the goal-directed cost, w_3, is increased to prioritize driving along paths headed in direction of the goal. It is important to note that this assertive, goal-oriented behavior does not jeopardize pedestrian

safety as all collision-bound maneuvers are filtered out and excluded in the RVO formulation.

We conducted a simulated experiment to evaluate the navigation performance of the two assistance policies in 4 typical navigation scenarios: (i) one-on-one approach, (ii) two-person crossing, (iii) multi-pedestrian approach with obstacles and (iv) multi-pedestrian crossing with obstacles. The experiment is conducted in the same virtual environment using the same virtual differential drive mobile robot as described in the previous chapter (see Section 4.3). The simulation trials were run several times and the resulting trajectories were used to evaluate the navigation performance (i.e., efficiency and safety) of the assistance policies using the following objective metrics:

1. *Path length (metres)*: Measured as the cumulative distance traveled from the start to the goal location.

2. *Task completion time (secs)*: Measured as time taken to reach the goal location from the start position.

3. *Average and minimum pedestrian clearance (metres)*: Measured as the average and minimum distances between the robot and the closest pedestrian along the path from start to the goal.

4. *Proxemics space intrusions (%)*: Following [136], this measure categorizes the robot's proximity to the nearest pedestrian during each time step into one of three proxemics spaces (based on the Proxemics theory proposed by Hall [83]): Intimate, Personal, and Social, in order to determine the percentage of time spent in each space. Both Intimate and Personal intrusions are considered in this study which correspond to a clearance of below $0.45m$ and $1.2m$ respectively.

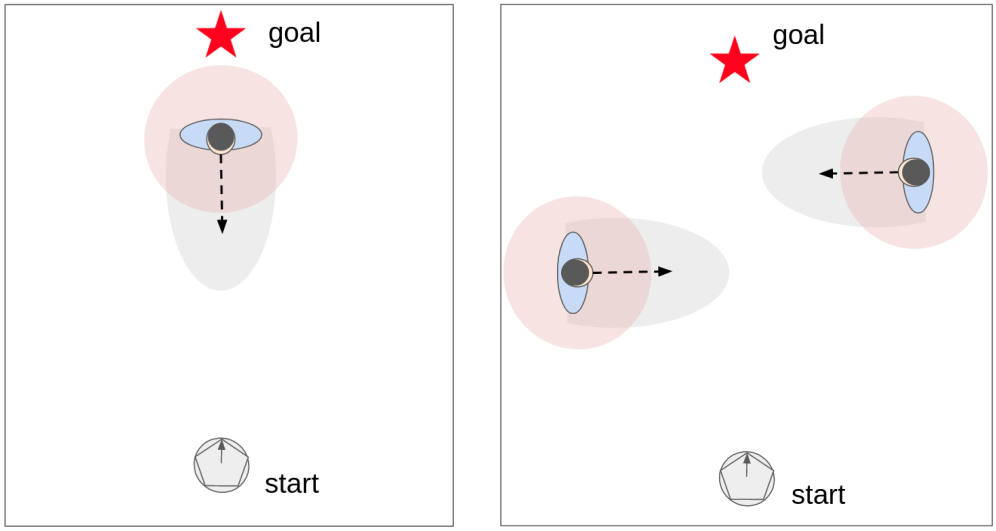

(a) One-to-one approach scenario (b) Two-person crossing scenario

Figure 5.2: Experimental scenarios 1 & 2 for evaluating the assistance policies

5.3.1 Scenario 1: One-to-One Approach

Fig. 5.2(a) shows the one-to-one approach scenario. The robot and one pedestrian are facing one another and moving in opposite directions towards each other with the robot's goal set behind the pedestrian. Table 5.1 summarizes the evaluation metrics (means and standard deviations) for both assistance policies. In terms of navigation efficiency, both the path length and the completion time were slightly lower for the goal-aligned (GA) policy compared to the safety-aligned (SA) (Fig. 5.3(a-b)). Whereas, the safety-aligned assistance policy resulted in safer navigation behavior with higher minimum pedestrian clearance and no personal space intrusion (Fig. 5.3(c-d)). The wider clearance distance from the pedestrian can also be seen from the trajectory plot in Fig. 5.4.

Table 5.1: Scenario 1: One-to-One Approach

	Path Length (m)	Completion Time (s)	Avg. Ped. Clearance (m)
Safety-Aligned (SA)	11.31±1.21	8.34±0.04	4.20±0.03
Goal-Aligned (GA)	10.30±1.21	8.13±0.07	3.92±0.02

	Min. Ped. Clearance (m)	% Intrusions	
		Intimate Space	Personal Space
Safety-Aligned (SA)	1.70±0.01	0.00±0.00	0.00±0.00
Goal-Aligned (GA)	1.05±0.02	0.00±0.00	6.57±0.11

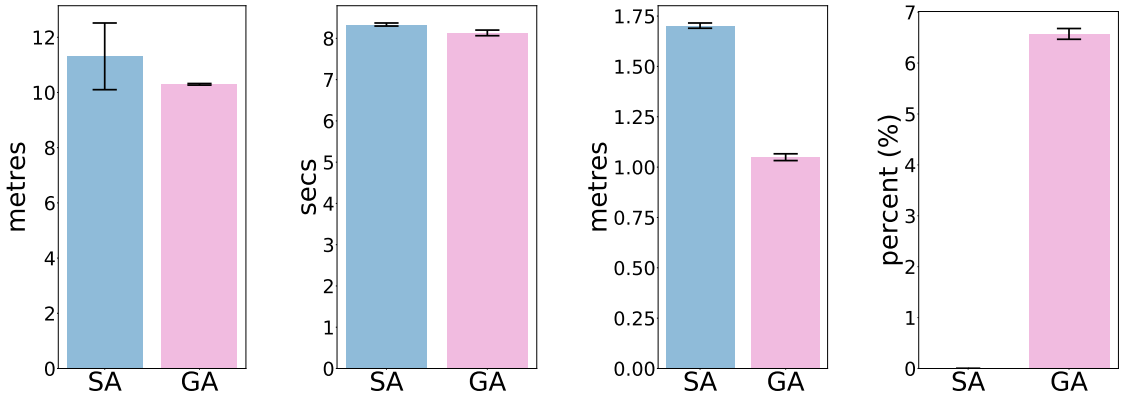

(a) Path Length (b) Completion Time (c) Min. Pedestrian Clearance (d) Personal Space Intrusion

Figure 5.3: Navigation performance metrics for safety-aligned (SA) and goal-aligned (GA) assistance policies in the one-to-one approach scenario. SA results in a safer navigation around the pedestrian (i.e., more clearance and no intrusion) at the expense of slightly longer path.

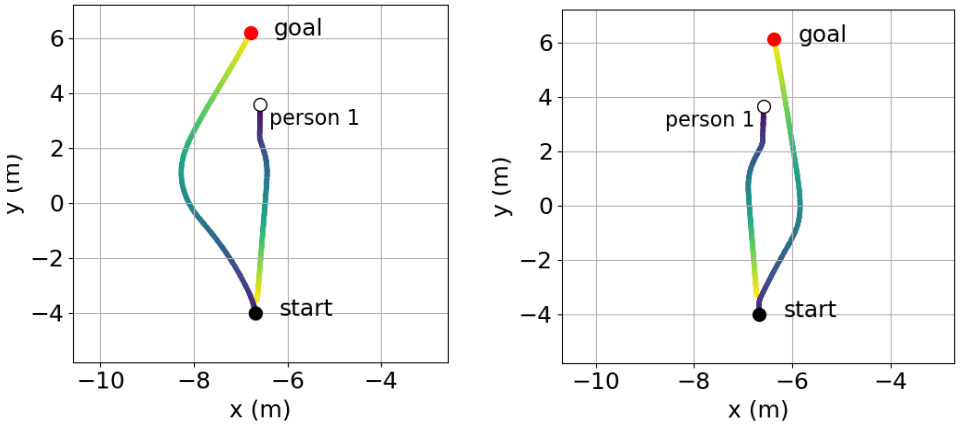

(a) Safety-Aligned (SA) assistance policy (b) Goal-Aligned (GA) assistance policy

Figure 5.4: Time-lapse trajectory plots showing the difference in navigation behavior between safety-aligned (SA) and goal-aligned (GA) assistance policies in the one-to-one approach scenario.

5.3.2 Scenario 2: Two-Person Crossing

Fig. 5.2(b) shows the two-person crossing scenario. One pedestrian starts at both the left and right end the space walking towards a goal in the opposite direction while the robot starts at the bottom middle of the space and would need to cross the paths of the pedestrians to get to the goal ahead. Table 5.2 summarizes the evaluation metrics (means and standard deviations) for both assistance policies. Similar to Scenario 1, both the path length and the completion time were slightly lower for the goal-aligned (GA) policy compared to the safety-aligned (SA) (Fig. 5.5(a-b)). Likewise, the safety-aligned (SA) assistance policy resulted in safer navigation behavior with higher minimum pedestrian clearance and no personal space intrusion (Fig. 5.5(c-d)). As can be seen from Fig. 5.6, frontal intrusion cost is in effect here, and the assistance policy adjusts its trajectory to avoid close crossing in front of the person 1.

Table 5.2: Scenario 2: Two-Person Crossing

	Path Length (m)	Completion Time (s)	Avg. Ped. Clearance (m)
Safety-Aligned (SA)	11.49±1.15	8.78±0.1	2.76±0.05
Goal-Aligned (GA)	10.94±1.22	8.45±0.04	2.34±0.03

		% Intrusions	
	Min. Ped. Clearance (m)	Intimate Space	Personal Space
Safety-Aligned (SA)	1.71±0.05	0.00±0.00	0.00±0.00
Goal-Aligned (GA)	0.97±0.01	0.00±0.00	11.34±0.54

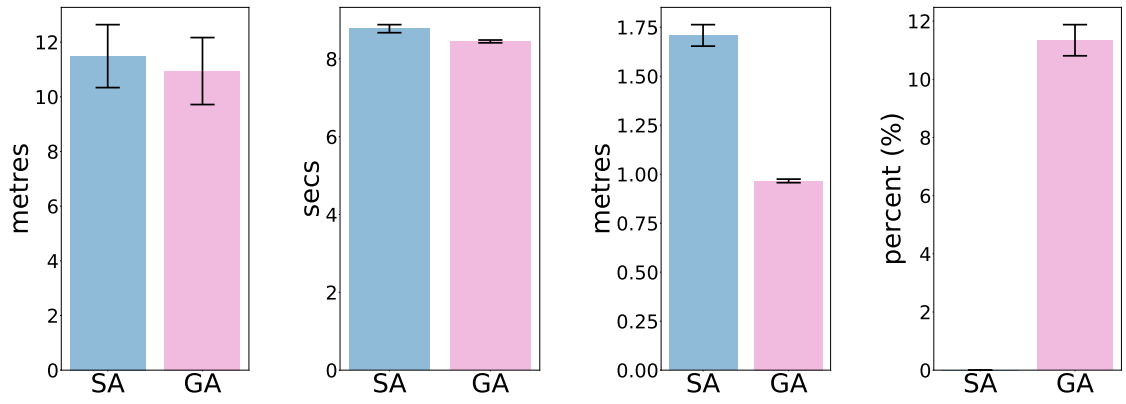

(a) Path Length (b) Completion Time (c) Min. Pedestrian Clearance (d) Personal Space Intrusion

Figure 5.5: Navigation performance metrics for safety-aligned (SA) and goal-aligned (GA) assistance policies in the two-person crossing scenario.

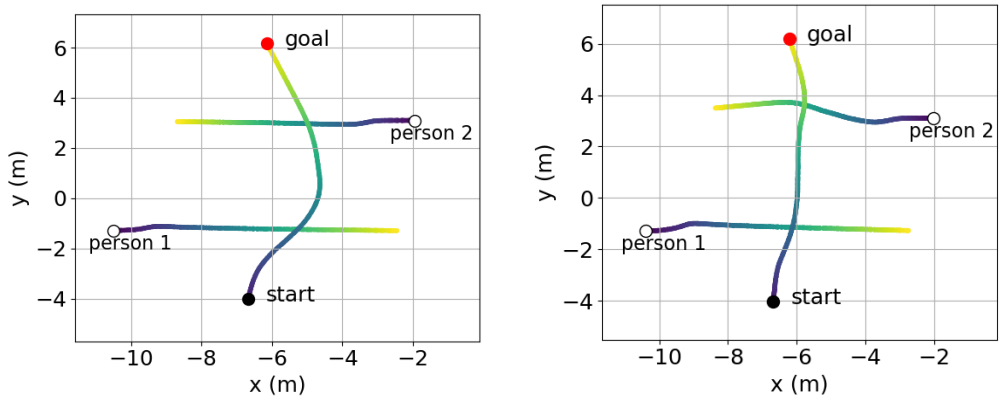

(a) Safety-aligned (SA) assistance policy (b) Goal-aligned (GA) assistance policy

Figure 5.6: Time-lapse trajectory plots showing the difference in navigation behavior between safety-aligned (SA) and goal-aligned (GA) assistance policies in the two-person crossing scenario.

5.3.3 Scenario 3: Multiple-Pedestrian Approach with Obstacles

Fig. 5.7(a) shows the multiple-pedestrian approach scenario with obstacles. The inclusion of static obstacles (e.g. tables) increases the complexity of the navigation task requiring the assistance policy to plan collision-free motions around multiple

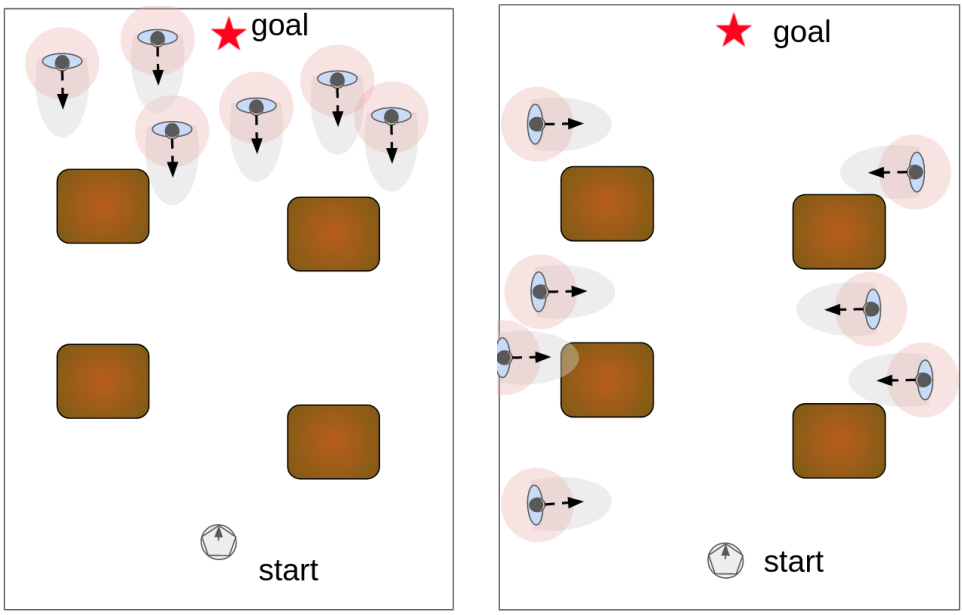

(a) Scenario 3: Multiple-pedestrian approach with obstacles

(b) Scenario 4: Multiple-pedestrian crossing with obstacles

Figure 5.7: Experimental scenarios 3 & 4 for evaluating the assistance policies

moving pedestrians while factoring obstacles in the environment.

The robot starts at one end of the hall while pedestrians are spawned at the other end walking in the direction towards the robot. Table 5.3 summarizes the evaluation metrics (means and standard deviations) for both assistance policies. With regards to navigation efficiency, goal-aligned (GA) assistance policy achieve much lower path length and completion time compared to the safety-aligned (SA) (Fig. 5.8(a-b)). SA results in not only higher values for navigation efficiency, but also with wide variance between trials.

Results for navigation safety show that even though SA had fewer personal space intrusions on average, the minimum pedestrian clearance was slightly higher in some trials than GA. This may be due to the robot getting stuck while negotiating a safe maneuver between multiple pedestrians and the static obstacles (Fig. 5.8(c-d)).

Table 5.3: Scenario 3: Multiple-Pedestrian Approach with Obstacles

	Path Length (m)	Completion Time (s)	Avg. Ped. Clearance (m)
Safety-Aligned (SA)	20.62±6.87	24.91±6.67	3.32±0.38
Goal-Aligned (GA)	13.54±0.12	11.93±0.55	4.04±0.05

		% Intrusions	
	Min. Ped. Clearance (m)	Intimate Space	Personal Space
Safety-Aligned (SA)	0.9±0.29	0.00±0.00	3.95±2.67
Goal-Aligned (GA)	1.00±0.00	0.00±0.00	9.94±0.54

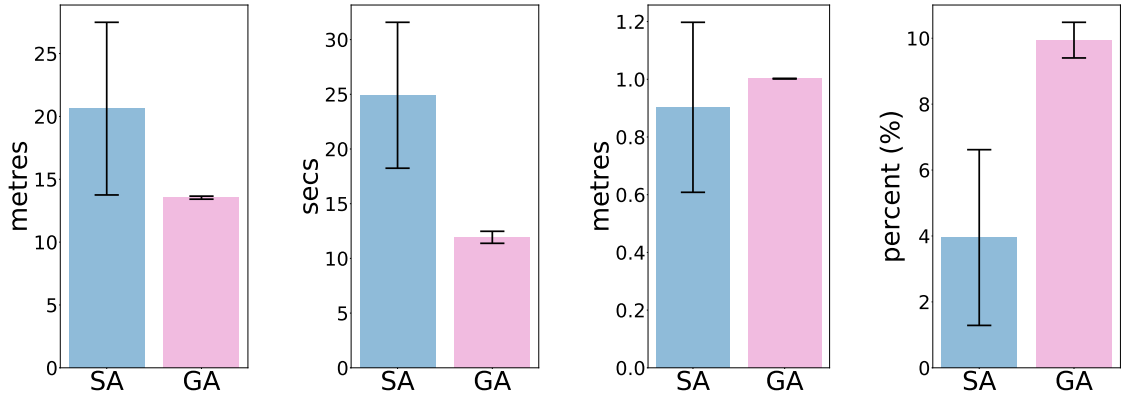

(a) Path Length (b) Completion Time (c) Min. Pedestrian Clearance (d) Personal Space Intrusion

Figure 5.8: Navigation performance metrics for safety-aligned (SA) and goal-aligned (GA) assistance policies in the multiple-pedestrian approach scenario with obstacles.

5.3.4 Scenario 4: Multiple-Pedestrian Crossing with Obstacles

Fig. 5.7(b) shows the multiple-pedestrian crossing scenario with obstacles. The robot starts at one end of the hall with its goal located at the other end while multiple pedestrians cross in front of the robot from the left side of the hall to the right and vice versa. Table 5.4 summarizes the evaluation metrics (means and standard deviations) for both assistance policies. With regards to navigation efficiency, goal-aligned (GA) assistance policy achieve much lower path length and completion time compared to the safety-aligned (SA) (Fig. 5.9(a-b)). In terms of navigation safety,

the safety-aligned (SA) assistance policy resulted in safer navigation behavior with higher minimum pedestrian clearance and no personal space intrusion.

Table 5.4: Scenario 4: Multiple-Pedestrian Crossing with Obstacles

	Path Length (m)	Completion Time (s)	Avg. Ped. Clearance (m)
Safety-Aligned (SA)	16.58±1.06	18.00±0.76	2.62±0.06
Goal-Aligned (GA)	14.12±0.34	12.38±1.00	2.36±0.06

		% Intrusions	
	Min. Ped. Clearance (m)	Intimate Space	Personal Space
Safety-Aligned (SA)	1.67±0.03	0.00±0.00	0.00±0.00
Goal-Aligned (GA)	0.96±0.45	0.03±0.07	8.03±4.14

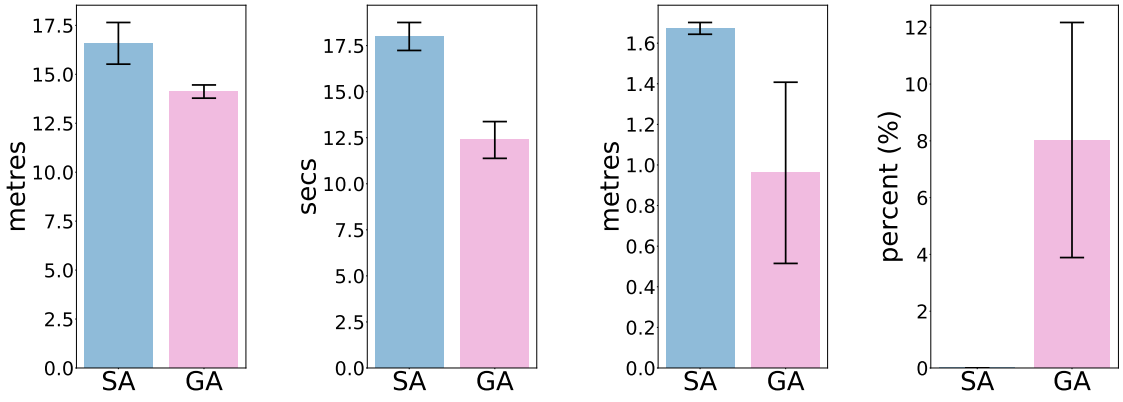

(a) Path Length (b) Completion Time (c) Min. Pedestrian Clearance (d) Personal Space Intrusion

Figure 5.9: Navigation performance metrics for safety-aligned (SA) and goal-aligned (GA) assistance policies in the multiple-pedestrian crossing scenario with obstacles.

5.4 User Study Design

A within-subject repeated measures design was used to evaluate the impact of adaptive navigation assistance on driving performance, human-robot cooperation, and user preference in a social navigation task. The Institutional Review Board (IRB) at Worcester Polytechnic Institute approved the study design and procedure.

The study hypotheses are as follows: First, we hypothesize that the objective-aligned assistance mode will improve driving performance over the contrasting assistance mode (**H1**). We also anticipate that participants will report considerably higher levels of cooperation and preference for objective-aligned assistance mode over contrasting assistance mode (**H2**). Furthermore, we hypothesize that the assistance adaptation will have a greater impact in H1 and H2 when participants are cognitively burdened with a secondary task (**H3**).

5.4.1 Experimental Setup

The pilot user study was designed as a virtual social navigation task just as in Chapter 4. Five (5) participants (4 males and 1 female) were recruited for the user study from the university student community. All participants stated that they had more than four years of driving experience. Participants controlled a differential drive mobile telepresence robot within a dynamic, human-populated virtual environment to navigate from a starting point in a hall to a specified goal location in a safe and socially acceptable manner. The populated environment and the virtual mobile robot were simulated with Gazebo Simulator. A forward-facing camera mounted on the mobile robot provided visual feedback to participants through a 24-inch computer monitor (see Fig. 4.3 (left)). A visual overlay of the visual guidance methods was displayed on the camera using OpenCV [137].

A conference hall style virtual environment was used with tables and walking space (see Fig. 4.3 (right)). In order to prevent participants from memorizing the hall layout across trials, two different layouts were adopted and randomly applied. Based on the social force model [85], we modeled the virtual pedestrian motion using

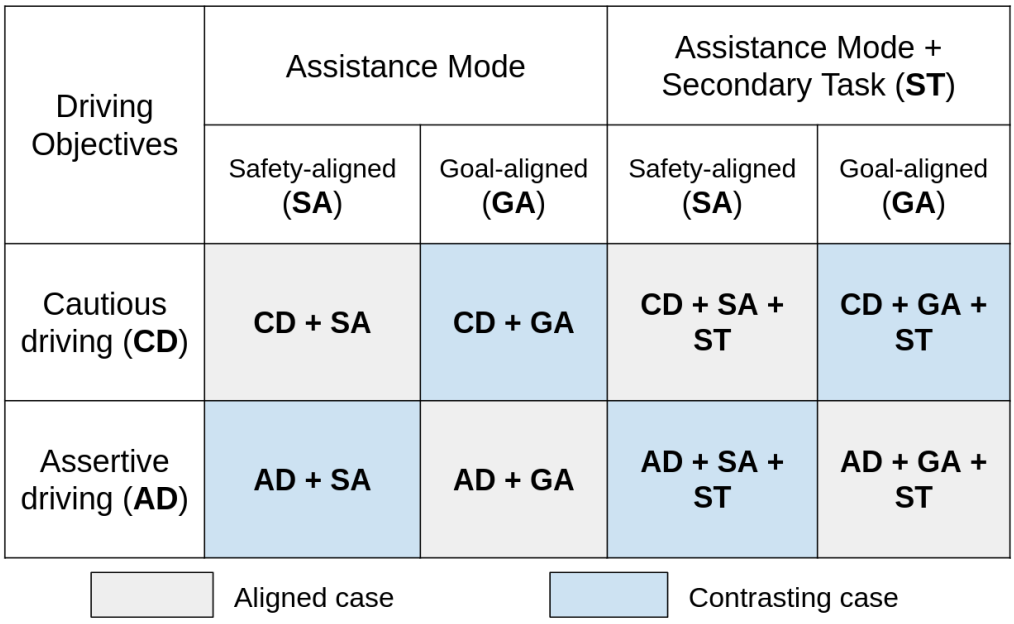

Figure 5.10: Pictorial description of the experimental conditions comprising 2 driving objectives, 2 assistance modes and 2 secondary task states (with or without). Aligned and contrasting cases are color-coded with light grey and light blue respectively.

a Gazebo actor plugin [3] [4] to enable reactive navigation behavior. Human control inputs and haptic guidance forces were applied through a commercially available haptic-enabled device (Novint Falcon, Novint Technologies). For robot control, only two of the 3-DOFs on the haptic interface are mapped to the differential-drive robot controller using a position-velocity mapping.

5.4.2 Experimental Conditions

Eight (8) conditions were defined in this study based on three criteria: driving objective applied, assistance mode used and presence of a secondary task (see Fig. 5.10).

1. **Driving Objectives:** Two driving objectives—Cautious and Assertive driving—were explored in this study to represent two common driving styles exhibited

[3] https://github.com/robotics-upo/gazebo_sfm_plugin
[4] https://github.com/robotics-upo/lightsfm

by humans in interaction with others either while walking or driving a vehicle [134].

(a) **Cautious driving (CD)**: For this objective, participants were prompted to drive "as cautiously as possible" around pedestrians. To induce this behavior, a proximity score, which increases based on the robot's proximity to surrounding pedestrians, is presented on the screen as a performance feedback (see Fig 5.11).

(b) **Assertive driving (AD)**: For this objective, participants were prompted to drive with the intent to reach the goal as quickly as possible while avoiding collisions or intrusions with pedestrians. Similarly, to induce this behavior, a timer was presented on the screen to provide feedback on their performance (see Fig 5.11).

2. **Assistance Modes:** The two navigation assistance policies—Safety-aligned and Goal-aligned—defined and evaluated earlier in this chapter are applied as the assistance modes in the pilot user study.

   (a) **Safety-aligned assistance (SA)**: This assistance mode corresponds to the cautious driving behavior and prioritizes larger clearance from pedestrians and obstacles as well as penalizing frontal passing at the expense of longer paths and completion time (See Section 5.3).

   (b) **Goal-aligned assistance (GA)**: This assistance mode corresponds to the goal driving behavior and prioritizes goal-directed paths with just enough deviation to avoid collision or intimate intrusion (See Section 5.3).

3. **Secondary Task (ST):** A cognitively demanding secondary task was included to the experiment to purposefully distract the participant and increase

their cognitive burden. Specifically, participants were asked to answer simple arithmetic questions (addition and subtraction of two numbers) presented at the bottom right corner of the visual display window (see Fig 5.11). The simple arithmetic questions are displayed at regular intervals (i.e., approx. six seconds) and participants were required to provide their answer verbally. This secondary task was used to simulate real-world scenarios where human operators may get both visually and cognitively distracted by social interaction or environment inspection while driving a vehicle or robot.

Conditions were further categorized into **aligned** and **contrasting** assistance cases based on the matching between the driving objective and the assistance mode. For instance, a condition is considered aligned if the participant is asked to drive cautiously (CA) (driving objective) while the assistance mode provided is safety-aligned (SA) (assistance mode). This also applies with and without the secondary task as can be seen with the color-coding in Fig. 5.10.

5.4.3 Experimental Procedure

Participants signed the IRB-approved informed consent form upon arrival at the study site. Afterwards, we began the study with an explanation of the study procedure and how to operate the virtual mobile robot. There were four phases in the study: familiarization, learning, validation, and testing.

Familiarization Phase: To get familiar with the robot controls, participants were allowed to drive it for up to 5-7 minutes in an open space (with no obstacles or other people). This phase was completed manually, without navigation assistance. After the participants are confident controlling the robot, they are moved onto the next step.

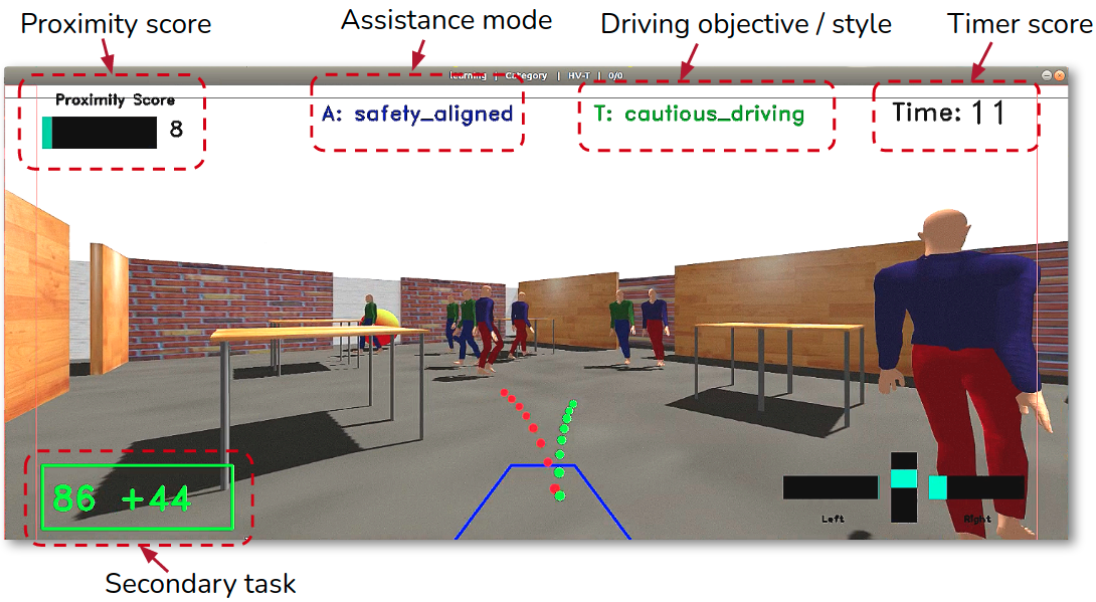

Figure 5.11: Visual display window showing the camera feeds from the forward-facing camera on the robot as well as other important visual features for the experiment.

Learning Phase: During this phase, the participants underwent a standardized training protocol in order to ensure they all reached a minimum skill level and were familiar with the experimental conditions. First, participants practiced freestyle driving towards a defined goal location in the virtual environment with only static pedestrians. The two assistance modes (safety-aligned and goal-aligned assistance) were introduced. They were then instructed to practice deliberate driving using two driving objectives (cautious and assertive). Two scoring measures—proximity score and timer score—provided immediate feedback to the participants on how well they were driving cautiously and assertively respectively (see Fig. 5.11). Finally, participants were introduced to the secondary task. They first performed the secondary task separately in order to obtain a baseline performance as suggested in [138]. Thereafter, they practiced driving in both driving objectives while performing the secondary task. In this phase, participants completed 24 driving trials, each of which took approximately 20 seconds.

Validation Phase: Before moving on to the testing phase, each participant was required to complete a validation phase. Participants in the validation phase were required to score above a minimum threshold score for proximity and time with no collision on at least four out of six driving trials. If they did not meet this requirement, they were given more practice before re-validation.

Testing Phase: In this phase, participants drove in a total of eight (8) conditions: **2** driving objectives X **2** assistance modes X **2** (with or without) secondary task, with two trials per condition, resulting in 16 trials in total. As shown in Fig. 5.10, half of the conditions were aligned cases (i.e., CD+SA, AD+GA, CD+SA+ST, AD+GA+ST), while the other half were contrasting cases (i.e., AD+SA, CD+GA, AD+SA+ST, CD+GA+ST). In order to avoid ambiguity, participant were informed what condition they were driving in through on-screen indicators (see Fig. 5.11). The order of the conditions was randomized and counterbalanced in order to reduce learning effect, recency bias, and fatigue. Break time options were provided in order to prevent fatigue. After each condition, participants filled out a post-condition questionnaire to provide subjective responses to their experience. Upon completion of all eight conditions, participants completed a post-study questionnaire in which they ranked the two assistance modes based on several criteria. The entire user study took approximately 1.5 hours to complete, depending on the participants.

5.4.4 Measures

Objective Measures

The same four (4) objective measures used in Section 5.3 are computed to evaluate the driving performance (both driving efficiency and safety) in the experiment. They are as follows: (i) *Path length (metres)*, (ii) *Task completion time (secs)*, (iii) *Average*

and minimum pedestrian clearance (metres), (iv) *Proxemics space intrusions (%).*

Subjective Measures

Post-condition Questionnaire: At the end of the two trials for each condition, participants completed the following questionnaire using a 7-point likert scale to evaluate the condition:

1. *System helpfuless and ease of use*: (1 - Strongly disagree, 7 - Strongly agree)
    - *Helpfulness*: "This assistance mode was very helpful for achieving the driving objective."
    - *Ease of use*: "I found this assistance mode to be easy to use for navigating the robot."
2. *Level of cooperation*: "To what extent did you cooperate or agree with the assistance mode in the task?" (1 - Never agreed, 7 - Always agreed)
3. *Level of difficulty*: "How difficult did you feel this trial was in achieving your driving objective?" (1 - Not difficult at all, 7 - Very difficult)

Post-block Questionnaire and Interview: After each participant completed a driving objective using both assistance modes, they completed the following questionnaire to reflect on their experience and rank the assistance modes.

1. Rank the two assistance modes in terms of the *most cooperation (or agreement)* with the navigation assistance in the task.
2. Rank the two assistance modes in terms of the *most preferred* for completing the task.

After the user study, we conducted a short, semi-structured interview with each participant to learn why they ranked the assistance modes and other follow-up questions.

5.5 Results

Objective Measures

For the cautious driving objective (CD), we evaluated the impact of aligned and contrasting assistance by comparing the safety-related metrics between CD+SA and CD+GA as well as in the secondary task cases, between CD+SA+ST and CD+GA+ST. We found no significant effect on the minimum pedestrian clearance, intimate intrusions and personal intrusion metrics (Table 5.5). Fig. 5.12 shows bar plots of min. pedestrian clearance and personal space intrusions across the cautious driving conditions. While plagued with high variability, we found a positive trend in the personal space intrusion metric (Fig. 5.12(b)).

In particular, CD+SA (cautious driving with safety-aligned assistance) had the lowest value of personal space intrusion, rising with CD+GA (cautious driving with assertive-aligned assistance) and rising even more with the inclusion of the secondary task. Interestingly, we found no significant effect of the secondary task (i.e., with or without secondary task) on navigation safety, although we observe a positive trend with secondary task conditions having higher rate of personal space intrusions.

For the assertive driving objective (AD), we evaluated the impact of aligned and contrasting assistance by comparing the navigation efficiency-related metrics between AD+SA and AD+GA as well as in the secondary task cases, between AD+SA+ST and AD+GA+ST. As with the cautious driving cases, we found no significant effect of assistance mode on the path length and completion time metrics

Table 5.5: Cautious Driving

Measures			Secondary Task (ST)	
	CD+SA	CD+GA	CD+SA	CD+GA
Objective Measures				
Path Length (m)	15.34±0.93	17.58±3.37	19.52±4.59	16.71±3.35
Completion Time (s)	15.17±1.12	16.09±2.63	21.37±7.45	20.10±5.21
Avg. Ped. Clearance (m)	2.71±0.11	2.77±0.27	2.74±0.18	2.76±0.26
Min. Ped. Clearance (m)	1.44±0.23	1.31±0.24	1.31±0.17	1.24±0.16
Intimate Intrusions (%)	0.01±0.03	0.01±0.03	0.00±0.00	0.00±0.00
Personal Intrusions (%)	0.00±0.00	0.59±0.87	2.86±2.45	3.86±3.27
Subjective Measures				
Helpfulness	4.80±1.48	4.80±1.79	4.80±1.92	5.60±0.89
Ease of Use	6.00±1.41	5.80±1.79	5.00±2.35	5.60±1.34
Cooperation	5.20±1.92	5.20±1.79	4.60±2.51	5.20±1.30
Level of Difficulty	2.20±0.84	2.80±1.79	5.80±1.30	4.60±2.07

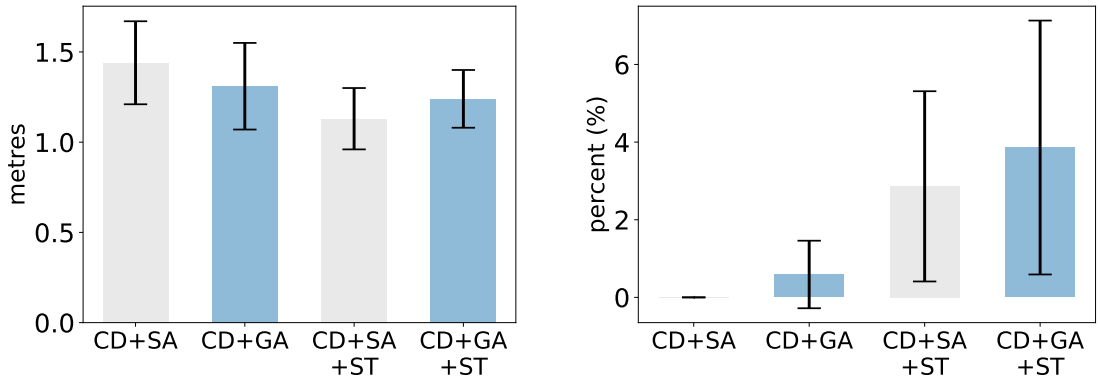

(a) Min Ped. Clearance (metres)

(b) Personal Space Intrusions (%)

Figure 5.12: Comparison of two main safety metrics across **Cautious driving (CD)** experimental conditions

(Table 5.6 and Fig. 5.13). We observed a slight increase (although not statistically significant) in the completion time between AD+SA ($M = 14.75, SD = 2.24$) and AD+GA ($M = 13.65, SD = 1.76$) as well as between AD+SA+ST ($M = 18.30, SD = 7.58$) and AD+GA+ST ($M = 16.42, SD = 4.57$) (Fig. 5.13(b)).

Table 5.6: Assertive Driving

Measures			**Secondary Task (ST)**	
	AD+SA	AD+GA	AD+SA	AD+GA
Objective Measures				
Path Length (m)	16.82±1.81	16.74±2.12	18.83±5.42	17.34±2.88
Completion Time (s)	14.75±2.24	13.65±1.79	18.30±7.58	16.42±4.57
Avg. Ped. Clearance (m)	2.66±0.14	2.55±0.14	2.58±0.30	2.46±0.23
Min. Ped. Clearance (m)	1.39±0.35	1.32±0.18	1.06±0.35	1.08±0.28
Intimate Intrusions (%)	0.00±0.00	0.00±0.00	0.01±0.03	0.00±0.00
Personal Intrusions (%)	1.62±3.10	2.65±2.56	6.47±6.95	5.83±4.14
Subjective Measures				
Helpfulness	4.40±2.07	5.00±0.71	4.20±1.10	2.80±0.84
Ease of Use	6.00±1.00	5.80±1.10	5.20±1.30	4.20±1.92
Cooperation	5.00±1.87	4.80±0.84	5.00±0.71	3.60±0.55
Level of Difficulty	4.60±1.52	4.20±0.45	6.60±0.89	6.00±0.71

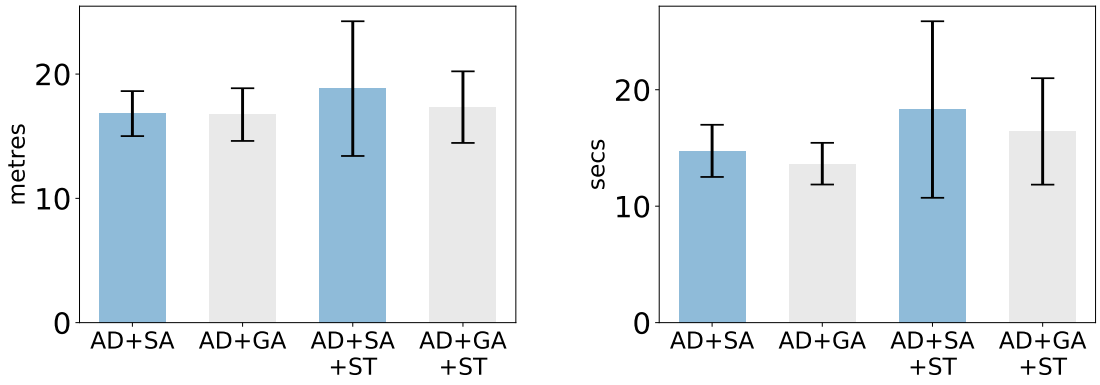

(a) Path Length (metres)

(b) Completion Time (secs)

Figure 5.13: Comparison of two main navigation efficiency metrics across **Assertive driving (AD)** experimental conditions

Subjective Measures

We analyzed the subjective measures to evaluate the effects of aligned and contrasting assistance on user perception of the assistance helpfulness, ease of use, level of cooperation with the assistance and level of difficulty. Starting with the cautious driving objective (CD), no significant effects of assistance mode were found across

conditions and metrics (Table 5.5). However, we note a slight positive trend between conditions with secondary task (CD+SA+ST and CD+GA+ST) across helpfulness, ease of use and cooperation, with slightly higher values using goal-aligned assistance (GA) over cautious-aligned assistance (CD). Additionally, participants reported the secondary task cases to have higher level of difficulty than the non-secondary task cases. This may serve as a manipulation check for the impact of the secondary task on the participant's workload and task difficulty.

For the assertive driving objective (AD), while no significant effects of assistance mode were found in the non-secondary task case, we found assistance adaptation had a marginal effect in the assistance helpfulness and cooperation ratings between CD+SA+ST and CD+GA+ST, $t(4) = 2.7, p = 0.052$, for both helpfulness and cooperation.

Fig. 5.14 shows the user preference ranking in both the non-secondary task and secondary task cases. As can be seen, all participants reported to prefer SA assistance in the cautious driving cases both with and without the secondary task. Whereas 60% of participants preferred SA over GA in assertive driving cases for non-secondary cases and 80% of participants preferred SA over GA with the secondary task.

5.6 Discussion

Our contribution in this chapter is to propose a socially aware navigation assistance approach that is adaptable to different distinct driving behaviors. The study considered two common driving behaviors: cautious driving and assertive driving. Two assistance policies—Safety-aligned and Goal-aligned—were designed to correspond to the cautious and assertive driving behaviors respectively. We subsequently

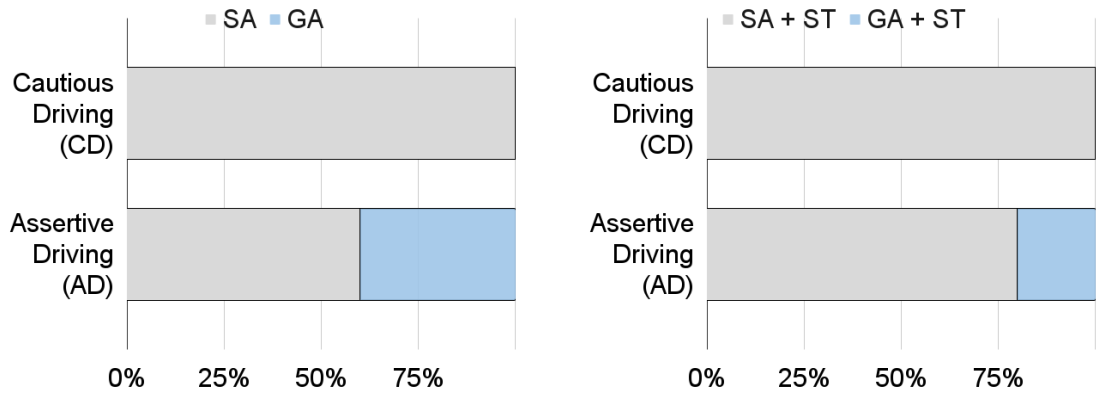

(a) Non-secondary task cases

(b) Secondary task cases

Figure 5.14: User preference ranking in both non-secondary task (a) and secondary task cases (b).

evaluated their navigation performance in four typical navigation scenarios utilizing objective metrics related to path efficiency and safety during social navigation. Using the social- and goal-related objective functions described in Section 5.2, we found that our adaptive SA-RVO approach was able to capture distinct characteristics of cautious and assertive driving. While the results show that hand-crafted cost weights produced reasonable behaviors, future work should consider using a learning-based approach to automatically determine the navigation cost weights based on expert human demonstrations of various behaviors [135, 136].

We further conducted an pilot user study to evaluate the impact of assistance adaptation on driving performance, human-automation cooperation and user preference. We first hypothesized that the aligned assistance modes will improve driving performance (both in efficiency and safety) over the contrasting assistance modes. According to our results, however, we observed no significant effect of assistance adaptation on driving performance, i.e., for efficiency in assertive driving, neither path length nor completion time reduced significantly when using goal-aligned assistance (GA) as opposed to safety-aligned assistance (SA). The same was observed

for navigation safety in cautious driving (see Fig. 5.12 & 5.13). A possible reason for this may be the actual driving behavior employed by the participants. While we instructed and trained participants on how to drive both cautiously and assertively in the learning phase, our analysis of their driving behavior in a manual case (i.e., without navigation assistance) showed that there was no significant difference in their navigation efficiency or safety between their cautious driving and assertive driving (AD) trials. Table 5.7 shows the mean and standard deviation values for both CD and AD across the driving performance metrics. We observe large variability in the results across participants, further obscuring any significant difference in driving behavior. Possible explanations for this may be that (i) participants defaulted to their normative driving style during the trials and thus didn't exhibit distinct behaviors, (ii) the variability in driving styles overpowered the limited sample size, (iii) the sample population—drawn primarily from young adults—tend to generally have higher reaction times in driving [139] and do so consistently in a more aggressive manner compared to older populations [140]. A few directions for future investigation can be considered. First, we consider streamlining the navigation task in order to focus more on single, pairwise social interactions where remote driving behaviors may be more distinct and easier to manipulate. Secondly, we could explore recruiting a more diverse participant pool across age groups in our future experiments. Furthermore, we can explore comparing different control interface devices in the pilot user study to ensure that the interface device currently in use is not introducing a limitation on the ability of participants to control the robot.

Table 5.7: Manual Driving: Comparison between Cautious and Assertive Driving

	Path Length (m)	Completion Time (s)	Avg. Ped. Clearance (m)
Cautious Driving (CD)	16.96±3.42	21.23±8.00	2.57±0.47
Assertive Driving (AD)	18.36±5.23	16.49±6.38	2.53±0.34

	Min. Ped. Clearance (m)	% Intrusions	
		Intimate Space	Personal Space
Cautious Driving (CD)	1.17±0.43	0.08±0.44	4.586±7.266
Assertive Driving (AD)	0.99±0.47	0.74±2.872	6.303±6.707

Regarding user preference and human-automation cooperation, we hypothesized that participants will report considerably higher levels of preference and cooperation for the objective-aligned assistance modes (i.e., CD+SA and AD+GA) over the contrasting assistance modes (i.e., CD+GA and AD+SA). The result of our subjective ranking only partially supports the hypothesis. In the case of user preference, all five participants ranked SA as preferred over GA for cautious driving (CD) tasks. In the post-study interviews, three participants mentioned that the guidance cues of SA were more helpful especially in cases when the pedestrians were outside their field of view (FOV). This echoes remarks reported by participants in the user study of Chapter 4.

When considering assertive driving (AD), however, three participants (60%) still ranked SA (the contrasting assistance) as more preferred over GA (the aligned assistance). When asked the reason for their ranking, they reported that the additional 'safety' against collisions provided by SA helped them even while heading towards the goal assertively. However, two participants, who preferred GA over SA, mentioned that the goal-oriented guidance of GA was preferred in assertive driving. This suggests that participants leveraged the assistance modes for different purposes. Additionally, in considering human-automation cooperation, our subjective metric revealed that no significant differences between aligned and contrasting assistance cases (see Table 5.5 & 5.6). In general, we found no significant distinction in participant responses across the subjective measures in the experimental conditions without the secondary task cases. However, in the assertive driving cases with secondary task, we found that SA had a marginally higher cooperation rating than

GA ($t(4) = 2.7, p = 0.052$). This may correspond to why participants preferred SA over GA even while requested to drive assertively.

The third hypothesis for the study was that assistance adaptation would have a greater impact on driving performance and user perceptions when there is a secondary task, as the participants would have a greater cognitive load. Our findings suggest that the participants' interactions with aligned and contrasting assistance modes were little influenced by the secondary task. In part, this may be due to the fact that rather than relying more on assistance due to increased cognitive load and distraction, the participants ignored it further. As reported in the post-study interviews, some participants weren't paying attention to the assistance during the secondary task cases and couldn't differentiate between them. However, some participants reported that while they ignored the visual guidance cues due to the visual distraction and cognitive load, they tended to rely on the haptic guidance on their hands.

5.7 Chapter Summary

In this chapter, we presented an adaptive shared autonomy approach for navigation assistance in dynamic, human-populated environments. This work extends the *SocNavAssist* approach presented in Chapter 4 to account for distinct driving behaviors/styles by incorporating socially-relevant objective functions that characterize these driving objectives. Specifically, two assistance policies—safety-aligned and goal-aligned—were developed in this study based on hand-designed cost function weights and evaluated in autonomous mode across four typical navigation scenarios. The evaluation results showed that the assistance policies portrayed the expected behaviors corresponding to cautious and assertive driving behaviors. We further

conducted an pilot user study ($n = 5$) to evaluate how the adaptive assistance affects driving performance (efficiency and safety), human-automation cooperation and user preference in a simulated social navigation task. Our preliminary results showed that more participants preferred the safety-aligned assistance mode in both cautious driving (aligned case) and assertive driving (contrasting case) due to the safety advantage. However, our results did not find any significant differences in driving performance (either in safety or navigation efficiency) on account of adaptation between aligned and contrasting assistance modes. This chapter sets preliminary work in evaluating how remote operators interact with different navigation assistance modes based on adaptation to common driving behaviors in social navigation. Future work would include more participants and implementation in a real-world navigation scenario.

Chapter 6

Learning-based Computational Human Driver Modeling for Assistive Driving Systems

6.1 Introduction

The goal of advanced driving assistance systems is to improve both human safety and overall mobility experience. However, these systems redefine how humans traditionally interact with their vehicles while driving. Understanding this interaction is crucial to the design and evaluation of the next generation of intelligent assistive driving systems.

Existing approaches for studying driver-vehicle interaction include the use of digital human driver models because simulation tests performed using real human drivers are costly, time-consuming and strictly limited due to safety constraints. Such surrogate models provide a safe and cost-efficient method for approximating realistic driver behavior in simulation. A review of the literature shows how the

use of digital driver models contribute to the design of active driver safety systems [93, 95], the usability and intelligence of driver-assistance systems [101], as well as vehicle ergonomics analysis [97, 98]. However, existing digital driver models do not consider the complex bi-directional, physical interactions that occur between the human driver and the driving interfaces (steering wheel and brake/throttle pedals) during naturalistic driving.

In recent work, Kimpara et al [2] proposed a novel simulation framework, Human Model-based Active Driving System (HuMADS), which integrates an active human driver model with a vehicle dynamics model to render high-fidelity simulation of driver-vehicle interaction. This chapter extends that work by addressing the problem of how to generate human-like driver control motions for a simulated driver model. This is achieved by taking a data-driven approach to learn motion planner policies for the two primary driving functions: steering wheel handling and pedal pressing. Specifically in this section, the following contributions are presented:

- Implementation of a data processing pipeline to identify the characteristic driver control styles (i.e., steering handling and brake/throttle pedal switching styles) from demonstration data obtained from experienced drivers.

- Analysis of the correlation between resulting characteristic steering handling styles, driving maneuver behaviors and driving contexts. This enables the mapping of road and driving task scenarios to respective handling styles.

- Learning driving motion primitive models based on the identified driver control styles, in order to construct the motion primitive library to enable realistic vehicle control motion generation on our simulated driver model [2].

The significance of the proposed approach is that it provides automotive researchers with a novel avenue to generate realistic driving behavior on a digital

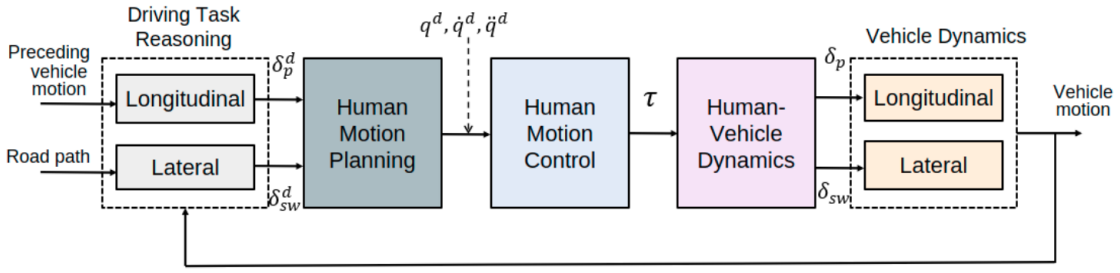

Figure 6.1: Driver-vehicle control framework for the Human Model-based Active Driving System (HuMADS) [2]. This framework enables the simulation of realistic driver-vehicle interaction in driving tasks.

human driver model in simulation and then perform more comprehensive analyses on the design and usability of advanced driver-assistance systems. For instance, in Level 2 autonomy systems [141], where both the human driver and system autonomy jointly share control of the vehicle, understanding how haptic authority on the shared steering wheel interface affects driver workloads is crucial to system usability and safety [142]. Other promising applications include leveraging these realistic simulations to improve vehicle ergonomics, occupant packaging and safety system design.

This chapter is organized as follows: the integrated framework for human-vehicle interaction is summarized in Section 6.2. The imitation learning pipeline for identifying, analyzing and modeling driver control styles is presented in Section 6.3. Results are presented and discussed in Sections 6.4 and 6.5, while concluding remarks are presented in Section 6.6.

6.2 Human-Vehicle Interaction Framework (HuMADS)

This section introduces the HUman Model-based Active Driving System (HuMADS) [2], which we have proposed as the framework for simulating realistic whole-body motion coordination in physical interactions between human driver and vehicle (Fig. 6.1). This integrated driver-vehicle model is adapted as a mid-sized human driver in a regular passenger vehicle cockpit. The human driver model comprises 37 degrees of freedom (DOF), actuated by torque actuators at each coordinate joint (Fig. 6.2). The vehicle model geometry and properties are obtained from the finite element model of a 2012 Toyota Camry. It includes vehicular components such as driver seat, pedals, steering wheel, etc. The following subsections will briefly describe each component of the HuMADS framework as illustrated in Fig. 6.1:

Driving Task Reasoning Layer: The driving task reasoning layer replicates the decision-making component of a human driver. It computes the reference pedal δ_p^r and steering angles δ_{sw}^r for longitudinal and lateral motion control respectively. The longitudinal motion controller is based on a car-following model following Saigo's model [143, 144]. The inputs to the model are the velocity of the preceding vehicle and the road pathway. The lateral motion controller is a forward-gaze steering model on the highway based on the theory of vehicle dynamics described by Abe [145].

Human Motion Planning Layer: This layer computes the coordinated *vehicle maneuver motions*, i.e. joint motion trajectories (angles, velocities and accelerations) of the driver model's whole body, to achieve the desired steering and pedal motions. Due to the complexity of planning multi-joint coordinated human motion especially in constrained contexts like driving, an imitation learning approach is

adopted in this layer and will be described in Section 6.3.

Human Motion Control Layer: This layer computes the desired joint torques τ given the desired joint angles q^d, angular velocities $\dot{q}^d$, and angular accelerations $\ddot{q}^d$ of the vehicle maneuver motion as well as external forces. The desired joint torques for the whole-body driver model are computed to maintain its body posture while tracking the desired arm/hand and foot trajectory for pedal pressing and steering respectively through inverse dynamics [2]. Inverse dynamics [146] adopts the feedback linearization approach to express the joint torques τ as the linear function of model states and their derivatives along with external forces, $f(q, \dot{q}, \ddot{q}, F_{ext})$. The human driver model is mathematically modelled as an n-link multi-body system expressed as:

$$M(q)\ddot{q} + C(q, \dot{q}) + N(q) + J^T F_{ext} = \tau \tag{6.1}$$

where q is the state vector in joint space, M is the mass matrix, C is the velocity vector which is the product of the Coriolis and Centrifugal force matrix, and $\dot{q}$ is the state velocity vector, N is the gravity vector, J^T represents the system Jacobian matrix, F_{ext} captures the external forces (contact forces between the human model and the vehicle such as thigh and seat cushion forces), and τ is the joint torque vector.

The nonlinearities in the dynamic system are resolved by computing the control input, τ_c, which approximates the nonlinear dynamics and then commands a control law, a_q:

$$\tau_c = \hat{M}(q)a_q + \hat{C}(q, \dot{q}) + \hat{N}(q) + \hat{J}^T F_{ext} \tag{6.2}$$

$$a_q = \ddot{q}^d - K_D(\dot{q} - \dot{q}^d) - K_P(q - q^d) - K_F J^T(F_{ext} - F_{ext}^d) \tag{6.3}$$

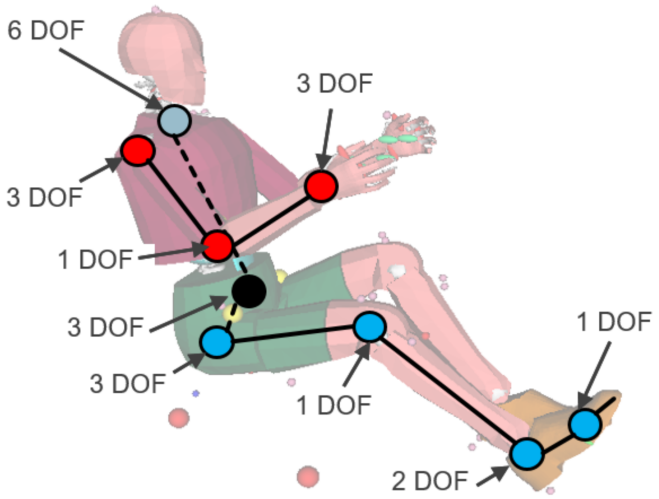

Figure 6.2: Kinematic model of the human driver based on full body models available on OpenSim [3]. The model comprises 37 degrees of freedom (DOF) actuated by coordinate torque actuators.

where $\hat{M}$, $\hat{C}$, $\hat{N}$ and $\hat{J}$ are approximate system dynamics obtained from the forward dynamics simulator, K_P, K_D and K_F are constant diagonal gain matrices for position, velocity and forces, q^d, $\dot{q}^d$ and $\ddot{q}^d$ are vectors of desired joint position, velocity and acceleration respectively, F^d_{ext} is the desired contact force vector.

Driver Dynamics Layer: The driver dynamics layer uses the whole-body human model to simulate the human driver's forward kinematics and dynamics, and the resulting steering and pedal motions. This layer simulates the dynamic interaction between the driver model and the vehicle cockpit. It also includes the contact forces on the driver seat, floor, pedals and steering wheel. This enables us analyze internal parameters such as joint reaction forces and muscle activity, which can be used to investigate the comfort/potential injury resulting from the driver's reactive motion.

Vehicle Dynamics Layer: The driver's commanded pedal angle δ_p and steering wheel δ_{sw} angle, resulting from the maneuver motions computed in the driver

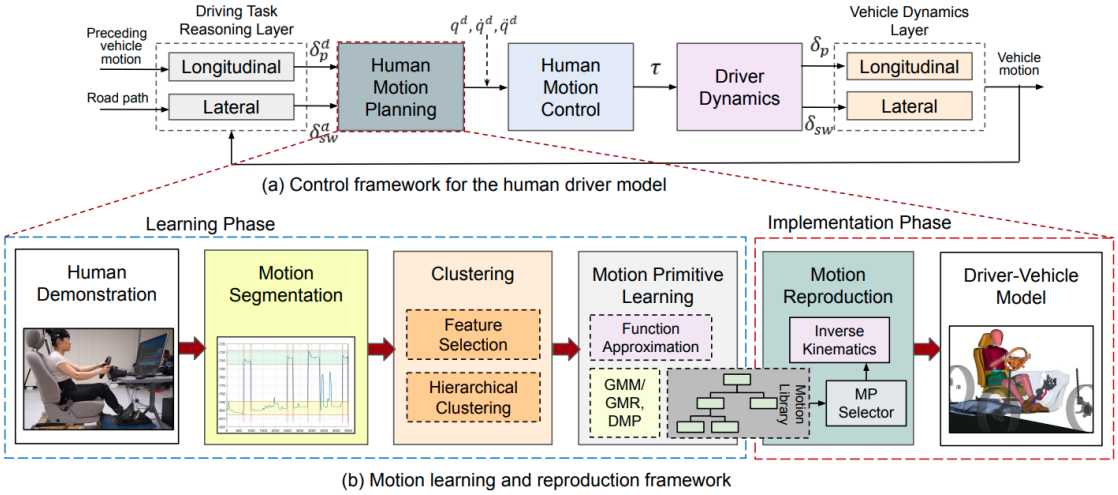

Figure 6.3: Framework for simulating realistic driver-vehicle interaction in driving tasks. (a) shows the control framework for the human driver model (HuMADS) [2]. This framework enables the rendering of whole-body coordination in driving tasks. (b) expands upon the Human Motion Planning layer to show the motion learning and reproduction framework using an imitation learning approach.

dynamics layer, are fed to the vehicle dynamics layer. Using the vehicle model proposed in [144], the vehicle dynamics (i.e. vehicle longitudinal and lateral acceleration, velocity) are determined from the commanded steering and pedal motions.

6.3 Learning and Reproducing Vehicle Maneuver Motions

This section presents our proposed methodology for identifying and learning the driver control motion styles as motion primitives from exemplar demonstration data from experienced drivers. To be clear in description, we define the following terms:

- *Driver control motion* refers to movement of the driver's arm/hands and leg(s)/feet to manipulate the steering wheel and pedals respectively
- *Driver control style* refers to a particular distinctive way a driver coordinates

their arm/hands and leg(s) motion in controlling the vehicle

- *Driving maneuver behavior* refers to high-level operational driving tasks as observed from the vehicle (e.g. lane keeping, lane change, discrete turning)

Our proposed approach consists of five steps (see Fig. 6.3(b)):

1. **Data collection:** we collected whole-body motion data from experienced drivers while driving a simulated vehicle on fixed-base driving test bed.
2. **Motion segmentation:** the motion data was then classified and segmented based on the characteristic *driving maneuver behaviors*.
3. **Clustering:** the segmented data were clustered into distinctive *driver control styles*.
4. **Motion primitive learning:** we extracted the regularity and variability of each control style cluster group using imitation learning.
5. **Motion reproduction:** Finally, a motion primitive library is built for reproducing contextual driver control motions in simulation.

The following subsections describe each step of the learning process.

6.3.1 Experiment and Data Collection

An experiment was conducted to collect the data of natural vehicle maneuver motions in typical driving tasks. Therein, $n = 8$ (5 Males, 3 Females; Age: 25 ± 2.2 years) healthy participants with at least two years of licensed driving experience were recruited. The average length of driving experience was 6.8 ± 2.3 years. During the experiment, the participant drove in a fixed-base driving simulation test bed (see Fig. 6.4(left)). The operator console supports the control of a vehicle within

Figure 6.4: A participant is driving in fixed-base simulation testbed within motion capture laboratory. (Left): Experimental setup. (Right): Screen capture of the driving simulator game.

a driving simulation environment (City Car Driving v1.5 Gaming Software) using Logitech G920 driving hardware and displays the simulated driving context via a 21" monitor (Fig. 6.4(right)).

Task description: The participants were asked to drive in three different driving contexts: *highway*, *in-city*, and *country road*. The participants drove under each condition for six minutes. These contexts were selected to capture a wide range of driving behaviors under various road and traffic conditions. To avoid fatigue, participants were allowed to take breaks between driving sessions.

Intake Survey: After giving informed consent, participants were asked to complete a survey to collect demographic information (age, gender) and a description of their driving experience, style and video gaming experience.

Practice session: The participants were required to pass a practice session before participating in the study. For each condition, the participant was allowed a maximum of 10 attempts to complete 3 successful practice runs. A practice run is considered successful if the participant drives for 2 minutes without getting into

an accident or accumulating more than 30 driving errors including driving against traffic, lane changing without signaling, etc. (reported by the gaming software). Participants who were unable to pass the practice session were excluded from the study.

Data Collection: A motion capture system (VICON Vero, 10 cameras) was used to track the upper and lower body motions of the participants at 100Hz. We simultaneously recorded the participant motions using video camera and driving context using screen capture, to facilitate data segmentation and labeling, and to match driver's motions to the driving context. The steering wheel angle, throttle opening and brake pedal displacement data were recorded through the Logitech G920 driving hardware at a rate of 100Hz. In total, 144 minutes (8 participants $\times$ 3 driving contexts $\times$ 6 minutes) of driving data was recorded. A 2nd-order low-pass butterworth filter with a cutoff frequency of 5 Hz was used for removing the high frequency noise from the recorded data.

6.3.2 Segmentation and Classification of Driving Motion Data

We segmented the continuous sequence of driving motion data and investigated the features that can distinguish different *driver control styles*. A feature vector thresholding method was used to segment the continuous sequence of driving motion data based on the characteristics of the data. To effectively determine feature threshold values, we first visually inspected the video recordings of the data and manually labeled them by their distinctive *driving maneuver behaviors*. The classes identified for steering maneuvers were as follows: (1) lane keeping on a straight road (LK-SR), (2) lane keeping on a curved road (LK-CR) or lane-change, and (3) discrete

turns (DT). We identified the steering wheel angle to be the characteristic feature and learned the threshold values from the manually labeled data. These threshold values were further used to determine the segment transition points in the data.

For the throttle/brake maneuvers, we noticed that drivers typically perform two basic foot movements: switching from one pedal to another, and pressing on a pedal. Our objective here is to extract motion segments when the driving foot is in the switching movement. We defined the foot position as the characteristic feature for data segmentation. Based on knowledge of the fixed positions of pedals, threshold values are set to define the segment transition points in the data. The data is thus segmented and classified into three characteristic behaviors: throttle-to-brake motion, brake-to-throttle motion and pedal pressing motion using the pre-defined threshold. The motion data within each segment is interpolated to a fixed length of 200 frames and normalized to ensure alignment across different demonstrations.

6.3.3 Clustering of Motion Segments

The resulting sequence of motion data segments are clustered based on their discriminatory features. This process aims to identify a set of *driver control styles* for wheel-steering and pedal-pressing. Because of the simplistic nature of the foot switching movement, we directly used the derived classes during segmentation for modeling and learning the foot switching motion primitives. Thus, this section will focus on clustering to extract distinctive steering handling styles from the data. For data processing, we employed the Statistics and Machine Learning Toolbox in MATLAB [147].

Feature selection

To obtain the natural clustering in the segmented motion data set, we defined a broad set of features and then manually labelled a subset of the data based on video inspection. These features include raw data features (3D position range of both hands, both elbows; minimum distance between hands; absolute distance covered by hands, etc.), statistical features (mean and standard deviation of distance between hands, hand velocity; correlation between hand 3D positions, hand velocities etc.) and other features such as steering wheel range, the arm swivel angle range which measures the arm posture by the rotation angle of elbow about the shoulder-wrist axis [148], and the steering angle range.

Using a filter feature selection method [147] on the partially labelled data, we selected the relevant features which have the highest discriminatory power in the distinction of patterns in the data. The resulting set of features[1] are shown in Table 6.1 and described in Fig. 6.5.

ID	Features
1	Position range of right hand in X-direction
2	STD of distance between both hands
3	Minimum distance between both hands in X-direction
4-5	Distance covered by right and left hand in X-direction
6	Steering angle range

Table 6.1: Relevant feature set

Hierarchical Clustering

The segmented motion data were clustered using the set of relevant features obtained from the data. We applied the *agglomerative hierarchical clustering* method [147],

[1] In our analysis, for feature ID 1, only the position range of the right hand, and not the left hand, had high discriminatory power. This may be related to the characteristics of our sample population.

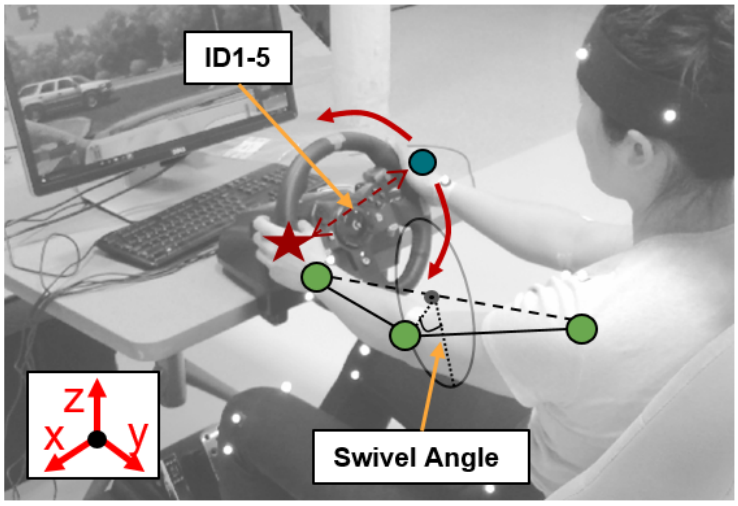

Figure 6.5: Graphical description of features defined in our analysis. ID1-6 are used in data clustering (Table 6.1). ID1-5 relates to distance metrics between both hands, ID6 (not shown in figure) is the range of the steering wheel during the motion segment. Swivel angle characterizes the driver's arm posture while steering.

which is a connectivity-based model, because its hierarchical structure well models the assumed classification of driver control styles in its inter-variability and coupling.

The agglomerative (or bottom-up) hierarchical clustering algorithm starts with considering each data point as a distinct cluster, then pairs of clusters are merged based on their distance/similarity metrics [149]. The *Ward's minimum variance* method [150] is used as the cluster linkage criteria for our data set. The result of the clustering is a dendrogram which graphically describes the natural groupings in the data set. To determine the number of clusters (or to cut the dendrogram), k, we choose k which maximizes the clustering quality index (CQI) represented by the Silhouette index [151]. This process assigned the segmented motion data into clusters which represent the characteristic steering maneuver styles exhibited across our experienced drivers.

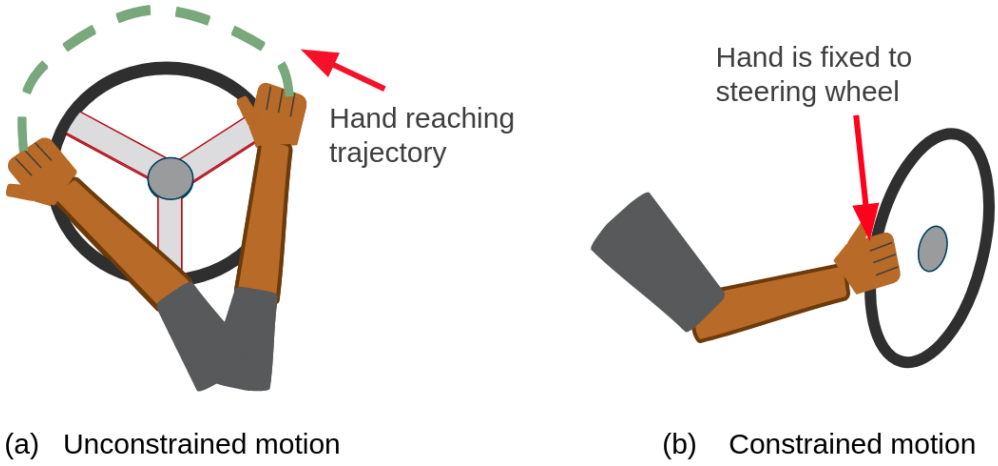

Figure 6.6: Graphical description of features defined in our analysis.

6.3.4 Learning Motion Primitives from Clusters

Here, we present our method for extracting the regularity and variability of respective driver control style groups using imitation learning algorithms and encoding them as *motion primitives* for steering and pedal pressing task. The first step is to determine the feature space in which to encode the demonstration data. This is usually defined based on domain knowledge. In our study, we distinguish driver control motions into *unconstrained* and *constrained* motions.

Unconstrained Motions

These are the reaching motions in free space. The active limb is modeled as a serial kinematic linkage moving its end-effector (hand or foot tip) from one point in 3D cartesian space to another. For this motion type, the task-specific structure is best captured by encoding the cartesian pose of the end-effector over time.

(a) Modeling motion regularity and variability: We use Gaussian Mixture Modeling/Gaussian Mixture Regression (GMM/GMR) to learn an averaged behavior (i.e. hand and foot trajectories) from the clustered segments [152]. Gaussian Mixture

Model (GMM) is parametric model of the probability distribution of the clustered motion data [153]. This mixture model represents the trajectories of multiple motion demonstrations as a weighted sum of M Gaussian component densities (Fig. 6.7(a)) expressed as:

$$p(x) = \sum_{i=1}^{M} w_i g(x|\mu_i, \Sigma_i) \tag{6.4}$$

where x is the N-dimensional vector of the time-aligned motion demonstration segments, w_i is the i-th mixture weight of the Gaussian distributions, μ_i is the mean vector of the i-th Gaussian, Σ_i is the covariance matrix of the i-th Gaussian and $g(x|\mu_i, \Sigma_i)$ is the i-th Gaussian distribution. The parameters of the mixture model, $\{w_i, \mu_i, \Sigma_i\}_{i=1}^{M}$, are estimated iteratively using the expectation-maximization (EM) algorithm [154]. The optimal number of Gaussian components, M, can be estimated by finding the value which maximizes the Bayesian Information Criterion (BIC) [155].

In addition, a Gaussian mixture regression (GMR) [156] process is implemented on the mixture model to retrieve a generalized trajectory [152]. This averaged trajectory, $\hat{x} = \{\hat{x}_{t,i}, \hat{x}_{s,i}\}$, representing temporal values and the corresponding spatial values respectively are estimated through regression [152]. By combining GMM with GMR, we can extract the averaged motion trajectory with the variability along that trajectory (Fig. 6.7(b)).

(b) Learning a generalized model: We further encode the averaged trajectories of the hands and foot using Dynamic Movement Primitives (DMP) [157]. The resulting generalized trajectory, $\hat{x}(t)$, is encoded by the DMP framework using a second-order differential equation which is interpreted as a linear spring-damper system perturbed by a non-linear forcing term [157, 158] expressed as:

$$\tau \dot{v} = K(x_d - \hat{x}) - Dv + (x_d - x_0)f \tag{6.5}$$

$$\tau \dot{x} = v \tag{6.6}$$

where $\hat{x}$ and v are the position and velocity of the differential equation system, x_0 and x_d are the start and final positions, τ is the temporal scaling factor, K and D are stiffness and damping constants respectively and f is the non-linear forcing term defined as a weighted Gaussian basis function, $\psi_i(s)$, with w weights which is used to encode the generalized trajectory:

$$f(s) = \frac{\sum_i w_i \psi_i(s) s}{\sum_i \psi_i(s)} \tag{6.7}$$

Note that $f(s)$ is a function of a phase variable, $s \in [0, 1]$, which tends monotonically from 1 to 0 along the trajectory from start to goal position [157].

The desired non-linear forcing function, $f_{des}(s)$, for a given behavior is computed by inserting the generalized trajectory, $\hat{x}(t)$, and its derivatives $v(t)$ and $\dot{v}$ into the differential equation (6.5). Then, a linear regression problem is solved to define the weights w_i that minimize the error criterion to drive the $f(s)$ to $f_{des}(s)$. The most common method used is the locally weighted regression (LWR). The weights, parameters of the DMP, are stored and retrievable from the motion primitive library.

Unconstrained Motions

These are motions where the active limb end-effector (hand or foot) is not free to move along an arbitrary trajectory, but must follow a defined trajectory that satisfies the motion constraints, such as the case when a driver's hand remains fixed on the steering wheel during a steering control (Fig. 6.6(b)). Thus, the motion of the hand

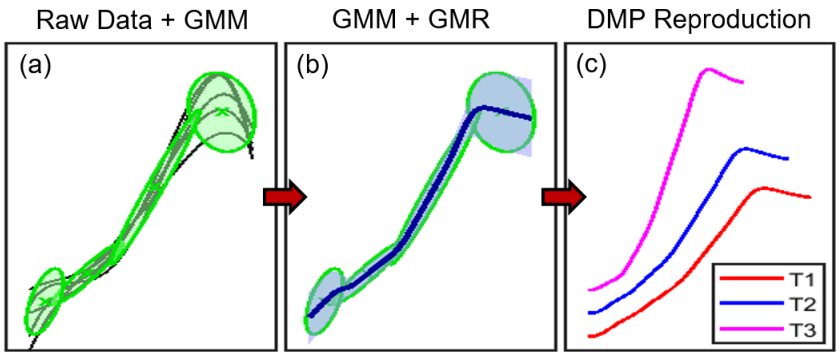

Figure 6.7: Combination of GMM/GMR and DMP to learn a generalizable trajectory model from multiple demonstrations. (a) shows a cluster of trajectories (black lines) with a GMM (green ellipses) fitted to it. (b) shows the mean trajectory (blue line) along with the variance (light blue shade) derived using GMR. (c) shows the reproduction of the mean trajectory adapted to 3 different start and end positions using DMP.

is constrained to follow the confined path of the steering wheel (circular path) as the driver remains in contact with it. For this motion style, the task-specific structure is best captured by defining a functional coupling between the steering wheel angle and the driver's arm posture measured by the arm swivel angle.

(a) Learning motion coupling as a motion primitive: For every motion segment with constrained motions, we first compute the arm swivel angle and analyze its correlation with the steering wheel angle across participants. Then we use a Gaussian model to learn the distribution (regularity and variability) between both angles. Our analysis resulted in a function which maps steering wheel angle to swivel angle which is dependent on arm and seating specifications (see Section 6.4.3).

6.3.5 Motion Reproduction Framework

Through imitation learning, a library of motion primitives can be constructed to represent regularity and diversity of driver control styles. This motion primitive library is integrated as a component in the human motion planning layer of our simulation

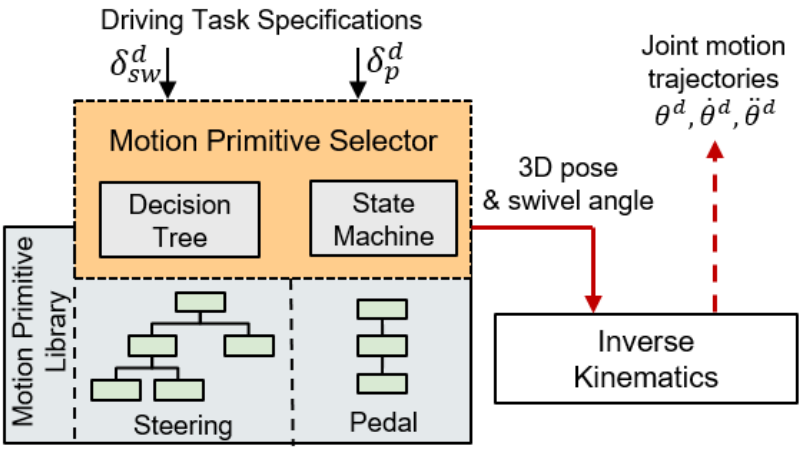

Figure 6.8: For motion reproduction, the motion primitive selector chooses the appropriate primitives from the motion library based on the desired driving task specifications and then sends the resulting parameters to the inverse kinematics (IK) solver. The result of the IK solver is joint motion trajectories.

framework (Section 6.2), to plan the appropriate *driver control motions* required to achieve the desired steering wheel motion (for lateral control) and throttle/brake pedal motion (for longitudinal control).

Fig. 6.8 illustrates the motion reproduction using motion primitive library. For **steering task**, we use a classification decision tree to abstract the decision-making process of selecting the most appropriate motion primitive in the library which fits the desired steering task, as defined from the driving task reasoning layer. The steering handling style clusters are used as classes for the entire motion data segment set and each observation has two labels: (1) associated driving maneuver behavior, and (2) associated driving context. The dataset is then used to train the decision tree model using the two labels as predictors. Therefore, the resulting decision tree takes in the current driving context (i.e., highway, in-city, country-road) and desired driving maneuver behavior (i.e. discrete turn, etc.) and predicts the steering handling style, and as a result, driver control motion primitive most suited to it. Once the driver control motion primitive is determined and the parameters of the

desired steering task (such as the desired angle trajectory) is passed from the driving task reasoning layer, the 3D hand and swivel angle trajectory is computed.

For **pedal pressing task**, we use a simplified finite state machine with two states: pressing throttle and pressing brake pedal. The switching actions are based on the sign of the desired pedal position (positive - throttle/accelerating; negative - brake/decelerating). For a given switching action, the corresponding pedal switching motion primitive is selected from the motion library. Then using the motion primitive, a 3D foot trajectory is computed by the DMP motion reproduction framework.

The resulting 3D trajectories are then fed through an inverse kinematics solver to determine the actual arm and leg joint trajectories which will be passed to the human motion control layer for torque generation at the joints for actuation.

6.4 Results

This section presents our results from the process of (1) motion segment clustering, (2) driver control style analysis, and (3) the resulting driver control motion primitive library. We also demonstrate the implementation of the dominant driver behavior — the most frequently used whole-body coordination in vehicle maneuver — using the learned motion primitives.

6.4.1 Clustering of Motion Data Segments

Fig. 6.9 shows the results of the clustering process. The agglomerative hierarchical clustering method was applied in two stages on the steering motion data segments. In each stage, the optimal number of clusters was obtained using a clustering quality index (CQI). In Stage 1 clustering, the discriminating behavior was whether the

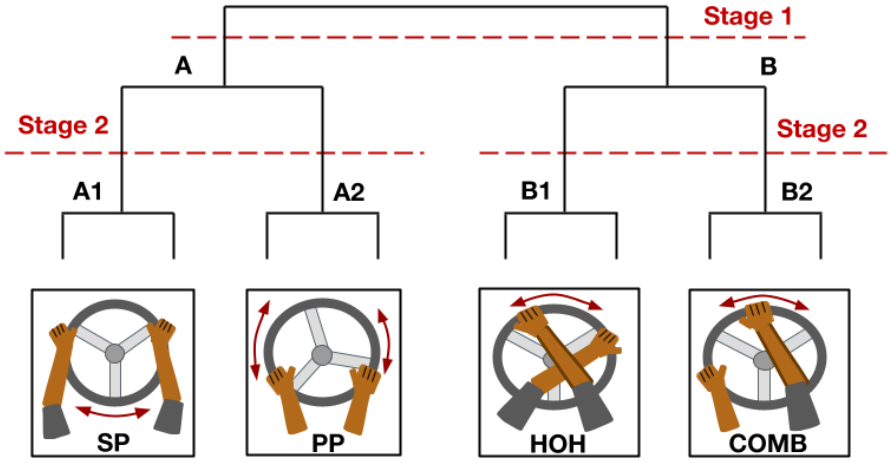

Figure 6.9: Clustering result showing the characteristic steering handling styles in the motion data. Four clusters were retrieved: standard pose (SP), push-pull (PP), hand-over-hand, and combination (COMB).

driver's hands remained within their respective halves of the steering wheel. In cluster A, we observed that both hands remained within their respective halves of the steering wheel throughout the motion segment. Whereas in cluster B, the driver's hands reached across the respective steering wheel half to pull the wheel.

In Stage 2, we applied clustering method to the two resulting clusters (A and B) to obtain further distinctive characteristics within the groups. We obtained four sub-clusters as shown in Fig. 6.9. In cluster A1, we observed that both hands held onto the steering wheel throughout the motion segment. We referred to this style as the standard pose (SP). In cluster A2, the dominant motion was a push-pull where both right and left hands slide along the steering wheel to make a turn. We referred to this style as push-pull (PP).

We observed that the dominant behavior in B1 was a hand-crossing motion, where the right or left hand breaks contact with wheel and reaches across to the other side of the wheel to pull it. We referred to this style as hand-over-hand (HOH). No distinct behavior was observed in B2, the motions related to a combination of

hand-over-hand, one-hand maneuvers, standard pose maneuvers, etc. We referred to this as COMB.

6.4.2 Driver Control Style Analysis

Fig. 6.10 shows the distribution of steering handling styles obtained from the clustering process. We compare the extracted handling style clusters across drivers, driving scenarios and driving maneuver behaviors and discuss their correlations. The styles are as follows:

- Standard pose (SP) - driver keeps both hands fixed to steering wheel during maneuver
- Push-Pull (PP) - driver sequentially rotates the steering wheel by sliding it from one hand to another
- Hand-over-Hand (HOH) - driver crosses one hand over the other to achieve a wide steering angle
- Combination (COMB) - driver combines HOH, PP, SP and other maneuvers to achieve a wide steering motion range

Fig. 6.10(a) shows the handling style distribution across the participants. For each participant, the plot represents the frequency of occurrence of each maneuver style. Across participants, we observed that the most dominant maneuver style is the standard pose (SP). Every participant adopts this style with the highest frequency, about half of all motion segments. All the participants also demonstrated the PP and HOH styles, however, in varying amounts. Almost all participants adopt the full set of styles (except Participant 1).

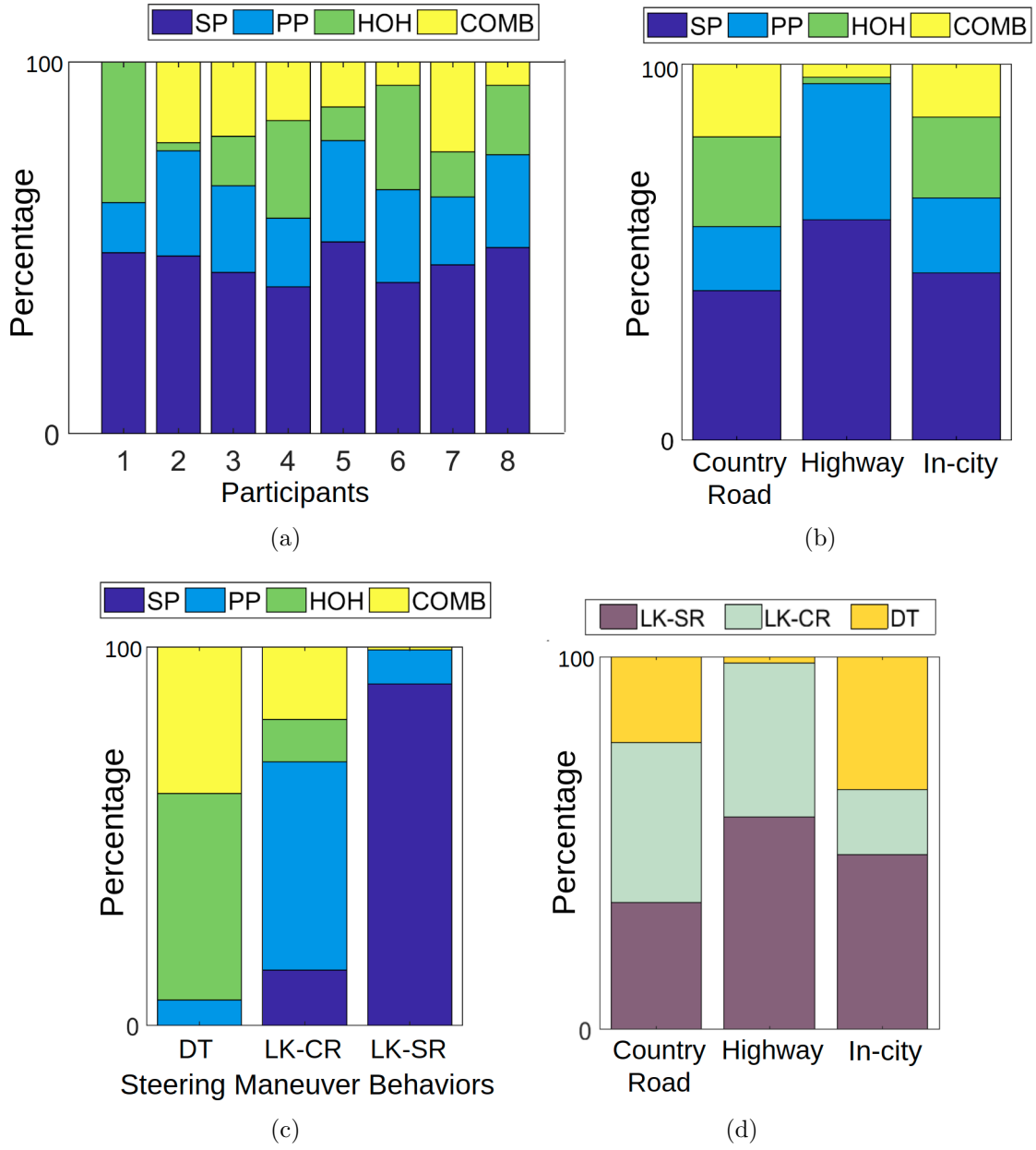

Figure 6.10: Analysis results from the steering handling style clustering. (a) shows the distribution of maneuver styles across respective participants, (b) shows the distribution of maneuver styles across driving contexts; (c) shows the distribution of maneuver styles across the steering maneuver behavior classes - Discrete turns (DT), Lane-keeping (curved road) (LK-CR), Lane-keeping (straight road) (LK-SR); and (d) shows the distribution of steering maneuver behaviors across driving contexts.

Fig. 6.10(b) shows the distribution of handling styles across driving contexts (i.e. country road, highway, and in-city driving). For each driving context, the plot shows the percentage of usage of each handling style. The percentage is computed by normalizing the frequency of each handling style against the total number of handling styles for each driving context. We can observe that in highway driving, over 90% of the handling styles adopted is either SP or PP. This is expected as drivers generally maintain both hands on the steering wheel or gently slide the wheel to make turns when driving at higher speeds (which is characteristic of highway driving). We also observe a near equal distribution between HOH and COMB style for both country road and in-city driving.

Fig. 6.10(c) shows a distribution of handling styles across steering maneuver behaviors. The plot shows that for making discrete turns (DT), only HOH, COMB and PP are adopted. Participant drivers didn't adopt SP for discrete turns. This is expected as, in discrete turns, the steering wheel is turned to over 200°, which is kinematically infeasible to perform with both hands fixed on the steering wheel. The dominant handling style in discrete turns is HOH. We can observe that the dominant style in lane-keep (curved-road) (LK-CR) is PP. That is, drivers slide the steering wheel along their hands (or adjust their grasping point) to make wider turns which may be discomforting with SP. In this plot, we also see that for lane-keep (straight road) (LK-SR), SP dominates almost entirely with over 90%.

Finally, Fig. 6.10(d) shows the distribution of steering maneuver behaviors across driving contexts. For each driving scenario, we plot the percentage usage of each maneuver behavior. We can observe that lane-keeping (straight road) (LK-SR) and lane-keeping (curved road) (LK-CR) steering behaviors dominate highway driving almost entirely, while discrete turn (DT) is most prominent in city driving compared to other contexts. This is expected as drivers rarely perform discrete turns on the

highway but do so more frequently while driving within the city.

Based on the maneuver style classification analysis shown in Fig. 6.10, we designed a high-level motion primitive selector to choose the most appropriate maneuver style that fits the driving scenario and current steering maneuver behavior required. The selector was modelled as a classification decision tree.

6.4.3 Driver Control Motion Primitives

This section presents our results from analyzing individual maneuver styles obtained from the clustering process. The regularity and variability of the respective styles are analyzed and modeled as maneuver motion primitives for both steering and pedal pressing tasks.

Steering Handling Motion Primitives

For the steering maneuver styles, we analyzed the characteristic features of the standard pose (SP), hand-over-hand (HOH), push-pull (PP) and combination (COMB) that distinguish the styles among participants, and then learn the diverse maneuver styles as maneuver motion primitives.

Standard Pose (SP): Motions in SP style are single-phase constrained motions, with both hands remaining fixed to the steering wheel throughout the maneuver. Fig. 6.11 shows the distribution of swivel angle (mean and S.D.) across all participants for both the left and right arms. To investigate the inter-participant differences in swivel angle during driving, we performed a multiple pair-wise comparison analysis (using Tukey's honestly significant difference criterion). We found that there is significant difference in swivel angle range across participants ($p < 0.001$). This suggests that drivers may employ a consistently distinct arm posture while driving.

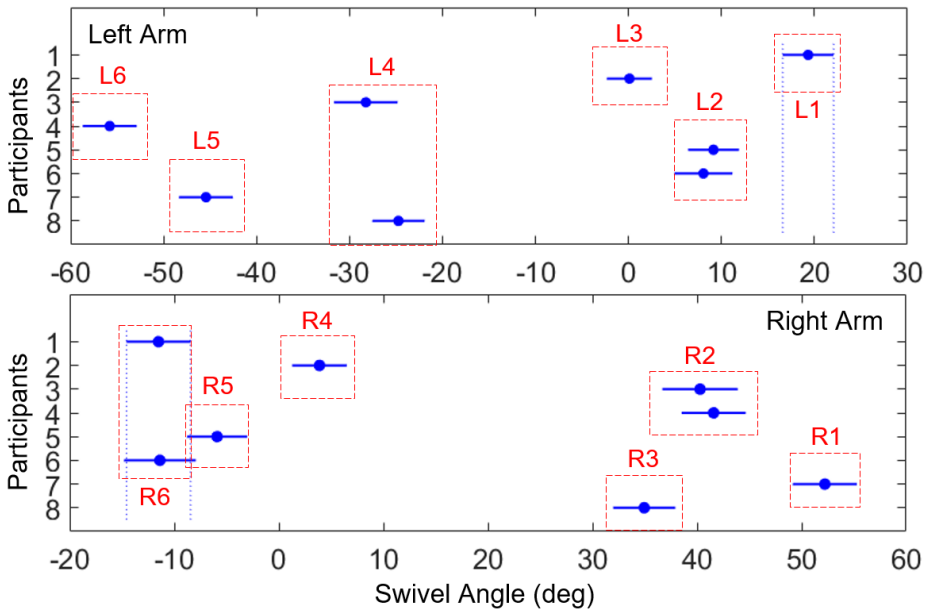

Figure 6.11: Multiple comparison analysis of arm swivel angle across participants. This plot shows the mean and standard deviation of the swivel angle for each participant's left (top) and right (bottom) arms performing the standard pose handling style. Participant data is grouped into clusters, L1-6 and R1-6, based on their pairwise similarity.

Note that some participant's means were not significantly different. We further clustered participants based on their pair-wise comparison results (i.e. participants with significantly different means are placed in different clusters while participants with insignificant differences are placed in same cluster). This resulted in six participant clusters labelled L1-6 and R1-6 in Fig. 6.11. An inverse symmetry between the left and right arm posture was also observed during this steering handling style.

Next, we evaluate the functional coupling between the swivel angle and the steering wheel across the defined participant clusters (see Fig. 6.12). We fit a multivariate Gaussian model to the data in each participant clusters and observed that the steering wheel variance is much larger than the swivel angle variance across groups. Therefore, for each cluster, we learn a standard pose motion primitive as the distribution of the swivel angle conditioned on a desired steering wheel angle.

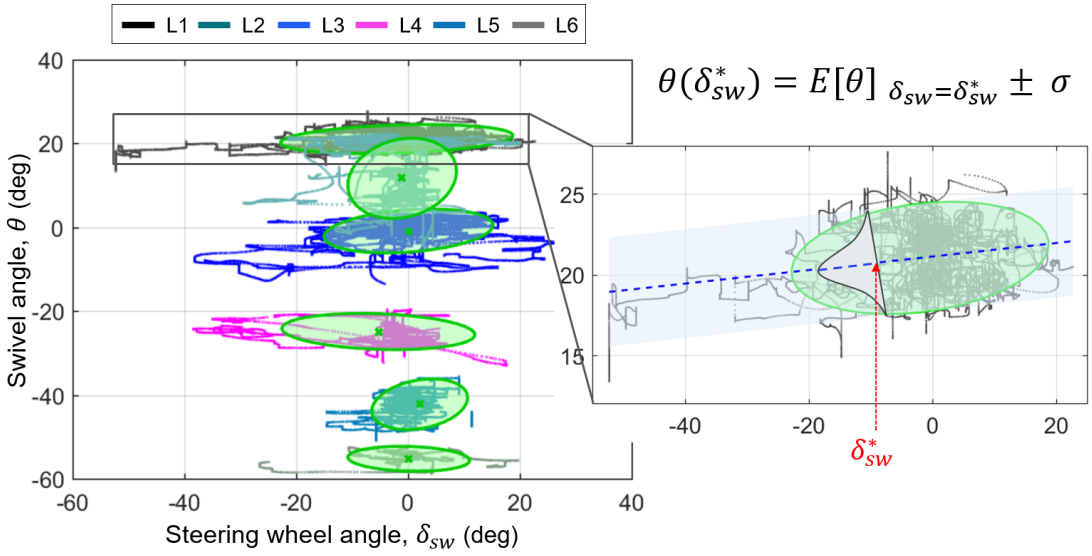

Figure 6.12: Functional coupling between steering wheel angle and swivel angle for left arm using a multivariate Gaussian model. The exploded graph shows the Gaussian model fit to the cluster L1 data. Using this model, we can obtain the swivel angle for a given steering wheel angle as the expected value, E, of the swivel angle, conditioned by the given steering wheel angle, along with the variance.

We investigated the factors that influence the driver arm posture. We performed a correlation analysis on two candidate factors: participant arm length and torso-to-steering wheel distance in seated position. The parameters are measured as shown in Fig. 6.13(b). Table 6.2 shows the Pearson correlation coefficient of both arm length (L) and torso-to-steering distance (C) against the swivel angle. We observe a moderate correlation across arms ($p < 0.001$). In Fig. 6.13(a), we plot the torso-to-steering distance (C) against arm length (L) for the left arm only, and observe a positive correlation ($r = 0.6510, p < 0.001$). This can be used in determining the swivel angle cluster in our simulation: based on the arm length of the driver model and the seating posture (which defines C), we determine what swivel angle cluster is best suited, by computing the shortest distance to the cluster center (indicated using 'X' in Fig. 6.13(a)).

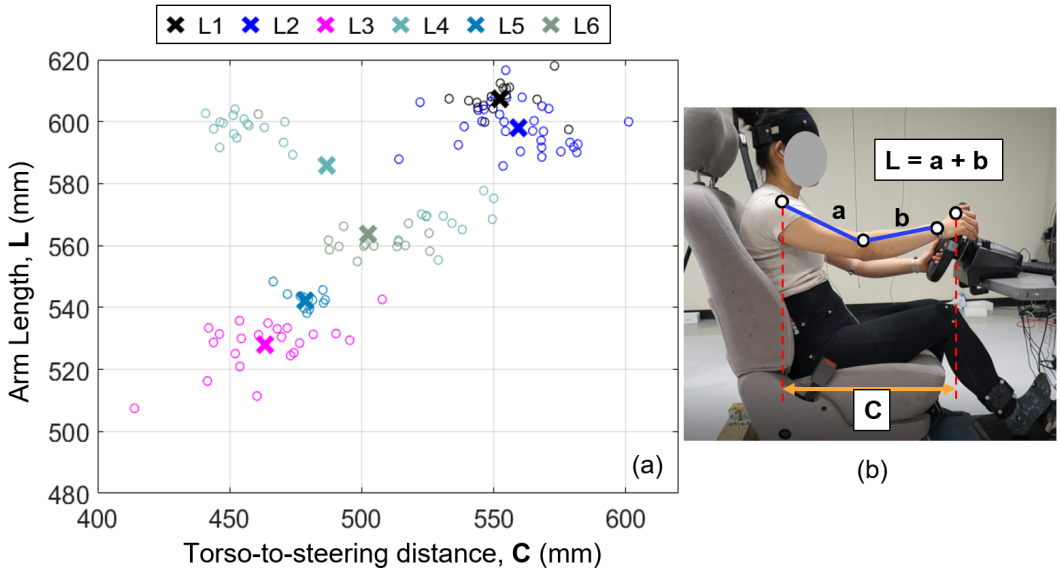

Figure 6.13: Correlation between arm length and torso-to-steering distance, factors that influence the driver's swivel angle during SP maneuver. (a) shows the plot of C against L with the swivel angle groups indicated. (b) shows how the parameters are measured.

Metric	Left Arm	Right Arm
Torso-to-steering wheel distance (C)	0.4750	-0.5706
Arm length (L)	0.4179	-0.4439

Table 6.2: Correlation analysis of torso-to-steering wheel distance and arm length against swivel angle

Hand-over-Hand (HOH): We observed two-phase bi-manual motion coordination from the analysis of the hand-over-hand demonstrations. The first phase is the *turn phase*, when the driver initiates a turn (either left or right); the second phase is the *return phase*, when a driver regularizes the steering wheel to 0° position after the turn. Both *turn* and *return phases* are symmetrical involving the same actions, but with opposite hands. Fig. 6.14 shows a graphical description of the *turn phase* alone with the actions involved in the phase. For each turn, we define a turning hand and a returning hand. The turning hand in HOH is the hand that pulls the steering wheel in the respective direction during the *turning phase*. When turning to the

left, the right hand is defined as the turning hand and vice versa. Each phase can be further decomposed into four actions: turn w/hold (S1), reach-A (S2), reach-B (S3) and compensate (S4) which take place sequentially (Fig. 6.14 (middle)). The figure illustrates the *turn phase* of a discrete turn to the left; the turning hand is the right hand. In S1, the right hand pushes the steering wheel to the left, while keeping contact with it. The left hand is inactive in this action. Then in S2, the active left hand reaches from below the right hand to a point above it to continue the left steering motion. In S3, the right hand reaches from its current position on the left side of the steering wheel back to the right side to stabilize the steering control. In S4, both hands adjust the steering wheel to achieve the desired motion.

Fig. 6.14 (top) shows the start and end points of the reaching motion (S2 & S3) as well as the trajectory for a representative participant. This is an unconstrained motion, hence as discussed in section 6.3, GMM/GMR and DMP are applied to extract and model the averaged hand trajectories from start to end point along with their variance as a motion primitive.

Fig. 6.14 (bottom-left) shows the plot of coupling between the swivel angle and the steering wheel angle during the constrained motion action (S1). We extract the average trajectory from multiple demonstrations using GMM/GMR and model this as a motion primitive. We also analyzed the temporal sequence of the maneuver that is shown in Fig. 6.14 (bottom-right). We observed a consistent overlap between the S1 and S2. This temporal sequence is used as we reproduce the coordinated bi-manual motion on our digital human model.

Push-Pull (PP): For the push-pull handling style (PP), we also observed a two-phase bi-manual coordinated motion with a combination of constrained and unconstrained motions by both hands. Fig. 6.15 represents the *turn phase* of the maneuver

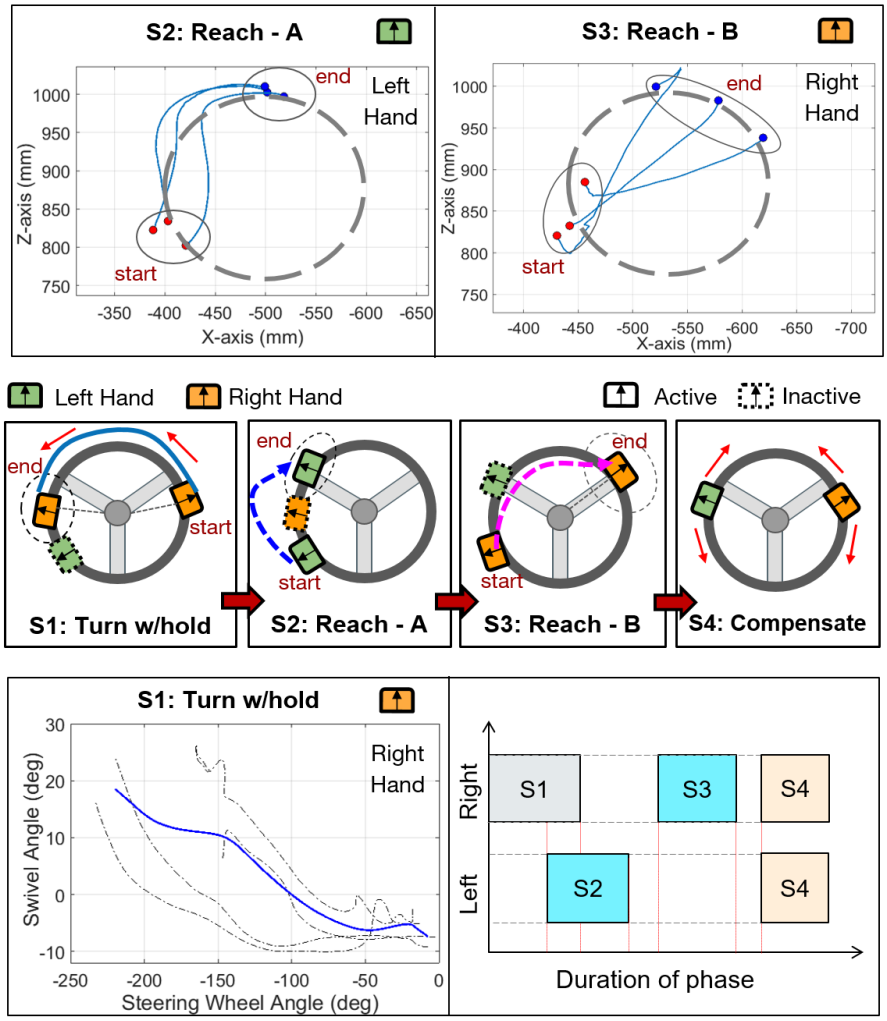

Figure 6.14: Illustration of the *turn phase* of the hand-over-hand (HOH) maneuver style. (Top): Trajectory for reaching motion action (S2 & S3) by both left and right hands. (Middle): Description of the phase actions: turn w/hold (S1), reach - A (S2), reach - B (S3), and compensate (S4). Dashed lines represent unconstrained hand motion while solid lines represent constrained hand motion. (Bottom-Left): Coupling between swivel angle and steering wheel angle during turn w/hold action. (Bottom-Right): Temporal sequence of the HOH maneuver.

which includes three sub-motions: push (by the turning hand) along with reaching of the returning hand, pull (by the returning hand) along with reaching of the turning hand and then compensation on steering wheel angle. The 3D plot at the bottom of Fig. 6.15 shows the hand trajectory of a single demonstration for one participant while under a PP handling style. As opposed to HOH, we observe that both hands are active during each sub-motion.

In Fig. 6.15, the steering wheel motion is to the right. In the push sub-motion, the left hand pushes the steering wheel along an arc, while the right hand moves from its current position at the lower half of the steering wheel upward to grasp the steering wheel for a pull. The left hand motion is modeled as a constrained motion (standard pose, SP) because the hand remains fixed on the wheel as it moves. The right hand motion, which is a reaching (unconstrained) motion is modeled and learned using GMM/GMR and DMP as in Fig. 6.14. The compensate motion is modeled as A standard pose (SP). The second phase of the motion, *return phase*, is identical to the turning phase with the hands switched (i.e. right hand pulls steering wheel while left hand moves in reaching motion). The push-pull sequence may occur multiple times depending on the desired steering angle motion.

Pedal Control Motion Primitives

For the pedal control, we obtained a motion primitive for each foot switching motion in the pedal task (i.e. brake-to-throttle motion and throttle-to-brake motion). Specifically, we applied GMM/GMR to extract the averaged trajectory from each of the demonstration data grouped together. Fig. 6.16 shows a plot overlaying the raw time-aligned foot tip trajectories for both switching motions (black dashed lines), the derived mixture model (green ellipses) and the averaged trajectory (blue solid line). The averaged trajectories for both switching motions are then encoded as

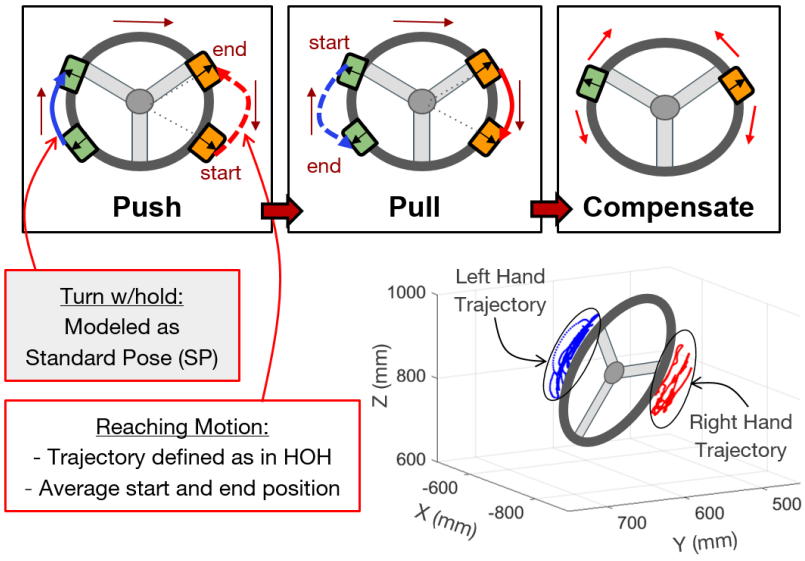

Figure 6.15: Illustration of the push-pull (PP) handling style. This shows the turn phase of the motion which includes 3 motions: push, pull and compensate. Dashed lines represent unconstrained (reaching) hand motion while solid lines represent constrained hand motion.

a generalizable motion primitive using the DMP framework, as described in Section 6.3.

6.4.4 Implementation on HuMADS

The *driver control motion primitives* for both steering handling and pedal control modeled above are stored in the motion primitive library and are used in the human motion planning module of the HuMADS. We demonstrate our implementation on the HuMADS given a pre-defined driving task (steering and pedal motion). The result of the human motion planning module is the desired whole-body joint kinematics motion best suited to achieve the driving task. Fig. 6.17 shows snapshots of the simulation at different steering and pedal actions. A demonstration video is accessible online [2].

[2]Demonstration video: https://youtu.be/LElY1ISa9uk

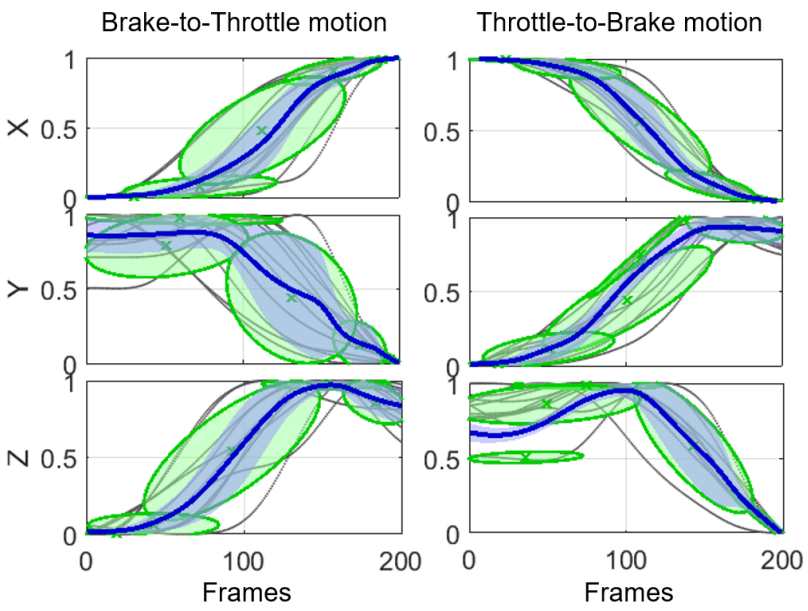

Figure 6.16: Modeling of foot tip motion in foot switching task for pedal activation. The black dashed lines are the raw time-aligned and normalized foot trajectory motions (x,y,z). The green ellipses are the mixture models used to fit the data. The solid blue line is the generalized trajectory derived using GMR. (Left): brake-to-throttle motion (Right): throttle-to-brake motion.

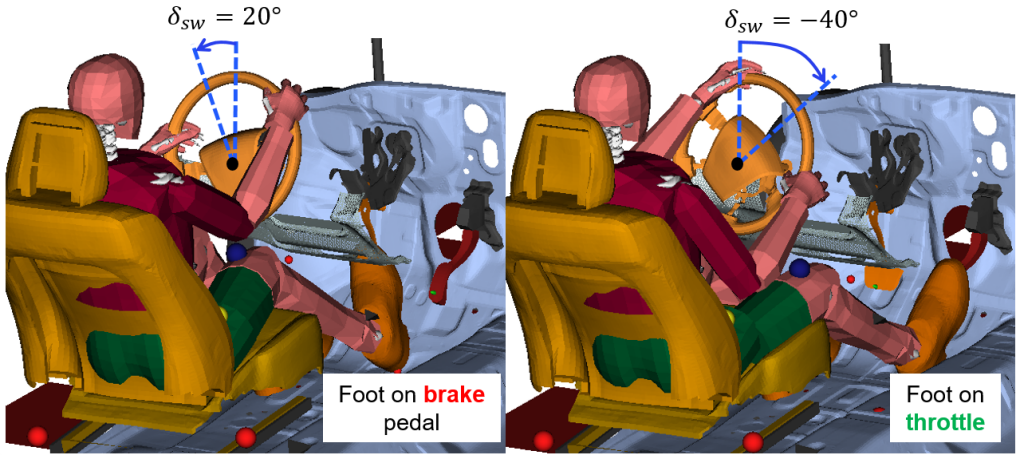

Figure 6.17: Snapshots of the implementation of our motion planning framework on the HuMADS

6.5 Discussion

Existing studies and digital human driver models have been limited to only the standard pose handling style [100, 101], perhaps due to the difficulty of modeling and planning other more complex steering handling styles in simulation. In this chapter, we presented an approach that extracts, analyzes and models these complex handling styles from human demonstrations. This framework will enable automotive researchers to perform more comprehensive analyses on the usability of vehicle active safety and driver-assistance technologies.

Our study reveals that human drivers tend to employ a consistent set of steering handling styles while controlling a vehicle, due to the regularity in developed human motor skills. These handling styles may have been learned while training to drive. In this work, we presented the feasibility of using machine learning methods to analyze and model the complex bimanual motion coordination involved in steering handling from human demonstration data. This is a crucial step beyond existing studies [159] which only investigate the steering handling styles through experimentation.

The results of our clustering on steering handling styles agree well with existing experimental studies [159] as well as guidelines defined by regulatory agencies such as the National Highway Traffic Safety Administration (NHTSA) [160]. According to NTSHA, the recommended steering handling style for large or discrete turns is the hand-to-hand (or push-pull) steering style. However, in our study, we found the dominant handling style for discrete turns to be the hand-over-hand (HOH) across our participants. The push-pull (PP) style is recommended because of its safety advantage over the hand-over-hand (HOH) specifically in the event of an air bag release. In such cases, the driver's hands may be over the steering wheel which could lead to injury, whereas, with push-pull, the hands remain at their respective

halves of the steering wheel throughout the driving task. Our simulation framework may enable automotive researchers to perform further predictive analysis on the impact of driver handling styles and steering wheel design on driver safety and workload during normal driving and safety-critical scenarios.

This work may also find relevance in human factors and ergonomics research in evaluating vehicle cockpit design. Our analysis of the standard handling pose (SP) shows that there is a positive correlation between the driver's arm swivel angle (which describes the arm posture) and factors such as their arm length and distance to steering wheel. While existing studies perform posture prediction and driver reachability in static or kinematics-based simulations [161], our framework can further enable dynamic evaluation of driver motions and hand reachability.

Recent studies in autonomous vehicles research have highlighted the need for smooth control transition mechanisms when the human operator needs to intervene either to a transition request or to avert an automation failure scenario [162,163]. To better design control interfaces and transition modalities, our approach to rendering realistic steering handling behaviors and our simulation framework can serve as a simulation testbed for automotive engineers to gain better understanding of impact of haptic interactions on transition time and stability.

From an imitation learning perspective, our work presents a data-processing pipeline for dealing with unstructured and heterogeneous human demonstration data. The question of *what to imitate* is crucial in defining the accurate feature space in which to learn the motion structure [152, 164]. We demonstrate how to learn both in the cartesian space as well as in the posture space (using the swivel angle). This work may ignite further investigation into learning and modeling other complex human manipulation tasks for different applications across computer animation and robotics fields.

It is also important to acknowledge the limitations of the study. Only a small sample size was used, which may not accurately represent the whole population. Therefore, there are concerns regarding the generalizability of our extracted driver control styles. However, we found a good correlation between our clustering results and those from studies with larger samples, despite the small sample size. This further suggests that humans exhibit similar style and behavior in driving. Furthermore, with the current version of the HuMADS framework, simulating the complex steering handling styles is limited. We experienced difficulties in modeling realistic forces during the making and breaking of contact between the driver model's hands and the steering wheel. Further physical contact modeling is required in future work to effectively reproduce arbitrary steering handling motions in simulation.

6.6 Chapter Summary

This chapter proposed a data-driven approach to model and render realistic driver control motions on an integrated human driver and vehicle model for physical human-vehicle interaction research. In particular, we proposed a systematic machine learning approach to extract a set of characteristic driver control styles from human demonstration. We then analyzed the driver control styles to determine the correlation between control styles, driving contexts and maneuver behaviors. We further used imitation learning methods (GMM/GMR and DMP) to model the handling styles as motion primitives for the human motion planning in simulation. Using the proposed approach, we learned the motion coordination for both steering handling and pedal activation motion from human driving data and demonstrated its reproducibility on an integrated cognitive-physical simulation framework (HuMADS). This work demonstrates the feasibility of our approach for rendering realis-

tic driving behavior on digital human driver models in simulation. This is significant as it extends the ability of automotive researchers to understand driver-vehicle interaction through more comprehensive simulations. Future work is needed to address the existing limitations in model generalization and simulation rendering.

Chapter 7

Concluding Remarks

7.1 Summary of Contributions

Mobility vehicles (e.g. passenger vehicles, wheelchairs, and mobile telepresence robots) are likely to rely on shared autonomy for the foreseeable future until autonomous navigation technology is well developed and societal perceptions change to support it. Consequently, it is crucial to continue improving the design of shared autonomy-based driving assistance systems. The versatility of shared autonomy has been demonstrated by its application across several mobility domains including unmanned aerial vehicles (UAVs) [50, 52, 73], unmanned ground vehicles (UGVs) [49, 165, 166] and passenger vehicles [7, 10, 51] to provide navigation guidance (e.g. path tracking, collision avoidance, etc.) to humans operating single or multiple vehicles using diverse interface modalities (e.g. visual, haptic, auditory). In particular, haptic shared autonomy systems have been shown to improve task performance [10] and enhance drivers' situational awareness while keeping the driver in the loop as final control authority [7, 35].

Yet, there are still a number of challenges in shared autonomy systems, including

control authority arbitration and control conflict caused by misalignment between the human and autonomous agent, which could result in user dissatisfaction and system abandonment [7]. Additionally, while SA has been applied across various domains, it has largely been focused on providing navigation assistance in static environments, with little attention paid to the more general case of providing navigation assistance in dynamic, human-populated settings. Human-centered design principles have been explored as a means to address the limitations of SA as well as to improve user satisfaction and acceptance [1]. The dissertation focuses on understanding and improving the design of human-centered shared autonomy systems by providing scientific contributions to the following four research questions:

1. *What are the implications of anticipation uncertainty on aligned intent and how can they be mitigated in force-based interactions?*

   System transparency is a crucial component of the human-centered design of human-machine systems. However, limited work has explored the impact of anticipation uncertainty on human motor control in force-based interactions. This is particularly relevant for haptic (kinesthetic) shared autonomy systems, where a haptic-enabled control device serves as the shared control interface between the human and the autonomous agent as described in Chapters 1 and 2. Chapter 3 of this dissertation presents findings from a simple pushing experiment designed and conducted to investigate the effect of force anticipation uncertainty and transparency on human motor control. Our findings indicate that task anticipation, including expected workload, influences human control strategy, particularly during force-based interactions. Particularly, our results revealed that the first peak of pushing force correlated with anticipated force workload. This accords with previous studies that humans rely on internal predictive models for motor control [56], which indicates that with properly

calibrated internal models, humans can accurately anticipate and predict force interactions. Furthermore, participants tended to perform more slowly and with lower forces when Heavy trials were preceded by Light trials. These findings reveal that force anticipation affects task performance in motion and force control, as well as how the workload of preceding tasks influences performance on the current task. These considerations are crucial in understanding the pivotal role of transparency and anticipation in force-based interaction, such as in haptic shared autonomy.

2. *How to design human-centered socially-aware navigation assistance with improved system transparency?*

   Navigation assistance in human-populated environments is crucial to ensuring the usability of mobile telepresence robots and the satisfaction and comfort of smart wheelchair users. Existing research on shared autonomy, however, has been confined to static environments or single moving pedestrian avoidance scenarios [13, 49] as discussed in Chapter 2. Chapter 4 of this dissertation addresses two questions that arise in designing intuitive and transparent shared autonomy systems that support socially aware navigation. The **first question** is: "How to plan and generate safe, socially-aware navigation paths within dynamic human environments?" I presented SA-RVO (Socially-Aware Reciprocal Velocity Obstacles) which is an extension of the original reciprocal velocity obstacle [86] approach for dynamic obstacle avoidance. By incorporating social proxemics constraints into the velocity obstacle formulation, SA-RVO achieves safe, non-intrusive navigation paths around people. Further, we modified the computation for optimal velocity by taking into account additional factors for navigation assistance, including (i) selecting the velocity that is as close

as possible to the operator's command velocity vector, (ii) penalizing large changes in consecutive optimal velocities to facilitate smooth guidance cues for the operator, and (iii) compensating for goal-directed velocities.

The **second question** is: "Which interaction modalities work best to communicate the generated guidance cues to the human operator in an intuitive and transparent manner?" In our study, we incorporated visual and haptic feedback channels into both single-modal and multimodal approaches. Specifically, two visual guidance designs and a haptic force rendering were proposed. A user study with fifteen participants was conducted to compare multimodal assistance to visual or haptic assistance alone in a shared navigation task. The key findings are that participants preferred multimodal assistance with visual guidance trajectory over haptic and visual modalities alone. Also, we found that despite no significant differences in navigation safety, visual cues significantly increased participants' understanding of intent and level of cooperation over haptic guidance alone.

3. *How to achieve assistance adaptation to distinct driving objectives/styles and how would this impact driving performance and human-automation cooperation?*

   Autonomy adaptation is a crucial element of human-centered autonomous systems for the reason that it allows autonomous agents to adjust their control level as needed to best align with human states or behaviors, tasks and/or environmental conditions [1, 14]. Existing research has examined autonomy adaptation to risk, level of trust and confidence [16,43], task and skill level [17,131]. Chapter 5 of this dissertation examines autonomy adaptation in the context of providing navigation assistance to remote operators of mobile telepresence

robots in human-populated environments. The focus of this work is twofold: (i) How to design socially-aware navigation assistance that is adaptive to user driving objectives/styles?, (ii) Will such an adaptive system impact driving performance, level of cooperation and user preference, and if so, by how much? By extending the SA-RVO approach presented in Chapter 4, I proposed two navigation assistance policies that correspond to the cautious and assertive driving behaviors studied in driver behavior literature [134]. An exploratory user study was conducted to examine the effects of adaptive assistance on driving performance, cooperation, and user preferences in a shared navigation task. Results showed that, even though assistance adaptation did not significantly affect driving performance, participants prefer safety-aligned assistance modes under both cautious and assertive driving conditions.

4. *How to model and render complex human driver behavior in simulation to advance our understanding of human driver-vehicle interaction and improve the design of driver assistance systems?*

   Shared driving has become more complex and disruptive as today's vehicles become more autonomous, affecting how drivers interact, adapt, and respond to vehicle systems. For assistive driving systems to be safe and comfortable, we must understand human driving behavior. Chapter 2 discussed how traditionally, ADS driver interactions have been studied using simulations or real-world human driver experiments, which have limited potential to evaluate dynamic interactions objectively or control workload on the human driver. Chapter 6 presented a new method for modeling and simulating human driver control behavior in ADS-driver interactions. We first outlined our novel simulation framework, Human Model-based Active Driving System (HuMADS) that in-

tegrates a whole-body human driver model and a vehicle dynamics model to provide a high-fidelity simulation of driver-vehicle interaction. Following this, we presented a systematic machine learning approach to identify, analyze, and model characteristic driving styles (such as steering handling and brake/throttle switching styles) from human demonstrations. Our analysis of the steering handling styles of human drivers, which agrees well with existing experimental studies [159], revealed that human drivers tend to control their vehicles with a consistent set of handling styles. Using this information, we determined a correlation between steering handling styles and driving contexts as well as maneuver behaviors. Additionally, we used a combination of imitation learning methods (GMM/GMR and DMP) to identify the regularity and variability of the steering handling and pedal switch styles across groups and modeled them as motion primitives that can be used for re-creating motion in simulations. Our work illustrates the feasibility of our method for simulating realistic driving behavior on digital human driver models. It is important because it opens up a novel avenue for automotive researchers to simulate realistic driving behavior and analyze the design and usability of advanced driver assistance systems based on it [28].

7.2 Limitations

1. **Experiment sample population:** The sample population for the experiments presented in this dissertation were primarily drawn from the WPI student population. As a result, the majority of participants were young adults (ages 18-29). Studies have identified age-related differences in driver behavior with and without interaction with driver assistance systems. In their study,

Bao et al. [140] discovered that younger drivers tend to engage in more aggressive driving behaviors than middle-aged and older drivers. Hong et al. [139] found that response time and driving skills generally diminish with age. Moreover, the level of trust and acceptance of driving assistance systems have been shown to vary with the age of the driver [167,168]. Consequently, we acknowledge that the lack of age-related diversity in our experiments may limit the generalizability of our findings.

2. **Influence of human-to-robot trust level and task difficulty:** The shared autonomy experiments in Chapters 4 and 5 did not evaluate the effects of human-to-robot trust on operator perceptions and performance. Research has shown that human-robot trust impacts joint task performance, with low human trust degrading task performance [129,169]. On the other hand, higher levels of trust increase overall task performance and user acceptance, and reduce operator workloads [16]. Trust, as a dynamic attribute, is continuously calibrated based on joint interaction with the robot partner and has also been shown to depend on the robot partner's past and current performance [16,169] as well as the transparency of the interface [170]. It is important to measure and evaluate trust levels across modalities and explore the interactions with navigation safety and team cooperation in future studies. Additionally, the level of task difficulty may have affected our ability to evaluate the impact of control conditions in Chapter 4. Kuiper et al. [69] found that navigation assistance systems are more effective when the task is more difficult. However, in our final questionnaire, participants reported high confidence in their skill to complete the task without navigation assistance. Another study, by Lee et al. [129], noted that people use autonomous systems based on the difference between their trust in the system and their self-confidence in completing the

task. ~~This may imply that, on average, participants did not rely on navigation assistance in the task.~~

3. **Haptic feedback rendering:** In the shared autonomy experiments described in Chapters 4 and 5, some participants commented that the haptic feedback cues changed rapidly and they weren't sure why or what the guidance was trying to achieve. This may be due to the dynamic nature of the navigation task. When operating in dense areas with many pedestrians in close proximity to the robot, there can be rapid consecutive changes in the optimal velocity heading computed by SA-RVO (see Section 4.2.1). In order to reduce jerky motions and distracting haptic force vibrations, we penalized consecutive velocity changes using a smoothness cost in the SA-RVO formulation. To further mitigate this effect, additional damping effects may be required in the haptic force rendering. Additionally, a fixed haptic gain was used throughout the experiments. The haptic gain parameter was set and calibrated through trial and tested in a pilot study. However, haptic force magnitude was perceived differently by participants during the main experiment. Some participants described the haptic force as too strong and overwhelming, yet others considered it to be mild and controllable. Previous studies have considered the influence of haptic gains on task performance and human-machine cooperation [171]. There is a need to further explore haptic gain tuning and adaptation for more comfortable haptic shared autonomy systems.

4. **Simulation-based vs. real-world experiments:** The discrepancy between simulation-based and real-world experiments must be acknowledged. Simulated experiments have been used extensively in the literature [8, 16, 41, 52] to study human-machine interactions in driving and navigation tasks since they

allow for more control of experimental conditions, relax human safety concerns, and still provide a method of investigating human-machine interactions effectively. However, we recognize the limitations of simulation-based studies in robustly validating our hypotheses. For instance, in the shared autonomy experiments in Chapter 4 and 5, one may expect that participants may control the robot differently while driving around real pedestrians, perhaps with a higher sense of safety and caution than when driving virtually around virtual pedestrians. Additionally, the driving data collection in Chapter 6 was performed on a fixed-base driving simulator in a lab setting. We agree that driver control motions may vary to accommodate the dynamic forces present while driving in a real vehicle, and hence, poses a limitation to the generalization of our learned models. However, it should be noted that the modeling and learning pipeline presented would be applicable irrespective of experimental protocol.

5. **Limited modeling capabilities on HuMADS framework:** In Chapter 6, the reproduction and rendering of the complex steering handling styles in simulation is limited by the current version of our HuMADS framework [2]. We experienced difficulties in modeling realistic forces during the making and breaking of contact between the driver model's hands and the steering wheel needed to achieve the complex hand-over-hand (HOH) or push-pull (PP) steering handling styles analyzed and modeled from human demonstration data. Further work is required in physical contact modeling and control in the OpenSim simulator [3] to enable us to effectively reproduce arbitrary steering handling motions in simulation.

7.3 Future Research Directions

The contributions presented in this dissertation strived to take a human-centered approach to design of haptic shared autonomy systems for assisted driving systems. Our findings offer a plethora of research directions for further addressing the challenges of shared autonomy, as you can see in this section.

1. **Learning social navigation styles from human demonstration:** The adaptive SocNavAssist approach presented in Chapter 5 used navigation objective functions to facilitate the modeling of different social navigation assistance styles, but the cost weights were custom-crafted and matched to the desired behaviors (i.e., cautious and assertive). This work could be extended by using a learning-based approach to automatically determine the navigation cost weights based on expert human demonstrations of various behaviors. Okal et al [135] demonstrated this approach for autonomous robot navigation using Bayesian inverse reinforcement learning to learn a predefined set of social cost behavior weights from human demonstration. It would also be interesting to take an unsupervised approach to identify and extract various driving styles from expert demonstrations by using the machine learning pipeline presented in Chapter 6. By doing this, we may be able to retrieve more nuanced social navigation behaviors. Additionally, in future work, this study should be performed in a real robot navigation scenario with real people to ensure realistic behaviors and perceptions as described in Section 7.2.

2. **Socially-aware navigation assistance for smart, powered wheelchairs:** This dissertation examined socially-aware navigation assistance in the context of telepresence robot navigation in remote driving situations. It would be worthwhile to adapt the proposed SocNavAssist approach to navigation as-

sistance for smart, powered wheelchairs in future investigations. In existing studies, wheelchair users with motor impairment have been shown to have difficulty driving in busy environments (e.g. airports, train stations, sidewalks, etc.) [172]. However, research on wheelchair navigation assistance has been focused mostly on collision avoidance tasks in static environments such as passing through doors [61, 80, 173]. Recently, a few studies [13, 89] have proposed semi-autonomous navigation methods for social navigation, but only considered scenarios with limited social interaction (e.g., narrow corridor crossing with a single person). Adapting the SocNavAssist approach proposed in Chapters 4 and 5 to assist wheelchair users in social navigation is a promising direction for future work. This would require exploring more compatible control and feedback interfaces for haptic and visual communication between the operator and the autonomous agent.

3. **Learning from control conflict:** The concept of control conflict was introduced in Chapter 2, which arises from a lack of intent alignment or control strategy between the human and the autonomous agent. In general, control conflicts are undesirable as they result in greater interaction forces by humans, which lowers user satisfaction and acceptance. What if the autonomous agent used conflict scenarios as interactive feedback to update its model of the user and their preferences in the task? There is a body of literature on learning from demonstrations that deal with interactive learning through feedback [174–176]. The mismatch in control commands can serve as continuous corrective feedback for online agent adaptation through incremental interactive learning. It could be a promising direction for improving the personalization and acceptance of haptic shared autonomy systems.

4. **Extending HuMADS:** The HuMADS framework presented in Chapter 6 provides an effective tool for simulating driver-ADS interaction in various scenarios. In our recent work [28], we explored how HuMADS can be used to evaluate the impact of different haptic-based ADS systems (with respect to presence and type of control conflict) on driving task performance and driver workloads. We envision extending this work in the future to evaluate ergonomic designs of interiors, to include muscle elements in HuMADS models to further study driver physical workload, and evaluate and validate active safety systems (e.g., frontal collision avoidance, steering handling, traction control, etc.) in simulation. Using this framework, we believe there is significant potential for improving future ADS design for safer driver assistance systems.

7.4 Broader Impact

Human mobility is fundamental to our everyday lives. Whether it is within our own home, on a wheelchair across a city street, commuting to work in a passenger vehicle, or traveling overseas, our ability to move from one place to another enriches our lives and enables society to function. In modern society, much of our mobility is mediated by machines and technology that not only make our transportation faster and more efficient, but also allow people with physical impairment to travel independently. Additionally, as outlined in Chapter 4, major advances in robot sensing capabilities and declining computing costs are driving the adoption of autonomous and intelligent systems in mobility vehicles. However, care must be taken to ensure that these systems are designed in a safe, trustworthy and reliable manner. In this dissertation, I primarily consider how assisted driving systems can be developed

from a human-centered approach so that they limit the adverse effects (e.g. control conflict), while improving the benefits (reduced workload and improved driving performance).

One primary area of concern is with safety. Safety is one of the most important design goals for any mobility system. Yet, a study by the United States National Highway Traffic Safety Administration (NTSHA) showed that in passenger vehicles, about 94% of accidents result from human error rather than from vehicle failure or system errors [177]. Many factors such as driver state (distractions, drowsiness, intoxication, fatigue), environmental conditions or a simple misjudgment can contribute to driving errors that compromise safety. This also holds true for other mobility systems. A key objective of intelligent assisted driving systems is to enhance overall driving safety by complementing the capabilities of the human driver. As described in Chapter 2, shared autonomy systems have been shown to not only improve driving performance (e.g. reduced collisions), but also reduce workload for the human [7]. However, as vehicles adopt more intelligent and autonomous features now and in the future, it is crucial to design these systems in a way that is human-compatible, ensuring understanding and cooperation between the humans and the autonomous system.

The findings of this dissertation suggest that multimodal shared autonomy systems (particularly with visual information) improve users' understanding of autonomous agents' intent and subsequently increase their satisfaction and preference for these systems. I believe that explainability, transparency and adaptation in autonomous and intelligent systems are crucial to ensure adequate human trust and cooperation is achieved, which would further ensure safety. In addition, the approach for human driver modeling and simulation proposed in this dissertation will offer automotive researchers a new avenue to perform model-based analyses on the

safety and usability of advanced driver assistance systems of the future.

Bibliography

[1] Y. Xing, C. Huang, and C. Lv, "Driver-Automation Collaboration for Automated Vehicles: A Review of Human-Centered Shared Control," in *IEEE Intelligent Vehicles Symposium, Proceedings*, pp. 1964–1971, Institute of Electrical and Electronics Engineers Inc., 2020.

[2] H. Kimpara, K. C. Mbanisi, J. Fu, Z. Li, D. Prokhorov, and M. A. Gennert, "Human model-based active driving system in vehicular dynamic simulation," *IEEE Transactions on Intelligent Transportation Systems*, vol. 21, no. 5, pp. 1903–1914, 2020.

[3] S. L. Delp, F. C. Anderson, A. S. Arnold, P. Loan, A. Habib, C. T. John, E. Guendelman, and D. G. Thelen, "Opensim: open-source software to create and analyze dynamic simulations of movement," *IEEE transactions on biomedical engineering*, vol. 54, no. 11, pp. 1940–1950, 2007.

[4] A. Nunes, B. Reimer, and J. F. Coughlin, "People must retain control of autonomous vehicles," 2018.

[5] N. Khojasteh, C. Liu, and S. R. Fussell, "Understanding undergraduate students' experiences of telepresence robots on campus," *Proceedings of the ACM Conference on Computer Supported Cooperative Work, CSCW*, pp. 241–246, 2019.

[6] L. Takayama, E. Marder-Eppstein, H. Harris, and J. M. Beer, "Assisted driving of a mobile remote presence system: System design and controlled user evaluation," in *Proceedings - IEEE International Conference on Robotics and Automation*, pp. 1883–1889, 2011.

[7] D. A. Abbink, M. Mulder, and E. R. Boer, "Haptic shared control: smoothly shifting control authority?,"

[8] D. A. Abbink, T. Carlson, M. Mulder, J. C. De Winter, F. Aminravan, T. L. Gibo, and E. R. Boer, "A topology of shared control systems-finding common ground in diversity," *IEEE Transactions on Human-Machine Systems*, vol. 48, pp. 509–525, oct 2018.

[9] C. E. Billings, *Human-centered aviation automation: Principles and guidelines*. National Aeronautics and Space Administration, Ames Research Center, 1996.

[10] S. M. Petermeijer, D. A. Abbink, M. Mulder, and J. C. De Winter, "The Effect of Haptic Support Systems on Driver Performance: A Literature Survey," oct 2015.

[11] M. Itoh, F. Flemisch, and D. Abbink, "A hierarchical framework to analyze shared control conflicts between human and machine," *IFAC-PapersOnLine*, vol. 49, no. 19, pp. 96–101, 2016.

[12] J. Rios-Martinez, ·. A. Spalanzani, and ·. C. Laugier, "From Proxemics Theory to Socially-Aware Navigation: A Survey," *Int J of Soc Robotics*, vol. 7, pp. 137–153, 2015.

[13] V. K. Narayanan, A. Spalanzani, and M. Babel, "A semi-autonomous framework for human-aware and user intention driven wheelchair mobility assistance," in *IEEE International Conference on Intelligent Robots and Systems*, vol. 2016-Novem, pp. 4700–4707, Institute of Electrical and Electronics Engineers Inc., nov 2016.

[14] M. Selvaggio, M. Cognetti, S. Nikolaidis, S. Ivaldi, and B. Siciliano, "Autonomy in physical human-robot interaction: A brief survey," *IEEE Robotics and Automation Letters*, 2021.

[15] A. W. De Jonge, J. G. Wildenbeest, H. Boessenkool, and D. A. Abbink, "The Effect of Trial-by-Trial Adaptation on Conflicts in Haptic Shared Control for Free-Air Teleoperation Tasks," Tech. Rep. 1, 2016.

[16] H. Saeidi, F. McLane, B. Sadrfaidpour, E. Sand, S. Fu, J. Rodriguez, J. R. Wagner, and Y. Wang, "Trust-based mixed-initiative teleoperation of mobile robots," in *Proceedings of the American Control Conference*, vol. 2016-July, pp. 6177–6182, Institute of Electrical and Electronics Engineers Inc., jul 2016.

[17] L. Milliken and G. A. Hollinger, "Modeling user expertise for choosing levels of shared autonomy," in *Proceedings - IEEE International Conference on Robotics and Automation*, pp. 2285–2291, Institute of Electrical and Electronics Engineers Inc., jul 2017.

[18] M. Gao and J. M. Zöllner, "Sparse Contextual Task Learning and Classification to Assist Mobile Robot Teleoperation with Introspective Estimation," *Journal of Intelligent and Robotic Systems: Theory and Applications*, vol. 93, pp. 571–585, mar 2019.

[19] A. Hosseini, F. Richthammer, and M. Lienkamp, "Predictive haptic feedback for safe lateral control of teleoperated road vehicles in Urban Areas," in *IEEE Vehicular Technology Conference*, vol. 2016-July, Institute of Electrical and Electronics Engineers Inc., jul 2016.

[20] Z. Wang, S. Suga, E. J. C. Nacpil, Z. Yan, and K. Nakano, "Adaptive driver-automation shared steering control via forearm surface electromyography measurement," *IEEE Sensors Journal*, vol. 21, no. 4, pp. 5444–5453, 2020.

[21] P. Maurice, V. Padois, Y. Measson, and P. Bidaud, "Human-oriented design of collaborative robots," *International Journal of Industrial Ergonomics*, vol. 57, pp. 88–102, 2017.

[22] H. Kimpara, K. C. Mbanisi, Z. Li, K. L. Troy, D. Prokhorov, and M. A. Gennert, "Force anticipation and its potential implications on feedforward and feedback human motor control," *Human Factors*, vol. 63, no. 4, pp. 647–662, 2021.

[23] K. C. Mbanisi, M. Gennert, and Z. Li, "Socnavassist: A haptic shared autonomy framework for social navigation assistance of mobile telepresence robots," in *2021 IEEE 2nd International Conference on Human-Machine Systems (ICHMS)*, pp. 1–3, IEEE, 2021.

[24] K. C. Mbanisi and M. Gennert, "Multimodal shared autonomy for social navigation assistance of telepresence robots," *in submission to IEEE Transactions on Human-Machine Systems*, 2022.

[25] K. C. Mbanisi and M. Gennert, "Adaptive socnavassist: Learning-based adaptation to dynamic user objectives in social navigation," *to be submitted to 2022 IEEE International Conference on Systems, Man, and Cybernetics*, 2022.

[26] K. C. Mbanisi, H. Kimpara, T. Meier, M. Gennert, and Z. Li, "Learning coordinated vehicle maneuver motion primitives from human demonstration," in *2018 IEEE/RSJ International Conference on Intelligent Robots and Systems (IROS)*, pp. 6560–6565, IEEE, 2018.

[27] K. C. Mbanisi, H. Kimpara, M. A. Gennert, and Z. Li, "Analysis and learning of natural driver control motion primitives for computational human driver modeling," *to be submitted to IEEE Transactions on Intelligent Vehicles*, 2022.

[28] K. C. Mbanisi, H. Kimpara, Z. Li, D. Prokhorov, and M. A. Gennert, "Human model-based evaluation of driver control workloads in driver assistance systems," *in submission to IEEE Transactions on Human-Machine Systems*, 2022.

[29] J. M. Beer, A. D. Fisk, and W. A. Rogers, "Toward a Framework for Levels of Robot Autonomy in Human-Robot Interaction," *Journal of Human-Robot Interaction*, vol. 3, no. 2, pp. 74–99, 2014.

[30] S. M. Petermeijer, A. Tinga, R. Jansen, A. de Reus, and B. van Waterschoot, "What makes a good team?-towards the assessment of driver-vehicle cooperation.," in *13th International Conference on Automotive User Interfaces and Interactive Vehicular Applications*, pp. 99–108, 2021.

[31] S. Musić and S. Hirche, "Control sharing in human-robot team interaction," *Annual Reviews in Control*, vol. 44, pp. 342–354, 2017.

[32] H. Wang and X. P. Liu, "Adaptive shared control for a novel mobile assistive robot," *IEEE/ASME Transactions on Mechatronics*, vol. 19, no. 6, pp. 1725–1736, 2014.

[33] M. Chiou, N. Hawes, and R. Stolkin, "Mixed-initiative variable autonomy for remotely operated mobile robots," *ACM Transactions on Human-Robot Interaction (THRI)*, vol. 10, no. 4, pp. 1–34, 2021.

[34] A. D. Dragan and S. S. Srinivasa, "A policy-blending formalism for shared control," *International Journal of Robotics Research*, vol. 32, no. 7, pp. 790–805, 2013.

[35] "A Review of Shared Control for Automated Vehicles: Theory and Applications," *IEEE Transactions on Human-Machine Systems*, vol. 50, pp. 475–491, dec 2020.

[36] R. Li, Y. Li, E. Li, E. Burdet, and B. Cheng, "Indirect Shared Control of Highly Automated Vehicles for Cooperative Driving between Driver and Automation," tech. rep., 2017.

[37] B. Hannaford and A. M. Okamura, *Haptics*, pp. 1063–1084. Cham: Springer International Publishing, 2016.

[38] N. Enayati, E. De Momi, and G. Ferrigno, "Haptics in robot-assisted surgery: Challenges and benefits," *IEEE reviews in biomedical engineering*, vol. 9, pp. 49–65, 2016.

[39] H. Culbertson, S. B. Schorr, and A. M. Okamura, "Haptics: The present and future of artificial touch sensation," *Annual Review of Control, Robotics, and Autonomous Systems*, vol. 1, pp. 385–409, 2018.

[40] Y. Che, A. M. Okamura, and D. Sadigh, "Efficient and trustworthy social navigation via explicit and implicit robot–human communication," *IEEE Transactions on Robotics*, vol. 36, no. 3, pp. 692–707, 2020.

[41] R. Boink, M. M. Van Paassen, M. Mulder, and D. A. Abbink, "Understanding and reducing conflicts between driver and haptic shared control," in *Conference Proceedings - IEEE International Conference on Systems, Man and Cybernetics*, vol. 2014-Janua, pp. 1510–1515, Institute of Electrical and Electronics Engineers Inc., 2014.

[42] "How boeing 737 max's flawed flight control system led to 2 crashes that killed 346." `https://abcnews.go.com/US/boeing-737-maxs-flawed-flight-control-system-led/story?id=74321424`. Accessed: 2022-04-04.

[43] H. M. Zwaan, S. M. Petermeijer, and D. A. Abbink, "Haptic shared steering control with an adaptive level of authority based on time-to-line crossing," in *IFAC-PapersOnLine*, vol. 52, pp. 49–54, Elsevier B.V., jan 2019.

[44] M. M. van Paassen, R. Boink, D. A. Abbink, M. Mulder, and M. Mulder, "Haptic Guidance, Interaction Between the Guidance Model and Tuning," Tech. Rep. July, 2015.

[45] J. Steen, H. J. Damveld, R. Happee, M. M. Van Paassen, and M. Mulder, "A review of visual driver models for system identification purposes," in *Conference Proceedings - IEEE International Conference on Systems, Man and Cybernetics*, pp. 2093–2100, 2011.

[46] S. J. Anderson, J. M. Walker, and K. Iagnemma, "Experimental performance analysis of a homotopy-based shared autonomy framework," *IEEE Transactions on Human-Machine Systems*, vol. 44, pp. 190–199, apr 2014.

[47] J. J. Abbott, P. Marayong, and A. M. Okamura, "Haptic virtual fixtures for robot-assisted manipulation," in *Robotics research*, pp. 49–64, Springer, 2007.

[48] L. B. Rosenberg, "Virtual fixtures: Perceptual tools for telerobotic manipulation," in *Proceedings of IEEE virtual reality annual international symposium*, pp. 76–82, IEEE, 1993.

[49] C. Ju and H. I. Son, "Evaluation of Haptic Feedback in the Performance of a Teleoperated Unmanned Ground Vehicle in an Obstacle Avoidance Scenario," *International Journal of Control, Automation and Systems*, vol. 17, pp. 168–180, jan 2019.

[50] T. M. Lam, H. W. Boschloo, M. Mulder, and M. M. Van Paassen, "Artificial force field for haptic feedback in UAV teleoperation," *IEEE Transactions on Systems, Man, and Cybernetics Part A:Systems and Humans*, vol. 39, pp. 1316–1330, nov 2009.

[51] A. Balachandran, M. Brown, S. M. Erlien, and J. C. Gerdes, "Predictive haptic feedback for obstacle avoidance based on model predictive control," *IEEE Transactions on Automation Science and Engineering*, vol. 13, pp. 26–31, jan 2016.

[52] D. Zhang, G. Yang, and R. P. Khurshid, "Haptic Teleoperation of UAVs through Control Barrier Functions," *IEEE Transactions on Haptics*, vol. 13, pp. 109–115, jan 2020.

[53] T. Battisti and R. Muradore, "A velocity obstacles approach for autonomous landing and teleoperated robots," *Autonomous Robots*, vol. 44, pp. 217–232, 2020.

[54] B. Shneiderman, "Human-centered artificial intelligence: Reliable, safe & trustworthy," *International Journal of Human–Computer Interaction*, vol. 36, no. 6, pp. 495–504, 2020.

[55] M. H. Martens and A. P. van den Beukel, "The road to automated driving: Dual mode and human factors considerations," in *16th international IEEE conference on intelligent transportation systems (ITSC 2013)*, pp. 2262–2267, IEEE, 2013.

[56] M. Kawato, "Internal models for motor control and trajectory planning," *Current opinion in neurobiology*, vol. 9, no. 6, pp. 718–727, 1999.

[57] N. AbuAli and H. Abou-zeid, "Driver behavior modeling: Developments and future directions," *International journal of vehicular technology*, vol. 2016, 2016.

[58] K. E. Schaefer, E. R. Straub, J. Y. Chen, J. Putney, and A. W. Evans III, "Communicating intent to develop shared situation awareness and engender trust in human-agent teams," *Cognitive Systems Research*, vol. 46, pp. 26–39, 2017.

[59] A. Yamazaki, K. Yamazaki, M. Burdelski, Y. Kuno, and M. Fukushima, "Coordination of verbal and non-verbal actions in human–robot interaction at museums and exhibitions," *Journal of Pragmatics*, vol. 42, no. 9, pp. 2398–2414, 2010.

[60] A. W. Evans III, S. G. Hill, and R. Pomranky, "Investigating the usefulness of soldier aids for autonomous unmanned ground vehicles, part 2," tech. rep., ARMY RESEARCH LAB ABERDEEN PROVING GROUND MD HUMAN RESEARCH AND ENGINEERING ..., 2015.

[61] M. Zolotas and Y. Demiris, "Towards Explainable Shared Control using Augmented Reality," in *IEEE International Conference on Intelligent Robots and*

Systems, pp. 3020–3026, Institute of Electrical and Electronics Engineers Inc., nov 2019.

[62] J. F. Mullen, J. Mosier, S. Chakrabarti, A. Chen, T. White, and D. P. Losey, "Communicating inferred goals with passive augmented reality and active haptic feedback," *IEEE Robotics and Automation Letters*, vol. 6, no. 4, pp. 8522–8529, 2021.

[63] Y. Che, H. Culbertson, C.-W. Tang, S. Aich, and A. M. Okamura, "Facilitating human-mobile robot communication via haptic feedback and gesture teleoperation," *ACM Transactions on Human-Robot Interaction (THRI)*, vol. 7, no. 3, pp. 1–23, 2018.

[64] K. Suzuki and H. Jansson, "An analysis of driver's steering behaviour during auditory or haptic warnings for the designing of lane departure warning system," *JSAE review*, vol. 24, no. 1, pp. 65–70, 2003.

[65] N. Koenig, L. Takayama, and M. Matarić, "Communication and knowledge sharing in human–robot interaction and learning from demonstration," *Neural Networks*, vol. 23, no. 8-9, pp. 1104–1112, 2010.

[66] K. Muelling, C. Takahashi, S. Nikolaidis, V. Alonso, and P. De La Puente, "System Transparency in Shared Autonomy: A Mini Review," *Frontiers in Neurorobotics — www.frontiersin.org*, vol. 12, p. 83, 2018.

[67] S. De Stigter, M. Mulder, and M. Van Paassen, "Design and evaluation of a haptic flight director," *Journal of guidance, control, and dynamics*, vol. 30, no. 1, pp. 35–46, 2007.

[68] W. Vreugdenhil, S. Barendswaard, D. A. Abbink, C. Borst, and S. M. Petermeijer, "Complementing Haptic Shared Control with Visual Feedback for Obstacle Avoidance," in *IFAC-PapersOnLine*, vol. 52, pp. 371–376, Elsevier B.V., jan 2019.

[69] R. J. Kuiper, D. J. Heck, I. A. Kuling, and D. A. Abbink, "Evaluation of Haptic and Visual Cues for Repulsive or Attractive Guidance in Nonholonomic Steering Tasks," *IEEE Transactions on Human-Machine Systems*, vol. 46, pp. 672–683, oct 2016.

[70] C. Brooks and D. Szafir, "Visualization of Intended Assistance for Acceptance of Shared Control," in *IROS 2020*, 2020.

[71] J.-M. Hoc, M. S. Young, and J.-M. Blosseville, "Cooperation between drivers and automation: implications for safety," *Theoretical Issues in Ergonomics Science*, vol. 10, no. 2, pp. 135–160, 2009.

[72] A. van den Berg, "Visual feedback for haptic assisted teleoperation of an industrial robot: With dross removal as a use case," 2020.

[73] V. Ho, C. Borst, M. M. van Paassen, and M. Mulder, "Increasing acceptance of haptic feedback in uav teleoperation by visualizing force fields," in *2018 IEEE International Conference on Systems, Man, and Cybernetics (SMC)*, pp. 3027–3032, IEEE, 2018.

[74] D. P. Losey, C. G. McDonald, E. Battaglia, and M. K. O'Malley, "A review of intent detection, arbitration, and communication aspects of shared control for physical human–robot interaction," *Applied Mechanics Reviews*, vol. 70, no. 1, 2018.

[75] C. Passenberg, A. Glaser, and A. Peer, "Exploring the design space of haptic assistants: The assistance policy module," *IEEE Transactions on Haptics*, vol. 6, pp. 440–452, oct 2013.

[76] M. Itoh and T. Inagaki, "Design and evaluation of steering protection for avoiding collisions during a lane change," *Ergonomics*, vol. 57, no. 3, pp. 361–373, 2014.

[77] J. Wang, G. Zhang, R. Wang, S. C. Schnelle, and J. Wang, "A Gain-Scheduling Driver Assistance Trajectory-Following Algorithm Considering Different Driver Steering Characteristics," *IEEE Transactions on Intelligent Transportation Systems*, vol. 18, pp. 1097–1108, may 2017.

[78] C. Neustaedter, S. Singhal, R. Pan, Y. Heshmat, A. Forghani, and J. Tang, "From Being There to Watching: Shared and Dedicated Telepresence Robot Usage at Academic Conferences," *ACM Trans. Comput.-Hum. Interact*, vol. 25, 2018.

[79] T. Kruse, A. K. Pandey, R. Alami, and A. Kirsch, "Human-aware robot navigation: A survey," *Robotics and Autonomous Systems*, vol. 61, pp. 1726–1743, dec 2013.

[80] "Learning Shared Control by Demonstration for Personalized Wheelchair Assistance," *IEEE Transactions on Haptics*, vol. 11, pp. 431–442, jul 2018.

[81] C. Mavrogiannis, F. Baldini, A. Wang, D. Zhao, P. Trautman, A. Steinfeld, and J. Oh, "Core Challenges of Social Robot Navigation: A Survey," Tech. Rep. 1, 2021.

[82] K. Charalampous, I. Kostavelis, and A. Gasteratos, "Recent trends in social aware robot navigation: A survey," jul 2017.

[83] E. T. Hall, *The hidden dimension*, vol. 609. Garden City, NY: Doubleday, 1966.

[84] J. Rios-Martinez, A. Spalanzani, and C. Laugier, "Understanding human interaction for probabilistic autonomous navigation using risk-rrt approach," in *2011 IEEE/RSJ International Conference on Intelligent Robots and Systems*, pp. 2014–2019, IEEE, 2011.

[85] D. Helbing and P. Molnar, "Social force model for pedestrian dynamics," *Physical review E*, vol. 51, no. 5, p. 4282, 1995.

[86] J. D. Van Berg, M. Lin, and D. Manocha, "Reciprocal velocity obstacles for real-time multi-agent navigation," in *Proceedings - IEEE International Conference on Robotics and Automation*, pp. 1928–1935, 2008.

[87] P. Trautman and A. Krause, *Unfreezing the robot: Navigation in dense, interacting crowds*. 2010.

[88] Y. F. Chen, M. Everett, M. Liu, and J. P. How, "Socially aware motion planning with deep reinforcement learning," in *IEEE International Conference on Intelligent Robots and Systems*, vol. 2017-Septe, pp. 1343–1350, Institute of Electrical and Electronics Engineers Inc., dec 2017.

[89] H. Kretzschmar, M. Spies, C. Sprunk, and W. Burgard, "Socially compliant mobile robot navigation via inverse reinforcement learning," *The International Journal of Robotics Research*, vol. 35, no. 11, pp. 1289–1307, 2016.

[90] O.-R. A. D. O. Committee, *Taxonomy and Definitions for Terms Related to Driving Automation Systems for On-Road Motor Vehicles*, apr 2021.

[91] A. Ziebinski, R. Cupek, D. Grzechca, and L. Chruszczyk, "Review of advanced driver assistance systems (adas)," in *AIP Conference Proceedings*, vol. 1906, p. 120002, AIP Publishing LLC, 2017.

[92] M. Hasenjager, M. Heckmann, and H. Wersing, "A Survey of Personalization for Advanced Driver Assistance Systems," jun 2020.

[93] A. Y. Ungoren and H. Peng, "An adaptive lateral preview driver model," *Vehicle system dynamics*, vol. 43, no. 4, pp. 245–259, 2005.

[94] M. Iwamoto, Y. Kisanuki, I. Watanabe, K. Furusu, K. Miki, and J. Hasegawa, "Development of a finite element model of the total human model for safety (thums) and application to injury reconstruction," *Proceedings of the 2002 International Research Council on Biomechanics of Injury, Munich, Germany*, pp. 31–42, 2002.

[95] H.-Z. Li, L. Li, J. Song, and L.-Y. Yu, "Comprehensive lateral driver model for critical maneuvering conditions," *International Journal of Automotive Technology*, vol. 12, no. 5, p. 679, 2011.

[96] S. Schnelle, J. Wang, H.-J. Su, and R. Jagacinski, "A personalizable driver steering model capable of predicting driver behaviors in vehicle collision avoidance maneuvers," *IEEE Transactions on Human-Machine Systems*, vol. 47, no. 5, pp. 625–635, 2017.

[97] M. P. Reed, J. Faraway, D. B. Chaffin, and B. J. Martin, "The humosim ergonomics framework: A new approach to digital human simulation for ergonomic analysis," tech. rep., SAE Technical Paper, 2006.

[98] J. Yang, J. H. Kim, K. Abdel-Malek, T. Marler, S. Beck, and G. R. Kopp, "A new digital human environment and assessment of vehicle interior design," *Computer-Aided Design*, vol. 39, no. 7, pp. 548–558, 2007.

[99] B. Dariush, "Real time posture and movement prediction in execution of operational tasks," Nov. 24 2015. US Patent 9,195,794.

[100] A. J. Pick and D. J. Cole, "A mathematical model of driver steering control including neuromuscular dynamics," *Journal of Dynamic Systems, Measurement, and Control*, vol. 130, no. 3, p. 031004, 2008.

[101] N. Mehrabi, R. Sharif Razavian, and J. McPhee, "Steering disturbance rejection using a physics-based neuromusculoskeletal driver model," *Vehicle System Dynamics*, vol. 53, no. 10, pp. 1393–1415, 2015.

[102] A. Hosseini, F. Richthammer, and M. Lienkamp, "Predictive haptic feedback for safe lateral control of teleoperated road vehicles in urban areas," in *2016 IEEE 83rd Vehicular Technology Conference (VTC Spring)*, pp. 1–7, IEEE, 2016.

[103] J. C. De Winter, R. Happee, M. H. Martens, and N. A. Stanton, "Effects of adaptive cruise control and highly automated driving on workload and situation awareness: A review of the empirical evidence," *Transportation research part F: traffic psychology and behaviour*, vol. 27, pp. 196–217, 2014.

[104] G. Zhenhai, "The driver's steering feel assessment using eeg and emg signals," *NeuroQuantology*, vol. 16, no. 2, 2018.

[105] E. J. C. Nacpil, Z. Wang, and K. Nakano, "Application of physiological sensors for personalization in semi-autonomous driving: A review," *IEEE Sensors Journal*, 2021.

[106] R. S. Woodworth, "Accuracy of voluntary movement.," *The Psychological Review: Monograph Supplements*, vol. 3, no. 3, p. i, 1899.

[107] D. Serrien, P. Kaluzny, U. Wicki, and M. Wiesendanger, "Grip force adjustments induced by predictable load perturbations during a manipulative task," *Experimental Brain Research*, vol. 124, no. 1, pp. 100–106, 1999.

[108] P. Jenmalm, C. Schmitz, H. Forssberg, and H. H. Ehrsson, "Lighter or heavier than predicted: neural correlates of corrective mechanisms during erroneously programmed lifts," *Journal of Neuroscience*, vol. 26, no. 35, pp. 9015–9021, 2006.

[109] A. M. Gordon, G. Westling, K. J. Cole, and R. S. Johansson, "Memory representations underlying motor commands used during manipulation of common and novel objects," *Journal of neurophysiology*, vol. 69, no. 6, pp. 1789–1796, 1993.

[110] C. E. Boettcher, K. A. Ginn, and I. Cathers, "Standard maximum isometric voluntary contraction tests for normalizing shoulder muscle emg," *Journal of orthopaedic research*, vol. 26, no. 12, pp. 1591–1597, 2008.

[111] T. D. Welch and L. H. Ting, "A feedback model explains the differential scaling of human postural responses to perturbation acceleration and velocity," *Journal of Neurophysiology*, vol. 101, no. 6, pp. 3294–3309, 2009.

[112] D. A. Nowak, S. Glasauer, and J. Hermsdörfer, "Force control in object manipulation—a model for the study of sensorimotor control strategies," *Neuroscience & Biobehavioral Reviews*, vol. 37, no. 8, pp. 1578–1586, 2013.

[113] D. A. Abbink and M. Mulder, "Exploring the dimensions of haptic feedback support in manual control," *Journal of Computing and Information Science in Engineering*, vol. 9, no. 1, 2009.

[114] C. C. Macadam, "Understanding and modeling the human driver," *Vehicle system dynamics*, vol. 40, no. 1-3, pp. 101–134, 2003.

[115] J. Cohen, "Statistical power analysis for the behavioral sciences. lawrence erlbaum associates," *Hillsdale, NJ*, pp. 20–26, 1988.

[116] J. Kotrlik and H. Williams, "The incorporation of effect size in information technology, learning, information technology, learning, and performance research and performance research," *Information Technology, Learning, and Performance Journal*, vol. 21, no. 1, p. 1, 2003.

[117] J. Miles and M. Shevlin, *Applying regression and correlation: A guide for students and researchers*. Sage, 2001.

[118] K. J. Mimnaugh, M. Suomalainen, I. Becerra, E. Lozano, R. Murrieta-Cid, and S. M. LaValle, "Analysis of user preferences for robot motions in immersive telepresence," *arXiv preprint arXiv:2103.03496*, 2021.

[119] C. Mavrogiannis, F. Baldini, and et al, "Core challenges of social robot navigation: A survey," *arXiv preprint arXiv:2103.05668*, 2021.

[120] J. Wang, A. Chellali, and C. G. Cao, "Haptic communication in collaborative virtual environments," *Human factors*, vol. 58, no. 3, pp. 496–508, 2016.

[121] X. T. Truong and T. D. Ngo, "Toward Socially Aware Robot Navigation in Dynamic and Crowded Environments: A Proactive Social Motion Model," *IEEE Transactions on Automation Science and Engineering*, vol. 14, pp. 1743–1760, oct 2017.

[122] S. Jain and B. Argall, "Probabilistic human intent recognition for shared autonomy in assistive robotics," *ACM Transactions on Human-Robot Interaction (THRI)*, vol. 9, no. 1, pp. 1–23, 2019.

[123] T. Linder and K. O. Arras, "Multi-model hypothesis tracking of groups of people in rgb-d data," in *17th International conference on information fusion (FUSION)*, pp. 1–7, IEEE, 2014.

[124] C. Brooks and D. Szafir, "Visualization of intended assistance for acceptance of shared control," in *2020 IEEE/RSJ International Conference on Intelligent Robots and Systems (IROS)*, pp. 11425–11430, IEEE, 2020.

[125] J. Rios-Martinez, A. Spalanzani, and C. Laugier, "From proxemics theory to socially-aware navigation: A survey," *International Journal of Social Robotics*, vol. 7, no. 2, pp. 137–153, 2015.

[126] R Core Team, *R: A Language and Environment for Statistical Computing*. R Foundation for Statistical Computing, Vienna, Austria, 2021.

[127] W. Vreugdenhil, S. Barendswaard, D. A. Abbink, C. Borst, and S. M. Petermeijer, "Complementing haptic shared control with visual feedback for obstacle avoidance," *IFAC-PapersOnLine*, vol. 52, no. 19, pp. 371–376, 2019.

[128] A. U. Batmaz, J. Maiero, E. Kruijff, B. E. Riecke, C. Neustaedter, and W. Stuerzlinger, "How automatic speed control based on distance affects user behaviours in telepresence robot navigation within dense conference-like environments," *Plos one*, vol. 15, no. 11, p. e0242078, 2020.

[129] J. D. Lee and N. Moray, "Trust, self-confidence, and operators' adaptation to automation," *International journal of human-computer studies*, vol. 40, no. 1, pp. 153–184, 1994.

[130] R. Luo, Y. Weng, Y. Wang, P. Jayakumar, M. J. Brudnak, V. Paul, V. R. Desaraju, J. L. Stein, T. Ersal, and X. J. Yang, "A workload adaptive haptic shared control scheme for semi-autonomous driving," *Accident Analysis & Prevention*, vol. 152, p. 105968, 2021.

[131] M. Gao, *Adaptive Shared Autonomy between Human and Robot to Assist Mobile Robot Teleoperation*. PhD thesis, KIT-Bibliothek, 2018.

[132] F. Durupinar, N. Pelechano, J. Allbeck, U. Güdükbay, and N. I. Badler, "How the ocean personality model affects the perception of crowds," *IEEE Computer Graphics and Applications*, vol. 31, no. 3, pp. 22–31, 2009.

[133] A. Bera, T. Randhavane, and D. Manocha, "Aggressive, tense or shy? identifying personality traits from crowd videos.," in *IJCAI*, pp. 112–118, 2017.

[134] B. Zhu, S. Yan, J. Zhao, and W. Deng, "Personalized lane-change assistance system with driver behavior identification," *IEEE Transactions on Vehicular Technology*, vol. 67, no. 11, pp. 10293–10306, 2018.

[135] B. Okal and K. O. Arras, "Learning socially normative robot navigation behaviors with bayesian inverse reinforcement learning," in *2016 IEEE International Conference on Robotics and Automation (ICRA)*, pp. 2889–2895, IEEE, 2016.

[136] N. Pérez-Higueras, F. Caballero, and L. Merino, "Teaching robot navigation behaviors to optimal rrt planners," *International Journal of Social Robotics*, vol. 10, no. 2, pp. 235–249, 2018.

[137] G. Bradski, "The OpenCV Library," *Dr. Dobb's Journal of Software Tools*, 2000.

[138] M. Chiou, M. Talha, and R. Stolkinl, "Learning effects in variable autonomy human-robot systems: how much training is enough?," in *2019 IEEE International Conference on Systems, Man and Cybernetics (SMC)*, pp. 720–727, IEEE, 2019.

[139] S. Hong, B. Min, S. Doi, and K. Suzuki, "Approaching and stopping behaviors to the intersections of aged drivers compared with young drivers," *International Journal of Industrial Ergonomics*, vol. 54, pp. 32–41, 2016.

[140] S. Bao, L. Wu, B. Yu, and J. R. Sayer, "An examination of teen drivers' car-following behavior under naturalistic driving conditions: With and without an advanced driving assistance system," *Accident Analysis & Prevention*, vol. 147, p. 105762, 2020.

[141] *Taxonomy and Definitions for Terms Related to Driving Automation Systems for On-Road Motor Vehicles*, jun 2018.

[142] D. A. Abbink and M. Mulder, "Motivation for a neuromuscular basis for haptic shared control," *IFAC Proceedings Volumes*, vol. 43, no. 13, pp. 299–303, 2010.

[143] S. Saigo, P. Raksincharoensak, and M. Nagai, "Investigation of inattentive driving estimation method by using longitudinal and lateral driver operational models," *SAE International journal of passenger cars-electronic and electrical systems*, vol. 6, no. 1, pp. 27–33, 2013.

[144] S. Saigo, "Study on driving state estimation method with on-board driver behavior model," *Dr. theis, Mechanical and System Engineering, Tokyo Univ. of Agriculture and Technology*, 2014.

[145] M. Abe, *Vehicle handling dynamics: theory and application*. Butterworth-Heinemann, 2015.

[146] M. W. Spong, S. Hutchinson, M. Vidyasagar, *et al.*, *Robot modeling and control*, vol. 3. Wiley New York, 2006.

[147] MATLAB, *version 9.5.0 (R2018b)*. Natick, Massachusetts: The MathWorks Inc., 2018.

[148] Z. Li, D. Milutinović, and J. Rosen, "From reaching to reach-to-grasp: the arm posture difference and its implications on human motion control strategy," *Experimental brain research*, vol. 235, no. 5, pp. 1627–1642, 2017.

[149] L. Kaufman and P. Rousseeuw, *Finding Groups in Data: an introduction to cluster analysis*. Wiley, 1990.

[150] J. H. Ward Jr, "Hierarchical grouping to optimize an objective function," *Journal of the American statistical association*, vol. 58, no. 301, pp. 236–244, 1963.

[151] P. J. Rousseeuw, "Silhouettes: a graphical aid to the interpretation and validation of cluster analysis," *Journal of computational and applied mathematics*, vol. 20, pp. 53–65, 1987.

[152] S. Calinon, F. Guenter, and A. Billard, "On learning, representing, and generalizing a task in a humanoid robot," *IEEE Transactions on Systems, Man, and Cybernetics, Part B (Cybernetics)*, vol. 37, no. 2, pp. 286–298, 2007.

[153] D. Reynolds, "Gaussian mixture models," *Encyclopedia of biometrics*, pp. 827–832, 2015.

[154] A. P. Dempster, N. M. Laird, and D. B. Rubin, "Maximum likelihood from incomplete data via the em algorithm," *Journal of the royal statistical society. Series B (methodological)*, pp. 1–38, 1977.

[155] D. Pelleg, A. W. Moore, *et al.*, "X-means: Extending k-means with efficient estimation of the number of clusters.," in *Icml*, vol. 1, pp. 727–734, 2000.

[156] D. A. Cohn, Z. Ghahramani, and M. I. Jordan, "Active learning with statistical models," *Journal of artificial intelligence research*, 1996.

[157] P. Pastor, H. Hoffmann, T. Asfour, and S. Schaal, "Learning and generalization of motor skills by learning from demonstration," in *Robotics and Automation, 2009. ICRA'09. IEEE International Conference on*, pp. 763–768, IEEE, 2009.

[158] A. J. Ijspeert, J. Nakanishi, H. Hoffmann, P. Pastor, and S. Schaal, "Dynamical movement primitives: learning attractor models for motor behaviors," *Neural computation*, vol. 25, no. 2, pp. 328–373, 2013.

[159] J. Schiro, P. Loslever, F. Gabrielli, and P. Pudlo, "Inter and intra-individual differences in steering wheel hand positions during a simulated driving task," *Ergonomics*, vol. 58, no. 3, pp. 394–410, 2015.

[160] "Using efficient steering techniques," tech. rep., NHTSA.

[161] M. P. Reed, M. B. Parkinson, and D. B. Chaffin, "A new approach to modeling driver reach," tech. rep., SAE Technical Paper, 2003.

[162] R. Kondo, T. Wada, and K. Sonoda, "Use of haptic shared control in highly automated driving systems," *IFAC-PapersOnLine*, vol. 52, no. 19, pp. 43–48, 2019.

[163] M. Blanco, J. Atwood, H. M. Vasquez, T. E. Trimble, V. L. Fitchett, J. Radlbeck, G. M. Fitch, S. M. Russell, C. A. Green, B. Cullinane, *et al.*, "Human factors evaluation of level 2 and level 3 automated driving concepts," tech. rep., 2015.

[164] B. D. Argall, S. Chernova, M. Veloso, and B. Browning, "A survey of robot learning from demonstration," *Robotics and autonomous systems*, vol. 57, no. 5, pp. 469–483, 2009.

[165] J. Storms, K. Chen, and D. Tilbury, "A shared control method for obstacle avoidance with mobile robots and its interaction with communication delay," *The International Journal of Robotics Research*, vol. 36, pp. 820–839, jun 2017.

[166] M. Gao, J. Oberlander, T. Schamm, and J. M. Zollner, "Contextual task-aware shared autonomy for assistive mobile robot teleoperation," in *IEEE International Conference on Intelligent Robots and Systems*, pp. 3311–3318, Institute of Electrical and Electronics Engineers Inc., oct 2014.

[167] A. H. Eichelberger and A. T. McCartt, "Toyota drivers' experiences with dynamic radar cruise control, pre-collision system, and lane-keeping assist," *Journal of safety research*, vol. 56, pp. 67–73, 2016.

[168] T. Günthner and H. Proff, "On the way to autonomous driving: How age influences the acceptance of driver assistance systems," *Transportation research part F: traffic psychology and behaviour*, vol. 81, pp. 586–607, 2021.

[169] P. A. Hancock, D. R. Billings, K. E. Schaefer, J. Y. Chen, E. J. De Visser, and R. Parasuraman, "A meta-analysis of factors affecting trust in human-robot interaction," *Human factors*, vol. 53, no. 5, pp. 517–527, 2011.

[170] S. Ososky, T. Sanders, F. Jentsch, P. Hancock, and J. Y. Chen, "Determinants of system transparency and its influence on trust in and reliance on unmanned robotic systems," in *Unmanned Systems Technology XVI*, vol. 9084, p. 90840E, International Society for Optics and Photonics, 2014.

[171] F. Mars, M. Deroo, and J.-M. Hoc, "Analysis of human-machine cooperation when driving with different degrees of haptic shared control," *IEEE transactions on haptics*, vol. 7, no. 3, pp. 324–333, 2014.

[172] B. Zhang, G. Barbareschi, R. Ramirez Herrera, T. Carlson, and C. Holloway, "Understanding interactions for smart wheelchair navigation in crowds," in *Proceedings of ACM CHI Conference on Human Factors in Computing Systems*, vol. 2022, ACM, 2022.

[173] T. Carlson, R. Leeb, R. Chavarriaga, and J. d. R. Millán, "Online modulation of the level of assistance in shared control systems," in *2012 IEEE International Conference on Systems, Man, and Cybernetics (SMC)*, pp. 3339–3344, IEEE, 2012.

[174] C. Celemin and J. Ruiz-del Solar, "An interactive framework for learning continuous actions policies based on corrective feedback," *Journal of Intelligent & Robotic Systems*, vol. 95, no. 1, pp. 77–97, 2019.

[175] D. Wout, J. Scholten, C. Celemin, and J. Kober, "Learning gaussian policies from corrective human feedback," *arXiv preprint arXiv:1903.05216*, 2019.

[176] R. Perez-Dattari, C. Celemin, G. Franzese, J. Ruiz-del Solar, and J. Kober, "Interactive learning of temporal features for control: Shaping policies and state representations from human feedback," *IEEE Robotics & Automation Magazine*, vol. 27, no. 2, pp. 46–54, 2020.

[177] "Critical reasons for crashes investigated in the national motor vehicle crash causation survey." `https://crashstats.nhtsa.dot.gov/Api/Public/Publication/812115`. Accessed: 2022-05-02.